PHENOMENOLOGICAL APPROACHES ON THE PHASE TRANSITION MECHANISMS OF SOME FERROELECTRIC MATERIALS

A THESIS SUBMITTED TO
THE GRADUATE SCHOOL OF NATURAL AND APPLIED SCIENCES
OF
MIDDLE EAST TECHNICAL UNIVERSITY

BY

NAZAN KARA

IN PARTIAL FULFILLMENT OF THE REQUIREMENTS
FOR
THE DEGREE OF DOCTOR OF PHILOSOPHY
IN
PHYSICS

JANUARY 2023

Approval of the thesis:

PHENOMENOLOGICAL APPROACHES ON THE PHASE TRANSITION MECHANISMS OF SOME FERROELECTRIC MATERIALS

submitted by **NAZAN KARA** in partial fulfillment of the requirements for the degree of **Doctor of Philosophy** i**n Physics, Middle East Technical University** by,

Prof. Dr. Halil Kalıpçılar
Dean, Graduate School of **Natural and Applied Sciences** _____

Prof. Dr. Seçkin Kürkçüoğlu
Head of the Department, **Physics** _____

Prof. Dr. Hamit Yurtseven
Supervisor, **Physics, METU** _____

Assoc. Prof. Dr. Ali Kiracı
Co-Supervisor, **Physics** _____

Examining Committee Members:

Prof. Dr. Bekir Sıtkı Kandemir
Physics, Ankara University _____

Prof. Dr. Hamit Yurtseven
Physics, METU _____

Prof. Dr. Şinasi Barış Emre
Physics, Ankara University _____

Prof. Dr. Nizami Hasanlı
Physics, METU _____

Prof. Dr. Mehmet Parlak
Physics, METU _____

Date: 25.01.2023

I hereby declare that all information in this document has been obtained and presented in accordance with academic rules and ethical conduct. I also declare that, as required by these rules and conduct, I have fully cited and referenced all material and results that are not original to this work.

Name Last name : Nazan Kara

Signature :

ABSTRACT

PHENOMENOLOGICAL APPROACHES ON THE PHASE TRANSITION MECHANISMS OF SOME FERROELECTRIC MATERIALS

Kara, Nazan
Doctor of Philosophy, Physics
Supervisor: Prof. Dr. Hamit Yurtseven
Co-Supervisor: Assoc. Prof. Dr. Ali Kiracı

January 2023, 105 pages

Several phenomenological studies were carried out to investigate the phase transition mechanisms of some ferroelectric crystals. In particular, we focused on the compressible Ising model to explain the anomalous behavior of specific heat for such ferroelectrics exhibiting second-order phase transitions in the vicinity of the transition temperatures. The temperature dependence of some thermodynamic functions such as internal energy, enthalpy, entropy, and free energy of some ferroelectric materials was also predicted. The thermodynamic quantities of ferroelectrics are obtained by calculating the order parameters using the experimental data from the literature. The calculated results are then interpreted with the ones stated in previous experimental studies.

Keywords: Phase Transitions, Ferroelectrics, Ising Model, Landau Theory

ÖZ

ÇEŞİTLİ FERROELEKTRİK MALZEMELERİN FAZ GEÇİŞ MEKANİZMALARINA FENOMENOLOJİK YAKLAŞIMLAR

Kara, Nazan
Doktora, Fizik
Tez Yöneticisi: Prof. Dr. Hamit Yurtseven
Ortak Tez Yöneticisi: Doç. Dr. Ali Kiracı

Ocak 2023, 105 sayfa

Bazı ferroelektrik kristallerin faz geçiş mekanizmalarını araştırmak için bir dizi fenomenolojik çalışma yapılmıştır. Özellikle, geçiş sıcaklıklarının yakınında ikinci derece faz geçişleri sergileyen bu tür ferroelektriklerin özgül ısısının anormal davranışını açıklamak için sıkıştırılabilir Ising modeline odaklandık. Bazı ferroelektrik malzemelerin iç enerji, entalpi, entropi ve serbest enerji gibi termodinamik fonksiyonlarının sıcaklığa bağlılığı da öngörülmüştür. Ferroelektrik malzemelerin termodinamik özellikleri, literatürdeki deneysel verilerden elde edilen düzen parametreleri kullanılarak hesaplandı. Hesaplanan değerler yine literatürdeki sonuçlarla karşılaştırılarak yorumlandı.

Anahtar Kelimeler: Faz Geçişleri, Ferroelektrikler, Ising Model, Landau Teori

To my dear family

ACKNOWLEDGMENTS

I would like to express my deepest gratitude to my advisor Prof. Dr. Hamit Yurtseven and co-advisor Assoc. Prof. Dr. Ali Kiracı. I would never have been able to take on and complete this work without their great supervision, encouragement, priceless comments and assistance, friendly attitude, patience, and unwavering support. And special thanks to Prof. Dr. Şinasi Barış Emre and Prof. Dr. Nizami Hasanlı for following the process and guiding with invaluable comments.

Most significantly, I want to thank my mother Cennet İnci Kara and father İlhan Kara for their unwavering moral support, inspiration, and encouragement throughout my entire life. Special thanks to my brother Ozan, sister-in-law Aylin and my life energy little Öykü for being in my life with endless love. The support of my family will inspire me to deal with all of the challenges in life.

Many great thanks are also due to my close friends İlhan Zeynep Karakılıç, Pınar Zeynep Çulfaz Emecen, Ayfer Duru, Günçe Çetin, Ezgi Bütev Öcal, Arda Öcal, Banu Cingöz Ulu, and Derya Antaş who were always nearby, willing to listen and give their endless support. I would like to thank Nihat Gökay Akgün and Ayşe Cansu Akgün for their understanding, friendship, and invaluable encouragement. I must express my very profound gratitude to Ayla Açelya Aslan and Cengiz Alp Aslan for providing me with unfailing support, continuous encouragement, and sharing the warm love in their home.

Lastly, words cannot express my gratitude to Yusuf Akkuş. I could not have undertaken this journey without his support throughout my entire life and without his love.

TABLE OF CONTENTS

ABSTRACT v

ÖZ vi

ACKNOWLEDGMENTS viii

TABLE OF CONTENTS ix

LIST OF TABLES xii

LIST OF FIGURES xiv

CHAPTERS

1 INTRODUCTION 1

2 LITERATURE REVIEW 5

2.1 Ferroelectric Materials 5

2.2 Properties of Examined Ferroelectric Materials 7

2.2.1 Lanthanum Borogermanate (Nd^{3+} doped $LaBGeO_5$, LBG) crystals 7

2.2.2 Pyridinium Fluorosulfonate $(C_5NH_6)FSO_3$ 9

2.2.3 Imidazolium Perchlorate $(ImClO_4)$ 12

2.2.4 Zirconium dioxide (Zirconia, ZrO_2) 14

3 THEORY 17

3.1 Phase Transition 17

3.2 The Compressible Ising Model 20

3.3 Landau Phenomenological Theory 22

3.4 Damping Constant 26

3.5 Grüneisen parameter 28

4 PHENOMENOLOGICAL APPROACHES ON THE Nd^{3+} DOPED FERROELECTRIC $LaBGeO_5$ 31

4.1 Analysis of the Specific Heat 31

4.2 Calculation of the Enthalpy, Entropy and the Free Energy for $LaBGeO_5$ 38

4.3 Analysis of the Birefringence and the Dielectric Constant 42

4.4 Results and Discussion of $LaBGeO_5$ 44

4.5 Conclusion of $La_{1-x}Nd_xBGeO_5$ 47

5 CALCULATION OF THE SPIN- LATTICE RELAXATION TIME AND THE ACTIVATION ENERGY NEAR THE IV-III PHASE TRANSITION IN PYRIDINIUM FLUOROSULFONATE $(C_5NH_6)FSO_3$ 49

5.1 Analysis of the Damping Constant 49

5.2 Results and Discussion of Pyridinium Fluorosulfonate $(C_5NH_6)FSO_3$ 58

6 ANALYSIS OF THE SPECIFIC HEAT AND CALCULATION OF THE RELAXATION TIME, ACTIVATION ENERGY, ENTROPY, AND ENTHALPY CLOSE TO THE LOWER PHASE TRANSITION IN IMIDAZOLIUM PERCHLORATE 61

6.1 Calculation of the Relaxation Time and Activation Energy 61

6.1.1 Calculations and Results 61

6.1.2 Discussion 67

6.2 Analysis of the Specific Heat 68

6.2.1 Calculation of the Entropy, Enthalpy, and Free Energy 68

6.2.2 Calculation of the Critical Exponents 73

6.2.3 Results and Discussions about Calculations of Im-ClO_4 77

6.2.4 Conclusion of Im-ClO_4 78

7 RAMAN WAVENUMBERS CALCULATED AS A FUNCTION OF PRESSURE FROM THE GRÜNEİSEN PARAMETER OF ZIRCONIA.....81

7.1 Calculations and Results 81

7.2 Discussion 86

8 SUMMARY.....89

REFERENCES 93

CURRICULUM VITAE.....105

LIST OF TABLES

TABLES

Table 4.1 Values of the critical exponent α and the fitting parameter JA according to Eq. (3.11) in both ferroelectric ($T<T_C$) and paraelectric ($T>T_C$) phases of $La_{1-x}Nd_xBGeO_5$ with x= 0 (T_C= 802.4 K) for the temperature intervals indicated. 33

Table 4.2 Values of the critical exponent α and the fitting parameter JA according to Eq. (3.11) in both ferroelectric ($T<T_C$) and paraelectric ($T>T_C$) phases of $La_{1-x}Nd_xBGeO_5$ with x= 0.03 (T_C= 816.6 K) for the temperature intervals indicated. 34

Table 4.3 Values of the critical exponent α and the fitting parameter JA according to Eq. (3.11) in both ferroelectric ($T<T_C$) and paraelectric ($T>T_C$) phases of $La_{1-x}Nd_xBGeO_5$ with x= 0.05 (T_C= 823.3 K) for the temperature intervals indicated. 35

Table 4.4 Values of the Landau coefficients a , a_4 (Eq. 4.6) and also the coefficients c_0 , c_1 (Eq. 4.7) for the ferroelectric ($T<T_C$) phase of $La_{1-x}Nd_xBGeO_5$ with x= 0; 0.03 and 0.05. 43

Table 5.1 Values of the $M_{2,max}$, the parameters a and b according to Eq. (5.4) and values of the α and a_4 according to the Eq. (5.6) below the solid-solid phase transition (IV-III) temperature of $T_C = 235\ K$. 52

Table 5.2 Values of the background damping constant Γ_0 (Γ_0') and the amplitude A (A') due to the PS (Eq. 5.1) and EF (Eq. 5.2) models both below and above $T_C = 235\ K$ using the experimental [48] spin-lattice relaxation time of the proton in P_yFSO_3. 54

Table 5.3 Values of the activation energy U for the cation reorientation and the constant $ln\ C$ according to Eq. (5.5) for the temperature interval indicated in P_yFSO_3. 55

Table 5.4 Values of the activation energy U and the constant lnC according to Eq. (5.5) for the reorientation of the dipole moment in P_yFSO_3. 57
Table 6.1 Values of the coefficients a_0 and a_1 according to Eq. (6.1) below the transition temperature (T_C= 247 K) of Im-ClO_4..... 62
Table 6.2 Values of the coefficients b_0, b_1 and b_2 according to Eq. (6.1) below and above the transition temperature (T_C= 247 K) of Im-ClO_4 63
Table 6.3 Values of the activation energy U and the constant C according to Eq. (6.3) for the cation reorientation in Im-ClO_4. 66
Table 6.4 Values of the critical exponent α and the fitting parameter JA according to Eq. (3.11) in the vicinity of these transition temperatures 245.8 K and 247.1 K in Im-ClO_4. 70
Table 6.5 The critical exponents deduced from the specific heat, polarization, and susceptibility in the vicinity of the second-order phase transition temperature T_C = 373 K. 76
Table 7.1 The values of the fitting parameter of Eq. (7.1) for the Raman modes in ZrO_2. 82
Table 7.2 The values of the fitting parameter of Eq. (7.2) for the cell volume in ZrO_2. 82
Table 7.3 Values of the damping constant Γ_0 (Γ_0') and the amplitude A (A') due to the PS (Eq. 5.1) and EF (Eq. 5.2) models both Raman frequency bands at 150 and 260 cm^{-1} in ZrO_2. 85

LIST OF FIGURES

FIGURES

Figure 2.1. A hysteresis loop illustrating the spontaneous polarization (P_S) and remnant polarization (P_R) [2]. 6

Figure 3.1. The order parameter dependence on temperature (a) first order phase transition (b) second order phase transition [70] 19

Figure 4.1. Specific heat [26], C_P, as a function of the reduced temperature ε in a ln-ln scale according to Eq. (3.11) for the temperature intervals of $801.1<T(K)<803.3$ (paraelectric phase) in $La_{1-x}Nd_xBGeO_5$ with x=0 (T_C=802.4 K). 32

Figure 4.2. Values of the critical exponent α as a function of temperature ΔT (Tables 1-3), calculated from the specific heat data [26] in both ferroelectric ($T<T_C$) and paraelectric ($T>T_C$) phases of $La_{1-x}Nd_xBGeO_5$ with x=0; 0.03 and 0.05 according to Eq. (3.11). 36

Figure 4.3. Values of the fitting parameter JA as a function of temperature ΔT (Tables 1-3) which was calculated from the specific heat data [28] in both ferroelectric ($T<T_C$) and paraelectric ($T>T_C$) phases of $La_{1-x}Nd_xBGeO_5$ with x=0; 0.03 and 0.05 according to Eq. (3.11). 37

Figure 4.4. The enthalpy difference ΔH as a function of temperature according to Eq (4.2) in both ferroelectric ($T<T_C$) and paraelectric ($T>T_C$) phases of $La_{1-x}Nd_xBGeO_5$ with x=0; 0.03 and 0.05. 39

Figure 4.5. The entropy difference ΔS as a function of temperature according to Eq (4.4) in both ferroelectric ($T<T_C$) and paraelectric ($T>T_C$) phases of $La_{1-x}Nd_xBGeO_5$ with x=0; 0.03 and 0.05. 40

Figure 4.6. The Gibbs free energy ΔG as a function of temperature according to Eq (4.5) in both ferroelectric ($T<T_C$) and paraelectric ($T>T_C$) phases of $La_{1-x}Nd_xBGeO_5$ with x=0; 0.03 and 0.05. 41

Figure 4.7. The normalized birefringence $\Delta n/\Delta n_{max}$ as a function of T-T_C according to Eq (4.1) in the ferroelectric phase ($T>T_C$) of $La_{1-x}Nd_xBGeO_5$ with x=0 and 0.05. 43
Figure 4.8. The inverse dielectric susceptibility χ^{-1} calculated from the observed [26] dielectric constant data using $\chi^{-1} = |\varepsilon - 1|^{-1}$ as a function of $La_{1-x}Nd_xBGeO_5$ with x=0; 0.03 and 0.05. 44
Figure 5.1. $M_2/M_{2,max}$ versus η graph (Eq. 5.4) below the IV-III solid-solid phase transition temperature of $T_C = 235\ K$ in P_yFSO_3..... 51
Figure 5.2. The experimental damping constant $(1/T_1)$ against our calculated Γ_{SP} from both PS and EF models below and above the IV-III solid-solid phase transition temperature of $T_C = 235\ K$ in P_yFSO_3..... 52
Figure 5.3. The temperature dependence of the spin-lattice relaxation time T_1 calculated from the PS (Eq. 5.1) and EF (Eq. 5.2) models both below and above the IV-III solid-solid phase transition temperature of $T_C = 235\ K$ in P_yFSO_3. The experimental [48] data were also given for comparison. 53
Figure 5.4. The damping constant Γ_{SP} calculated from Eqs. (5.1) and (5.2) as a function of the reciprocal temperature to extract the activation energy for the cation reorientation in P_yFSO_3..... 55
Figure 5.5. Temperature dependence of the inverse dielectric susceptibility χ^{-1} below the IV-III solid-solid phase transition temperature $T_C = 235\ K$ in P_yFSO_3. 56
Figure 5.6. The temperature dependence of the spontaneous polarization P below the IV-III solid-solid phase transition temperature of $T_C = 235\ K$ in P_yFSO_3. 57
Figure 6.1. The order parameters (observed ($M_2/M_{2,max}$) [61] and calculated η (Eq. 5.3)) versus temperature graph below the phase transition temperature of T_C = 247 K in $ImClO_4$. 62

Figure 6.2. The experimental [61] versus calculated (Eqs. 5.1 and 5.2) spin lattice relaxation time at various temperatures. The solid curves represent the best fit to the experimental data. 64
Figure 6.3. The temperature dependence of the inverse spin lattice relaxation time τ that was calculated from the PS and EF models both below and above the solid-solid phase transition temperature of $T_C = 247\ K$ in $ImClO_4$. 65
Figure 6.4. The damping constant Γ_{SP} calculated from Eqs. 5.1 (PS) and Eqs. 5.2 (EF) as a function of the reciprocal temperature to extract the activation energy for the cation reorientation in $ImClO_4$. 66
Figure 6.5. Temperature dependence of the specific heat observed during the heating at the lower-temperature phase transition [63] 68
Figure 6.6. Specific heat (C_P) [63] as a function of the reduced temperature ε in an ln-ln scale according to Eq. (3.11) in the vicinity of these transition temperatures 245.8 K and 247.1 K in Im-ClO_4 69
Figure 6.7. The enthalpy difference ΔH as a function of temperature according to Eq. (6.4) around both transition temperatures 245.8 K and 247.1 K in Im-ClO_4. 71
Figure 6.8. The entropy difference ΔS as a function of temperature according to Eq. (6.5) around both transition temperatures 245.8 K and 247.1 K in Im-ClO_4. 72
Figure 6.9. The Gibbs free energy difference ΔG as a function of temperature according to Eq. (6.6) around both transition temperatures 245.8 K and 247.1 K in Im-ClO_4. 72
Figure 6.10. Specific heat (C_P) [63] as a function of reduced temperature ε in an ln-ln scale according to Eq. (3.11) in the vicinity of second-order phase transition temperatures 373 K in Im-ClO_4. 74
Figure 6.11. Critical exponent α as a function of temperature interval ΔT that approaches the second-order phase transition temperatures (373 K) in Im-ClO_4. 74

Figure 6.12. Polarization P as a function of reduced temperature ε in an ln-ln scale in the vicinity of the second-order phase transition temperatures 373 K in Im-ClO_4. 75
Figure 6.13. The susceptibility χ as a function of reduced temperature ε in an ln-ln scale in the vicinity of the second-order phase transition temperatures (373 K) in Im-ClO_4. 76
Figure 7.1. Isothermal Grüneisen parameter γ_T(P) calculated (Eq 3.44) as a function of pressure for the Raman frequencies of ZrO_2. 83
Figure 7.2. The damping constant Γ_{SP} calculated from Eqs. (5.1) and (5.2) as a function of pressure for the Raman frequency band at 150 cm^{-1} in ZrO_2. 84
Figure 7.3. The damping constant Γ_{SP} calculated from Eqs. (5.1) and (5.2) as a function of pressure for the Raman frequency band at 260 cm^{-1} in ZrO_2. 85

CHAPTER 1

INTRODUCTION

Ferroelectric materials demonstrate electric dipole moments even in the absence of an external electric field, which has spontaneous electric polarization [1,2]. These materials offer a wide range of useful properties, such as hysteresis loop, high permittivity, high piezoelectric effects, high pyroelectric coefficients, strong electro-optic effects, and anomalous temperature coefficients of resistivity [3]. Also, they can occur in a wide variety of forms, including single crystals, ceramics, polymers, and thin films [3]. Ferroelectric materials can be used in a wide variety of fields due to their non-linear nature such as electronics, medicine, material science, marine, memory devices, and many applications in daily life. However, there are still lot of research ongoing on various promising ferroelectric materials.

As a typical behavior of ferroelectric materials, ferroelectricity usually disappears above a special temperature known as transition temperature (Curie temperature, T_C) and material becomes paraelectric. This phenomenon has been defined as a phase transition. The present study aims to investigate the phase transition mechanism in terms of various dynamical properties such as order parameter, damping constant, activation energy, etc. in the vicinity of transition temperatures for ferroelectric materials; Lanthanum Borogermanate (LBG) crystals, Pyridinium Fluorosulfonate, Imidazolium Perchlorate, and Zirconia.

In the scope of present study, firstly, two phenomenological models, namely the compressible Ising model and the Landau model, have been used to analyze the specific heat and the dielectric constant data, respectively, for the pure and Nd^{3+} doped $LaBGeO_5$ (LBG) crystals. The critical exponent of the specific heat was extracted in both ferroelectric and paraelectric phases of the crystals studied here

within the temperature intervals of $|T - T_C| < 4\ K$. The extracted values of critical exponent were then utilized to make predictions about a variety of thermodynamic parameters, including enthalpy, entropy, and the Gibbs free energy. The measured values of birefringence were related to the order parameter below the transition temperature T_C in terms of the analysis of dielectric constant data within the Landau theory framework.

Secondly, the spin-lattice relaxation time T_1^H for protons nuclei is calculated in terms of the pseudospin-phonon (PS) coupled and the energy fluctuation (EF) models close to the IV-III solid-solid phase transition of $T_C = 235\ K$ in Pyridinium Fluorosulfonate ($(C_5NH_6)FSO_3$). Calculation was performed by associating the observed second moment of the ^1H as the order parameter below T_C and as the disorder parameter above T_C. Values of the activation energies for the cation reorientation in the $(C_5NH_6)FSO_3$ crystal are also deduced by using both PS and EF models. Additionally, the observed dielectric permittivity of this crystal is analyzed within the framework of the Landau theory, and values of the spontaneous polarization (SP) are determined as a function of temperature. The normalized values of SP are used in PS and EF models to extract the activation energy for the reorientation of the dipole moment of this compound arising from cation-anion interaction. The results show that the PS and EF models can describe the observed behavior of the spin-lattice relaxation time adequately for the IV-III solid-solid transition in $(C_5NH_6)FSO_3$.

Thirdly, the temperature dependence of the relaxation time of imidazolium perchlorate (Im-ClO_4) was calculated from the pseudospin-phonon coupled (PS) and the energy fluctuation (EF) models close to the first order phase transition temperature of 247 K. Calculation was performed in terms of the proton second moment that was associated with the order parameter as predicted from the mean field theory. The results were in good agreement with the observed data. In addition, values of the activation energy were deduced in terms of the Arrhenius plot using the calculated values of the relaxation time from both PS and EF models.

The anomalous behavior of the specific heat of Im-ClO_4 was analyzed in terms of a power-low formula (including the critical exponent α and the interaction parameter JA) deduced from the Ising model in the vicinity of the lower phase transition temperature of T_C = 247 K. Moreover, some thermodynamic functions such as entropy and enthalpy were predicted as a function of temperature using the values of α and JA extracted from the observed specific heat data of Im-ClO_4.

In addition, the critical exponents of the Im-ClO_4 were examined, which correlated the reduced temperature to the specific heat C_P, polarization and susceptibility in the vicinity of second-order transition temperature T_C = 373 K, so that the critical exponents were extracted for each relation. Their values have been examined if they are compatible with any of the universality classes as given in the literature. Finally, as the well-known scaling relation, Rushbrooke inequality (RI) has been investigated whether it is compatible with the values of the critical exponent, which were obtained.

Finally, the isothermal Grüneisen parameters γ_T of various Raman modes in Zirconia (ZrO_2) were calculated as a function of pressure at room temperature. For this calculation of γ_T, the pressure dependence of both Raman frequencies for the bands at 150, 260, 320, 480, 602, and 650 cm^{-1}, with the cell volume of the ZrO_2, were obtained from the literature. The two lowest modes (150 and 260 cm^{-1}) exhibit an unusual over-damped soft mode behavior upon increasing pressure, as stated earlier. Therefore, the pressure dependencies of the frequencies of those two lowest modes were associated with the order parameter S to predict the half width at half maximum (HWHM or damping constant) from the pseudo-spin phonon coupled (PS) and the energy fluctuation (EF) models for the pressure gaps from 0 GPa to 5 GPa.

CHAPTER 2

LITERATURE REVIEW

Ferroelectricity was not observed in any other material for many years after it was discovered with Rochelle salts [4] until it was observed in KH_2PO_4 (KDP) in the 1930s and barium titanate (BTO) in the 40s [5]. It can be claimed that molecular ferroelectrics could be alternatives to perovskites, if some of their features, like spontaneous polarization, can be measured closer to perovskites [6-7]. After many studies in the field, it has been revealed that molecular ferroelectrics can meet the need and have more environmentally friendly [8] solutions than perovskites. With the inclusion of these new materials in ferroelectrics, many new features have been added; such as being soft and flexible [9-10], having lightweight [7], being lead-free [8], being able to work at low temperatures [7,10], and being biocompatible [11].

2.1 Ferroelectric Materials

The electric dipole moment per unit volume of a substance is used to define polarization (P) and is related to dielectric displacement (D) linearly [1,2]. In ferroelectric materials both P and D, are non-linear functions of electric field (E). A ferroelectric crystal typically consists of fields referred to as domains of homogenous polarization, where each one has the same direction of polarization. The magnitude of the polarization within a single ferroelectric domain is defined as spontaneous polarization (P_S). However, the polarization could be in different directions for the adjacent domains, therefore at first, when there is no electric field (E=0) applied, the net polarization of the sample is equal to zero. Since the relation is non-linear, the

polarization displays the closed curve known as the hysteresis loop by a change of the electric field.

Hysteresis shows how a material's current state depend on its history. To investigate the properties of ferroelectric materials, the electric field polarization (P-E) cycle is measured. As demonstrated in the Figure 2.1, the polarization does not change linearly with the electric field for ferroelectric materials.

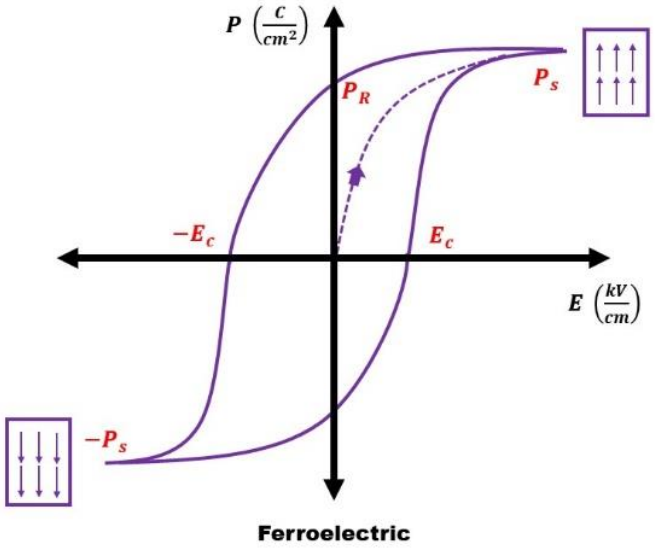

Figure 2.1. A hysteresis loop illustrating the spontaneous polarization (P_S) and remnant polarization (P_R) [2].

When an electric field is applied to the crystal, the domains containing polarization components along the applied field direction expand, that causes an increase in the polarization. In time, the polarization saturates and the crystal becomes a single domain when all the domains are oriented in the direction of the applied field. There will be some distortion in the polarization direction of the crystal. As seen in the Figure 2.1, the up and down states correspond to the points where the ferroelectric is fully saturated, either positive or negative, respectively. These points also refer to spontaneous polarization. As expected, the polarization decreases when the applied electric field decreases, but it follows a different path and does not reach zero when the electric field vanishes. Remanent polarization (P_R) is the value of polarization

where the electric field disappears as shown in the figure. Additionally, as the reverse electric field increases, the polarization in the opposite direction becomes saturated. The hysteresis curve will be obtained (Figure 2.1) by once more inverting the electric field.

2.2 Properties of Examined Ferroelectric Materials

2.2.1 Lanthanum Borogermanate (Nd^{3+} doped $LaBGeO_5$, LBG) crystals

At about a Curie temperature of Tc 804K, the ferroelectric material lanthanum borogermanate, $LaBGeO_5$ or simply LBG, passes through a phase transition. According to a Rulmont and Tarte [13], LBG has a crystalline structure similar to that of stillwellite ($CeBSiO_5$)., At about room temperature, in ferroelectric phase, LBG is in the trigonal polar space group $P3_1$ containing three formula units per cell (24 atoms) and the unit cell parameters are a= 6.9995 Å, c= 6.8596 Å [14]. In the ferroelectric phase the crystal structure of LBG has been reported [15] as the boron (B), germanium (Ge) and lanthanum (La) ions are surrounded by oxygen (O) forming BO_4, GeO_4 tetrahedra and LaO_9 polyhedra. In order to create helical chains along the c-axis, the BO_4 tetrahedra are connected by their corners. By sharing the oxygen atoms at the corners, the GeO_4 tetrahedra connect two subsequent BO_4 tetrahedra in the chain. The chain of BO_4 and GeO_4 tetrahedra is connected by the large LaO_9 polyhedra. Below T_C, LBG crystals exhibit the following advantageous characteristics; spontaneous polarization Ps = 9μC/cm^3 at 300K [16], high Curie-Weiss constant (order of 10^4 K) [17], high pyroelectric coefficient $\gamma = dP_S/dT \approx$ 10nC/cm^2 at 300K, relatively low permittivity ($\varepsilon_{\parallel c} = \varepsilon_{\perp c}$ = 13.4 at 1 MHz) [18], high electrical resistivity ($\rho_\gamma > 10^7 \Omega$.cm) and low dielectric loss ($\tan\delta \approx 0.001$) [18]. This model states that the LBG in non-polar space group $P3_121$ has three formula units per cell (z = 3), and the unit cell parameters are a = 6.9926 Å and c = 6.9315 Å above T_C (paraelectric phase) [18]. The BO_4 tetrahedra disorder above T_C that was revealed by this model [18] can be explained by the dynamical displacement of the La and Ge

atoms to place them on the twofold axis. These displacements of La and Ge concern the B and O_5 atoms close to the c-axis which occupy with equal probability two sites with distance of approximately 0.6 Å and 0.15 Å, respectively.

There have been a lot of conflicting reports regarding the structural phase transition mechanism of LBG. An order-disorder process is indicated by the Rhodes-Wohforth plot referred by Tokunaga [19] and the minimal entropy change $\Delta S = 0.114\ R = R \ln (1.121)$ [16] for the LBG resembling displacive type transition. Similarly, Onodera et al. [16] and Stefanovich et al. [17] reported the Landau coefficients that indicated order-disorder mechanism. Moreover, it has been stated by Hrubá et al. [20] that small excess entropy is consistent with the disorder of the atom which is one of the eight atoms in the formula unit, supporting the order-disorder aspect of transition. According to Kaminskii et al. [12] and Rulmont and Tarte [13], the unpolarized infrared (IR) and Raman spectra of LBG have been described. Pisarev and Serhane [21] noted a partial softening of the low frequency created by the A symmetry close to the T_C. The polarized Raman spectra of LBG glasses were published by Califano et. al. [22]. Milov and Strukov experimentally determined the piezoelectric moduli of the LBG crystal [23]. To describe the structural, electrical, and vibrational characteristics of LBG crystals, density functional theory (DFT) computations were carried out [15,24].

Despite B_2O_3 evaporation, a high melt viscosity, and a significant tendency for undercooling, it is very challenging to create LBG crystals [25]. They offer a great deal of promise for application in the creation of nonlinear optical devices such tunable waveguides and fiber gratings. Nd^{3+} or Pr^{3+} doped LBG in particular shows promise as a self-frequency-doubling (second harmonic generation, SHG) crystal that can meet the needs of the development of short-wavelength lasers. It has reported in the literature on how the rare-earth metals (Gd, Eu, Tm, and Nd) doping affect the ferroelectric characteristics of LBG [25,26]. On the basis of the compressible Ising model, the anomalous behavior of the specific heat, which is a spin for the potential phase transition, has been examined. According to Rice [27], the specific heat at constant volume (C_V) for a first order transition reaches infinity

at the transition temperature. On the other hand, Larkin and Pikin [28] claimed that for weakly first order or almost second order transitions, the specific heat at constant pressure (C_P) goes to infinity at the transition temperature. As the transition temperature is approached from below, Baker and Essam [29] shown that C_P does not change from being finite. For such crystals displaying weakly first order or almost second order transitions, Yurtseven [30] developed a compressible Ising model superimposed on an Einstein and/or Debye model in light of these research. In order to explore the unusual behavior of the specific heat at the phase transition temperatures for several ferroelectric materials, such as ammonium halides [31,32], $LiKSO_4$ [33], TMA-$ZnBr_4$ [34], and $PyBF_4$ [35], Yurtseven and/or coworkers have employed his model.

In terms of the compressible Ising model with the critical exponent, the critical behavior of the specific heat for $(La_{1-x}Nd_x)BGeO_5$ crystals [26], where x= 0; 0.03; 0.05, was examined in the region of the phase transition temperatures of T_C = 802.39 K (x = 0), T_C = 816.63 K (x = 0.03), T_C = 823.27 K (x = 0.05). The critical exponent, which was taken from the measured [26] specific heat data, was used to determine the temperature dependence of the enthalpy (H), the entropy (S), and the Gibbs free energy (G) of these three compositions. Additionally, the Landau phenomenological theory was used to examine the inverse dielectric susceptibility (χ^{-1}) obtained from the observed [26] dielectric constant data, and the Landau coefficients were calculated. The measured [26] birefringence (normalized) of these compositions was used as the order parameter (squared) in this investigation.

2.2.2 Pyridinium Fluorosulfonate $(C_5NH_6)FSO_3$

The pyridinium (C_5NH_6 cation, or shortly P_y) salts can be formed as a result of the reaction of the pyridine (C_5NH_5), a strong organic base, with various acids. These salts are widely applied as disinfectants in the medical field (foams, eye drops, and solutions). Moreover, pyridinium compounds have been used as dyes (acylating agents), phase transfer catalysts, and intrinsic fluorescence [36]. They are synthetic

building blocks for obtaining piperdine, dihydropyridire and substituted pyridine [37]. A simple principle of classification for pyridinium salts has been proposed [38] by considering the number of solid-solid phase transitions: salts of type N undergo N transformations. A few monomorphic compounds (Type 0) of these salts including tetrahaloarutes [39] and nitrate [40] anions have been reported. Some examples of the Type 1 salts with the inclusion of chloride, bromide, iodide [41], hexafluorophosphate [42] and antimonite [43] anions have been reported to undergo one solid-solid phase transition. Besides, the tetrafluoroborate [44], percholarete [45] and perhenate [46] salts have exhibited two successfully phase transitions (Type 2). The dynamic orientational disorder of the Py cations in the high temperature phases of the Type 2 salts has been described by a model of stochastic jumps among the equivalent potential barriers [47]. The orientational order below the lower phase transition is lost on heating as a result of the Py cation's infrequent reorientation between likely non-equivalent potential barriers in the low-temperature phases of Type 2 salts. It is also noteworthy that for Type 2 salts, the alignment of the permanent dipole moments of the P_y cations in an applied electric field gives rise to the existence of a reversible spontaneous polarization in the intermediate phases (mesophases), as stated before [46]. As a member of Type 3 of these salts, pyridinium fluorosulfonate $(C_5NH_6)FSO_3$ or shortly P_yFSO_3 undergoes three solid-solid phase transitions at $235\ K$ (IV-III transitions), $272\ K$ (III-II transition), and $282\ K$ (II-I transition) as the temperature was lowered from the room temperature [48]. At room temperature (paraelectric phase), P_yFSO_3 belongs to the trigonal crystal system with the space group $R\bar{3}m$ and its lattice parameter in this structure was reported as $a = 5.762$ Å, $\alpha = 97.86^0$ and $Z = 1$ [48]. Both Py cation and FSO_3 anion reveal $\bar{3}m$ symmetry and they are dynamically strongly disordered. Also, it is reported that the P_y cation reorients around its pseudohexad axis perpendicular to the ring plane. The center of the gravity of P_y cation occupies site a (0,0,0) while the S atom occupies site b (½, ½, ½), as reported previously [48]. On the other hand, since the position of the nitrogen (N) atom could not be determined, all the pyridine ring atoms are refined as carbon atoms so that each site f(x, x, 0) contains 5/6 C and 1/6

N. For the same reason, fluorine (F) atom was refined together with the three oxygen atoms as the $(SO_4)^-$ anion so that one can obtain six positions for both F and O atoms, each containing 1/6 F and ½ O with relatively large temperature factors [48].

The ferroelectric properties of P_yFSO_3 have been studied experimentally by Polish scientists [48]. In their study, they reported the temperature dependence of the specific heat and the entropy by using Differential Scanning Calorimetry (DSC). Also, they measured the temperature dependence of the seconds moments and spin lattice relaxation time T_1 of ^1H and ^{19}F by using the nuclear magnetic resonance (NMR) spectrometer. In addition, they performed the measurements of the complex dielectric permittivity and obtained the dielectric hysteresis loop of P_yFSO_3 [48].

The spin lattice relaxation time (SLRT) for proton nuclei (T_1^H) was calculated as a function of temperature close to the IV-III transition ($T_C = 235\ K$) using the pseudospin-phonon coupled (PS) model [49] and the energy fluctuation (EF) model [50]. For this calculation, we used the temperature dependence of the observed proton second moment [48] as an order parameter. By fitting the SLRT calculated from both models (PS and EF) to the observed data [48], the parameters were determined and the observed behavior of SLRT was explained close to the IV-III solid-solid transition in P_yFSO_3. In addition, values of the activation energy for the cation reorientation in P_yFSO_3 were deduced by using the damping constant which was calculated from both models (PS and EF) in the temperature range studied.

Finally, the observed [48] dielectric permittivity of P_yFSO_3 was analyzed by means of the Landau theory in the vicinity of the IV-III solid-solid transition and the Landau coefficients a_2 and a_4 were determined. These coefficients were then used to predict the spontaneous polarization and to calculate the activation energy for the reorientation of the dipole moment within the framework of both PS and EF models.

2.2.3 Imidazolium Perchlorate ($ImClO_4$)

Imidazolium salts (IMSs) are derived from imidazole rings, which are found all over nature and have the capacity to form hydrogen bonds with both drugs and proteins as well as metals as ligands [51]. IMSs can interact electrostatically with biological systems in a way that their parent imidazoles cannot because they lost the ability to link both metals and hydrogen [52]. Imidazolium salts are referred to room temperature ionic liquids (RTILs), which include substantial organic cations and inorganic anions, and can be employed as electrolytes due to their broad chemical stability [53] and remarkable catalytic capabilities [54,55]. Moreover, they have been utilized to dissolve carbohydrates [56], cover metal nanoparticles with metal ions [57], and produce polyelectrolyte brushes on surfaces [58]. In contrast to ferroelectric oxides, organic-inorganic molecular ferroelectrics have gained prominence due to their favorable traits, including being environmentally friendly (particularly due to their lead-free structure), having both a low cost and mechanically flexible structure [6, 59]. In particular, as a member of organic-inorganic molecular ferroelectrics, imidazolium perchlorate ($C_3N_2H_5ClO_4$ or Im-ClO_4) can be used as an effective 3D printed metamaterial that produces rapid-prototype for reducing the manufacturing time of ferroelectrics from hours to minutes, as pointed out previously [7]. Moreover, it has been noted [60] that Im-ClO_4 thin films demonstrate superior electromechanical coupling over PZT films, making them a desirable lead-free option for a variety of uses in sensor technology and electro-optics.

Im-ClO_4 is reported to go through three successive solid-solid phase transitions at 487, 373, and 247 K [61]. According to Pająk et al. [61], the Im-ClO_4 crystal structure is trigonal, with a space group of R3m, Z=1 and a lattice parameter a = 5.484(1) Å with a value of α = 95.18(2)º. Moreover, as previously reported [61], cations are very disordered where perchlorate ions are ordered at room temperature. The crystal structure is also trigonal above room temperature, with a space group of $R\bar{3}m$, a = 5.554(1) Å and α = 95.30(2)º, but all of the ionic sublattices are disordered

[61].The dielectric and optical properties of Im-ClO_4 have been declared by Czapla *et al.* [62] by studying the x-ray diffraction, dielectric and birefringence measurements. The precise measurements of specific heat changes of this crystal have been performed by Przeslawski and Czapla [63] using an ac calorimeter. The polymorphic phase transitions, appearance of the ferroelectricity, molecular structure, and molecular dynamics of Im-ClO_4 have been investigated by Pajak *et. al.* [61] using differential scanning calorimetry (DSC), proton NMR relaxation and second moment, x- ray diffraction and dielectric spectroscopy measurements.

In the present study, the proton spin lattice relaxation time (SLRT), denoted as T_1 (s) has been calculated as a function of temperature in the vicinity of the solid-solid phase transition temperature T_C = 247 K, by using both the pseudospin-phonon (PS) coupled and the energy fluctuation (EF) models. This calculation has been performed by using the observed [61] proton second moment (M_2) as an order parameter below T_C and as a disorder parameter above T_C according to both models. Moreover, the fitting procedure was implemented for the calculated data of SLRT, by obtaining the fitting parameters at first, then the attitude of the observed values of SLRT was denoted around the transition temperature. Finally, the activation energy values are computed from the correlation of the damping constant with respect to the reciprocal of temperature.

As an example of molecular ferroelectrics, Croconic acid was found to have a high spontaneous polarization of roughly 23 $\mu C\ cm^{-2}$ [60], which is comparable to BTO. Also, diisopropylammonium bromide (DIPAB), as another example, has a high ferroelectric phase transition temperature of 426K, which is higher than that of BTO, and also has a strong piezoelectric response with well-defined ferroelectric domains [59,61]. Similarly, with strong spontaneous polarization, low coercivity, superior electromechanical coupling, and high Curie temperature imidazolium perchlorate ($ImClO_4$) can be accepted as promising molecular ferroelectric. As a trigonal crystal Im-ClO_4 has a high melting temperature and high ferroelectric transition temperature so that it can be processed at high temperatures [63, 64].

Im-ClO_4 is a molecular ionic crystal with pseudopentagonal cation symmetry that can be categorized by disordered molecular structure [62]. Thanks to the foregoing features mentioned also for molecular ferroelectrics, $ImClO_4$ can be used in sensing, actuation, data storage, electro-optics, and molecular flexible electronics [60]. Im-ClO_4 has been reported [61] to undergo three successive solid-solid phase transitions at 487, 373 and 247 K. Im-ClO_4 is polar below T_C= 373.6 K according to the structural analysis and second harmonic generation measurement [62].

In the previous study, we dealt with the structural anomalies at the temperatures close to the first-order phase transition temperature of 247 K. The temperature dependence of the relaxation time of Im-ClO_4 was computed using the pseudospin-phonon coupled (PS) and energy fluctuation (EF) models [66]. In the present study, the anomalous behavior of the specific heat of the same material Im-ClO_4 was analyzed in terms of a power-low formula deduced from the Ising model in the vicinity of the lower phase transition temperature of T_C = 247 K and the critical exponents which were deduced from the specific heat, polarization, and susceptibility, have been investigated around the second-order phase transition temperature T_C = 373 K. So, we aimed to have a detailed series of study about Im-ClO_4.

2.2.4 Zirconium dioxide (Zirconia, ZrO_2)

Zirconium dioxide (Zirconia, ZrO_2) has complex polymorphism, including high-pressure and high-temperature phases. The unique properties of these phases ensured the broad and diverse application of ZrO_2 and ZrO_2-based materials in various fields [67]. Many remarkable properties can be possessed; refractoriness, low volatility, high chemical resistance, extraordinary mechanical strength, wear resistance, low thermal conductivity, wide bandgap, oxygen conductivity, high refractive index, and biological inertness [68]. The significance of Zirconia in engineering ceramics is widely acknowledged; among the many useful uses are high-temperature equipment, thermal barriers, and oxygen sensors. The reason why prospective application of

particular current interest is its possible use to replace SiO_2 as the gate-dielectric material in metal-oxide-semiconductor (MOS) device [69].

Currently, ZrO_2 is a major component of modern ceramic material which is well acknowledged as possesses three polymorphic modifications under standard pressure: monoclinic, tetragonal, and cubic [68].

CHAPTER 3

THEORY

3.1 Phase Transition

Every condensed matter system has homogeneous forms called states which can be identified in terms of various properties, such as density, crystal symmetry, magnetization, electric polarization, etc. Since changes in these properties are important to learn about phases, therefore materials, the phase transition is one of the most studied topics. Phase transition can be defined as significant changes in symmetry and properties of a system; that arise from changes in external conditions such as temperature, pressure, chemical potential, etc. The transition occurs when the system becomes unstable. The stability of any system is characterized by the condition of the minimum thermodynamic potential at a finite temperature.

In other words, each system state in thermodynamics is determined by a certain amount of energy. This energy is referred to as free energy if the system's state is determined by its temperature T, pressure P, and volume V [70]. The stability condition can be written as

$$\Delta U + P\Delta V - T\Delta S \geq 0 \tag{3.1}$$

where U is internal energy, V is volume, and S is entropy.

This potential could be the Helmholtz free energy $F = E - TS$ if the independent variables are temperature and volume, whereas it is Gibbs free energy $G = E - TS + PV$ if the variables are temperature and pressure. It is clear from these expressions that with increasing temperature, the highest possible entropy will be reached, and the system will have a disordered state.

Classification of Phase Transition

Paul Ehrenfest who presented the classification of phase transitions in 1933, divided them into two groups; first order and second order transitions [71]. The main idea of the classification is continuity/discontinuity of the thermodynamic potentials which define the phase of matter.

Whether discontinuities take place in the first derivatives of Gibbs free energy G, as given in Eq. 3.2, in entropy and volume the transition is defined as a first order phase transition [70].

$$S = -\left(\frac{\partial G}{\partial T}\right)_P \qquad V = \left(\frac{\partial G}{\partial p}\right)_T \qquad H = -T\left(\frac{\partial (G)}{\partial (T)}\right) \tag{3.2}$$

If the transition is of a second order type, the first derivatives of the Gibbs free energy are continuous. Different from the first order type, the second derivatives of the Gibbs free energy, which are given in Eq. 3.3, are discontinuous. At the transition point, several thermodynamic quantities also approach infinity asymptotically or are reduced to zero.

$$\frac{C_P}{T} = -\left(\frac{\partial^2 G}{\partial T^2}\right)_P = \left(\frac{\partial S}{\partial T}\right)_P \qquad \kappa_T V = -\left(\frac{\partial^2 G}{\partial p^2}\right)_T = -\left(\frac{\partial V}{\partial p}\right)_T \tag{3.3}$$

C_P denotes the heat capacity at constant pressure and κ_T is the isothermal compressibility at a constant temperature.

As well as continuity in the first and second derivatives of thermodynamic potential defines the type of it, latent heat is also a method to distinguish. The presence or absence of latent heat during phase transformations accounts for the primary distinction between these two types of transitions since it reflects the change of enthalpy [70]. Whether there exists a latent heat during the transition, it can be defined as the first order, and an absence of the latent heat indicates a second order transition.

Another way of classifying the phase transitions is based on the dependence of the order parameter on temperature. The quantities that characterize the state of the system have certain ordering and they can be matched by order parameters [70]. The idea was suggested by Landau phenomenological theory which will be introduced in detail later. The theory put forward that if the order parameter changes discontinuously around the transition point (if there is a jump) with respect to the temperature as shown in Figure 3.1 (a), the transition is called a first order phase transition. On the other hand, it can be defined as a second order phase transition if the dependence is continuous as indicated in Figure 3.1 (b). The transition occurs over a definite temperature called critical temperature (Curie temperature) where one can talk about an order below it. As seen in the figure, there is an order below the critical temperature T_C, whereas the order parameter vanishes above this temperature. The order parameter is used by normalization, which takes a value between 0 and 1.

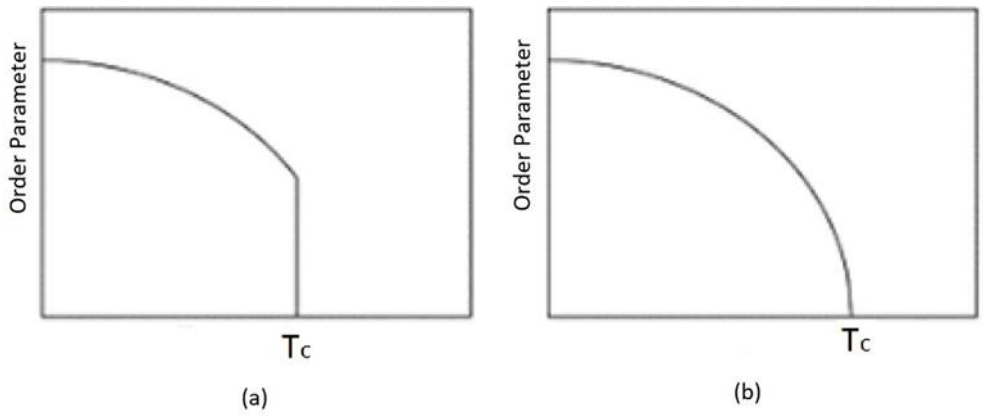

Figure 3.1. The order parameter dependence on temperature (a) first order phase transition (b) second order phase transition [70]

3.2 The Compressible Ising Model

The Ising model can be defined as a microscopic approach to phase transitions, based on the interaction between particles. Essentially, Ernst Ising developed the Ising model to simulate the behavior of phase transitions in ferromagnets [70]. The model explains how short-range interactions between molecules in a crystal result in long-range, correlative behavior, and predicts the possibility of a phase change. It is one of the simplest thermodynamic models, based on three assumptions:

(1) The particles of the system that are located on the sites of a crystal lattice.
(2) Each particle exists in one of two potential states (in magnetic case, spins), which are $S_i = \pm 1/2$.
(3) The energy of the system can be defined as $E = -J \sum_{i,j} S_i S_j$, where J is a constant interaction parameter and sum is over all pairs of nearest neighbors i and j [70].

The main problem is calculating the mechanical energy of the system with all the particles, especially for many particle systems. The Hamiltonian for an Ising system which considers the nearest neighbor spin interactions is described in the usual form

$$H_{I} = -J \sum_{i,j} \sigma_i \sigma_j \tag{3.4}$$

where J is the interaction parameter between the nearest neighbor molecules, and σ_i, σ_j represent the spin variables. The Ising free energy G_I of an Ising system is defined as

$$G_I = -kT \ln Z \tag{3.5}$$

where k is the Boltzman constant and Z is the partition function given as

$$Z = \sum_{i,j} e^{-\frac{H}{kT}} \tag{3.6}$$

The critical behavior of the Ising free energy G_I close the phase transition temperature can be expressed as a power-law formula as stated before [30] which reads as

$$G_I = A_0' + A'|\varepsilon|^{2-\alpha} \tag{3.7}$$

where α is the critical exponent, ε = |T-T_C|/T_C is the reduced temperature and $A_0' = JA_0$ and $A' = JA$ are the parameters in the dimensions of energy with constants A_0 and A. The specific heat C which is the second derivative of the free energy G with respect to the its argument J/kT is,

$$C = k(J/kT)^2[\partial^2 lnZ/\partial(J/kT)^2] \tag{3.8}$$

From Eq. (3.5) and (3.7), one gets

$$\ln Z = -(J/kT)\,(A_0 + A\,|\varepsilon|^{2-\alpha}) \tag{3.9}$$

The second derivative of the Eq (3.9) with respect to J/kT is

$$\partial^2 lnZ/\partial(J/kT)^2 = -\frac{VT^2}{JT_C}(2-\alpha)\left[(A-1)\,|\varepsilon|^{1-\alpha} + \frac{AT}{T_C}(1-\alpha)|\varepsilon|^{-\alpha}\right] \tag{3.10}$$

Inserting Eq (3.10) into the Eq (3.8), Yurtseven and Sherman [72] have reported an analytical expression for the specific heat C by neglecting the weakly divergent $|\varepsilon|^{1-\alpha}$ term, given by

$$C = -\frac{JAT}{T_C^2}\,(1-\alpha)\,(2-\alpha)\,|\varepsilon|^{-\alpha} \tag{3.11}$$

Enthalpy, Entropy, and the Gibbs Free Energy

The temperature dependence of the enthalpy H can be calculated as follows

$$H = \int C dT + H_0 \tag{3.12}$$

where H_0 is the enthalpy value at $T = T_C$. Inserting Eq. (3.11) into the Eq (3.12) one gets

$$\Delta H = -JA[(1-\alpha)|\varepsilon|^{2-a} + (2-\alpha)|\varepsilon|^{1-a}] \tag{3.13}$$

ΔH denotes the change in the enthalpy ($\Delta H = H - H_0$).

Likewise, the temperature dependence of the entropy S can also by calculated according to the following equation;

$$S = \int \frac{C}{T}\, dT + S_0 \tag{3.14}$$

where S_0 is the entropy value at $T = T_C$. Inserting Eq (3.11) into the Eq (3.14) one gets

$$\Delta S = -\frac{JA}{T_C}(2-\alpha)|\varepsilon|^{1-\alpha} \tag{3.15}$$

Similarly, ΔS denotes the entropy change ($\Delta S = S - S_0$)

The obtained vales of ΔH and ΔS are used to calculate the Gibbs free energy ΔG given as

$$\Delta G = \Delta H - T\Delta S \tag{3.16}$$

3.3 Landau Phenomenological Theory

The Landau phenomenological theory was initially proposed to explain the mechanism of second order phase transition in the region close to the transition temperature. The main idea of the theory is determining the free potentials of the system by investigating the changes in macroscopic properties such as spontaneous polarization, magnetization, elasticity, probability of occupancy of atoms, etc.

In Landau theory, free energy can be both Helmholtz F(V,T) and Gibbs G(P,T) free energies that are defined as continuous functions of order parameter η. As mentioned before, order parameter is a variable that is determined to characterize the ordering

of the homogeneous states (phases) in systems. Since free energy of the system in equilibrium is directly related to pressure and temperature, order parameter η must be a function of them. In the vicinity of transition temperature T_C, the order parameter η is small, so free energy can be expanded in Taylor series;

$$G(P,T,\eta) = a_0(P,T) + a_1\eta + a_2\eta^2 + a_3\eta^3 + a_4\eta^4 + \cdots \tag{3.17}$$

where sequence of coefficients $a_0, a_1, a_2, a_3,$ and a_4 are known as Landau coefficients which are functions of temperature and pressure.

There are two assumptions in the Landau phenomenological theory. The first one is that the order parameter can be defined by the conditions;

$$\frac{\partial G}{\partial \eta} = 0 \qquad and \qquad \frac{\partial^2 G}{\partial \eta^2} > 0 \tag{3.18}$$

which are the expressions for minimum free energy. Second assumption is about vanishing the order parameter at the phase transition, $\eta(T_C) = 0$. To achieve the first assumption for all η, it is clear that a_1 must be zero in the case of no external field. Otherwise, by the presence of linear term, order parameter cannot disappear for any temperature above T_C and free energy cannot display a minimum at $\eta = 0$.

According to the symmetry arguments that arise from magnetic systems, which is positive and negative magnetization of the system, must be equivalent so that the odd power terms of the magnetization in the free energy are omitted. Similarly, only the even power terms of order parameter are accepted here, and the free energy G can be expressed in terms of the order parameter η as

$$G(P,T,\eta) = a_0(P,T) + a_2\eta^2 + a_4\eta^4 \tag{3.19}$$

To simplify the expression, we treat the system at constant pressure as being equivalent to the critical one and omit the pressure from the arguments. In addition, when we consider the second requirement in Eq. 3.18, it follows that $a_2 > 0$ must be satisfied for $T > T_C$ while $a_2 < 0$ for $T < T_C$. So, the coefficients a_2 can be written around T_C as;

$$a_2 = a\,(T - T_C) \tag{3.20}$$

where the positive constant a. Then the free energy takes its simplest form;

$$G(T, \eta) = a_0 + a\,(T - T_C)\eta^2 + a_4\eta^4 \tag{3.21}$$

From the minimization condition $dG/d\eta = 0$, one gets

$$\eta(a\,(T - T_C) + 2a_4\eta^2) = 0 \tag{3.22}$$

which can be solved for the order parameter η as

$$\eta = 0 \quad and \quad \eta^2 = -\frac{a(T - T_C)}{2a_4} \tag{3.23}$$

$\eta = 0$ corresponds to the paraelectric phase for $T > T_C$. By taking $a_4 > 0$, a positive η solution of Eq (3.23) defines the ferroelectric phase. The η^4 term in the Eq. 3.21 is needed since the η^2 term vanishes at the transition temperature, however its temperature dependence can be ignored and accepted as a constant.

The equilibrium condition of the free energy can be obtained by putting Eq. 3.23 back into energy expression for T < T_C;

$$G_{min} = a_0 + \frac{a^2}{2a_4}(T_C - T)^2 \tag{3.24}$$

It can be easily seen that the first derivative of the free energy has continuous behavior where it would have a jump in second derivative that is the characteristic behavior of second order phase transition.

Since the temperature dependence expression of the free energy has been obtained, thermodynamic quantities such as entropy S, heat capacity C_P, and the inverse dielectric susceptibility χ^{-1} can be calculated by means of the Landau phenomenological theory for the second order phase transition.

The derivative of the free energy gives the entropy S of the transition as

$$S = -\frac{\partial G}{\partial T} = S_0(T) - a\eta^2 \tag{3.25}$$

It follows that

$$S = \begin{cases} S_0(T) & T > T_C \\ S_0(T) + \dfrac{a^2(T - T_C)}{2a_4} & T < T_C \end{cases} \tag{3.26}$$

where entropy demonstrates continuous behavior with respect to order parameter as a given condition for second order phase transition. The heat capacity is another thermodynamic quantity, which can be derived from the free energy by the relation;

$$C_P = T\left(\frac{\partial S}{\partial T}\right) = C_0(T) + \frac{a^2 T_C}{2a_4} \tag{3.27}$$

at constant pressure in the ferroelectric phase $T < T_C$. Since the order parameter vanishes in the paraelectric phase $T > T_C$, behavior of the heat capacity depends on the temperature in this phase and there exists a discontinuity at the transition temperature. The jump in the specific heat $C_P(T)$ defines a divergent λ shape curve so that this transition is known as a λ-transition.

The second derivative of Eq (3.21) with respect to the order parameter η defines the inverse dielectric susceptibility χ^{-1} which reads

$$\chi^{-1} = \frac{\partial^2 G}{\partial \eta^2} = 2\,a\,(T - T_C) + 12a_4\eta^2 \tag{3.28}$$

Inserting η^2 (Eq 3.23) into the Eq (3.28), one gets the following expression for χ^{-1} in the ferroelectric phase ($T < T_C$).

$$\chi^{-1} = -4a(T - T_C) \tag{3.29}$$

First Order Phase Transition in Landau Theory

There are two assumptions which we accept to investigate the Landau phenomenological theory up to here. One of them is omitting the cubic term of order parameter in energy expression (Eq 3.17). What if the cubic term is also considered? The Landau expression Eq. 3.21 turns to;

$$G(T,\eta) = a_0 + a\,(T - T_C)\eta^2 + a_3\eta^3 + a_4\eta^4 \tag{3.30}$$

By minimizing the free energy with respect to η, $dG/d\eta = 0$, one can obtain

$$\eta_1 = 0 \quad and \quad \eta_2 = -\frac{3a_3}{8a_4} \mp \sqrt{\left(\frac{3a_3}{8a_4}\right)^2 - \frac{a(T - T_C)}{2a_4}} \tag{3.31}$$

where these two solutions need to satisfy the energy equation for a specific temperature T_0;

$$G(\eta_1, T_0) = G(\eta_2, T_0) \tag{3.32}$$

There is a discontinuity in the order parameter from η_1 to η_2, which means that the first order phase transition occurs at T_0.

The second assumption is about the coefficient a_4 of the η^4 term which has been accepted as positive previously. In the case of negative a_4, the sixth order term needs to be added to the free energy expression for extracting the minimum of it. The expression can be written as;

$$G(T,\eta) = a_0 + a\,(T - T_C)\eta^2 - |a_4|\eta^4 + a_6\eta^6 \tag{3.33}$$

The roots of the equation for the order parameter can be extracted as;

$$\eta_1 = 0 \quad and \quad \eta_2 = \frac{1}{\sqrt{3a_6}}\left\{|a_4| + \sqrt{a_4^2 - 3a_6 a(T - T_C)}\right\}^{\frac{1}{2}} \tag{3.34}$$

The discussion of Eq. 3.27 can be repeated here. Since there is a jump between the values of order parameter for a specific temperature, this is also defined as a first order phase transition.

3.4 Damping Constant

The damping constant $\Gamma_{sp}(\vec{k}\nu, \omega_\nu)$ due to the pseudospin-phonon interaction is given by the imaginary part of the self-energy which reads as [73]

$$\Gamma_{sp}(\vec{k}\nu, \omega_\nu) \simeq A \int_{BZ} S(\vec{q}, \omega) \left[\frac{n(\omega_\nu)}{n(\omega)+1} + 1\right] d^3q + B \qquad (3.35)$$

In Eq. (3.35) the integral is taken over all the wavevector q in the Brillouin zone (BZ). A and B are constants, $\vec{k}$ is the wavevector of the ν^{th} phonon ω_ν is the peak frequency and S is the dynamic scattering function of the pseudospins that describes the anomalous behavior of the damping constant close to the transition temperature (T_C), which is given by [49]

$$S(q, \omega) = \langle n(\omega) + 1 \rangle \frac{\chi(q, 0)\omega\tau_q}{1 + (\omega\tau_q)^2} \qquad (3.36)$$

where, χ is the dielectric susceptibility, τ_q is the relaxation time of the order parameter with the wavevector q. Eq. (3.36) can be expressed as follows (Eq 3.37) by using the approximations $n(\omega) + 1 = (kT/\hbar\omega)$, $(\omega\tau_q)^2 \ll 1$ and $n(\omega_\nu)/[n(\omega)+1] \ll 1$ for $\omega \simeq 0$,

$$\Gamma_{sp} \approx \frac{AkT}{\hbar} \int_{BZ} \chi(q, 0)\tau_q \, d^3q + B \qquad (3.37)$$

In their study, Laulicht and Luknar [73] have reported the following expression using the random phase approximation which reads as

$$\chi(q, 0)\tau_q = \frac{C\,(1 - P^2)}{T} \frac{\tau_q^2}{\tau} \qquad (3.38)$$

Here C is the Curie constant, P is the fractional spontaneous polarization (order parameter), τ is the proton flipping time.

Lahajnar et. al. [74] have calculated the integration of Eq. (3.37) using Eq. (3.38) for the KDP crystal given by

$$\Gamma_{sp} \propto \frac{1}{T_1} \propto (1 - P^2) ln \left[\frac{T_C}{T - T_C(1 - P^2)}\right] \qquad (3.39)$$

where T_1 represents the proton spin lattice relaxation time. Eq (3.39) defines the temperature dependence of the damping constant (or relaxation time) for the pseudospin-phonon coupled (PS) model.

On the other hand, the damping constant (relaxation time) is related to the fluctuation of the frequencies at zero wavevector [50] given by

$$\Gamma_{sp}^2 \propto \frac{kT\chi(0)}{V} \tag{3.40}$$

where V is the volume of the crystal.

Schaack and Winterfelt [50] have reported the following expression for the damping constant by inserting Eq. (3.38) in Eq. (3.40) that reads as

$$\Gamma_{sp} \propto \frac{1}{T_1} \propto \left(\frac{T(1-P^2)}{T-T_C(1-P^2)}\right)^{\frac{1}{2}} \tag{3.41}$$

Eq. (3.41) defines the critical broadening of the damping constant due to the energy fluctuation (EF model).

3.5 Grüneisen parameter

The Grüneisen parameter is related to the volume dependence of mode frequency by regarding the quantum harmonic oscillator of Einstein's theory as a mode of crystal vibration;

$$\gamma = \frac{\alpha K_T}{\rho C_V} \tag{3.42}$$

where α denotes the volume expansion coefficient, ρ is the density, K_T is the isothermal bulk modulus and C_V denotes the specific heat.

The Grüneisen parameter value for each mode of the frequency ν_i in the crystal is;

$$\gamma_i = -\left(\frac{\partial ln\nu_i}{\partial lnV}\right)_T \tag{3.43}$$

where ν_i denotes the frequency of the ith mode and V is the volume of the unit cell.

By differentiating the previous function with respect to pressure (P), the isothermal Grüneisen parameter is derived as;

$$\gamma_T(P) = -\frac{V(P)}{\nu(P)} \frac{\left(\frac{\partial \nu}{\partial P}\right)_T}{\left(\frac{\partial V}{\partial P}\right)_T} = \frac{\left(\frac{1}{\nu}\right)\left(\frac{\partial \nu}{\partial P}\right)_T}{\kappa_T} \tag{3.44}$$

where κ_T is the isothermal compressibility.

CHAPTER 4

PHENOMENOLOGICAL APPROACHES ON THE Nd^{3+} DOPED FERROELECTRIC $LaBGeO_5$

Ferromagnetic Nd^{3+} doped Lanthanum Borogermanate ($LaBGeO_5$ or LBG) crystals were examined in three samples (pure and two more compositions) in terms of the compressible Ising model and the Landau model to analyze their specific heat and the dielectric constant, respectively. The formula that is used for the sample is $La_{1-x}Nd_xBGeO_5$ and the compositions are given as x= 0, 0.03, and 0.05. The calculations were performed separately at the three transition temperatures; 802.4K, 816.6K, and 823.3K. The measured values of birefringence were related to the order parameter below the transition temperature Tc by analyzing dielectric constant data within the framework of the Landau theory.

4.1 Analysis of the Specific Heat

The specific heat C_P data were used from the literature [26] for $La_{1-x}Nd_xBGeO_5$, by the specific heat versus temperature graph, which has three peaks at temperatures; 802.4K, 816.6K, and 823.3K for three compositions; x= 0, 0.03, and 0.05, respectively. These temperature values were taken as transition temperatures, depending on the behavior of specific heat of the samples. The specific heat data of $La_{1-x}Nd_xBGeO_5$ were analyzed according to Eq. 3.8 approximately 4K below and above the phase transition temperatures (T_C) for x= 0, 0.03, and 0.05. The $\ln(C_P/T)$ versus $\ln|\varepsilon|$ graphs were plotted as shown in Figure (4.1) to extract the critical exponent α and the fitting parameter JA Eq. (3.11). The slope of the graph gives α value and the intersection point can be related with the parameter JA.

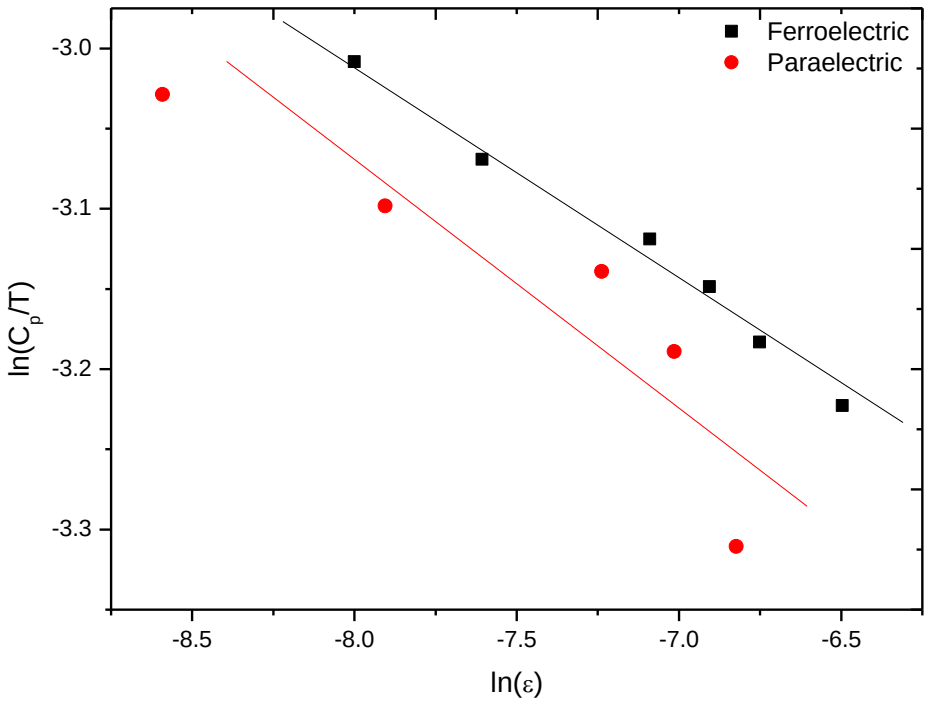

Figure 4.1. Specific heat [26], C_P, as a function of the reduced temperature ε in a ln-ln scale according to Eq. (3.11) for the temperature intervals of $801.1<T(K)<803.3$ (paraelectric phase) in $La_{1-x}Nd_xBGeO_5$ with x=0 (T_C=802.4 K).

The calculation procedure of α and JA of Eq. (3.11) were repeated for these three compositions of LBG crystals at all three transition temperatures. Each calculation has been done in both ferroelectric and paraelectric phases of the crystals within the temperature intervals $\Delta T = |T - T_C| < 4\ K$. In other words, while ΔT getting smaller, we approach the transition temperature.

The extracted values of the critical exponent α and the fitting parameter JA from the heat capacity (Eq. 3.8) were indicated in Tables (4.1)- (4.3) for various temperature intervals (ΔT) in the vicinity of critical temperature both in ferroelectric and paraelectric phases for the x= 0.03 and 0.05 compositions of $La_{1-x}Nd_xBGeO_5$, respectively.

Table 4.1 Values of the critical exponent α and the fitting parameter *JA* according to Eq. (3.11) in both ferroelectric ($T<T_C$) and paraelectric ($T>T_C$) phases of $La_{1-x}Nd_xBGeO_5$ with x= 0 (T_C= 802.4 K) for the temperature intervals indicated.

Phase		**JA**	**α**	**Temp. interval (K)**	**ΔT (K)**
T_{C1} = 802.4 K (x= 0)	**Ferroelectric ($T<T_C$)**	4673 ± 864	0.201 ± 0.011	798.6 < T < 802.1	3.5
		5072 ± 814	0.185 ± 0.010	799.4 < T < 802.1	2.7
		5559 ± 890	0.168 ± 0.009	800.2 < T < 802.1	1.9
		6183 ± 834	0.149 ± 0.008	800.6 < T < 802.1	1.5
		6594 ± 962	0.138 ± 0.008	801.2 < T < 802.1	0.9
		7196 ± 1165	0.123 ± 0.009	801.6 < T < 802.1	0.5
	Paraelectric ($T>T_C$)	252 ± 210	0.871 ± 0.124	802.5 < T < 805.8	3.3
		268 ± 318	0.773 ± 0.138	802.5 < T < 804.9	2.3
		545 ± 816	0.575 ± 0.135	802.5 < T < 804.3	1.8
		1402 ± 1971	0.387 ± 0.112	802.5 < T < 804.0	1.5
		2626 ± 2913	0.275 ± 0.084	802.5 < T < 803.7	1.2
		4251 ± 3781	0.195 ± 0.065	802.5 < T < 803.4	0.9
		6308 ± 3256	0.132 ± 0.036	802.5 < T < 803.3	0.7
		8058 ± 1504	0.094 ± 0.012	802.5 < T < 803.1	0.6

Table 4.2 Values of the critical exponent α and the fitting parameter *JA* according to Eq. (3.11) in both ferroelectric ($T<T_C$) and paraelectric ($T>T_C$) phases of $La_{1-x}Nd_xBGeO_5$ with x= 0.03 (T_C= 816.6 K) for the temperature intervals indicated.

Phase		**JA**	**α**	**Temp. interval (K)**	**ΔT (K)**
T_{C2} = 816.6 K (x= 0.03)	**Ferroelectric ($T<T_C$)**	6219 ± 1564	0.150 ± 0.015	813.1 < T < 816.5	3.4
		6684 ± 1774	0.137 ± 0.016	813.8 < T < 816.5	2.7
		7278 ± 2033	0.122 ± 0.016	814.3 < T < 816.5	2.2
		7649 ± 2187	0.113 ± 0.017	814.6 < T < 816.5	1.9
		8701 ± 2294	0.093 ± 0.015	815.1 < T < 816.5	1.4
		9273 ±2423	0.083 ± 0.015	815.4 < T < 816.5	1.0
		10050 ± 1999	0.070 ± 0.011	815.5 < T < 816.5	0.9
	Paraelectric ($T>T_C$)	343 ± 108	0.528 ± 0.018	817.1 < T < 822.4	4.2
		330 ± 140	0.541 ± 0.024	817.1 < T < 821.0	2.8
		328 ± 202	0.543 ± 0.035	817.1 < T < 820.5	2.2
		300 ± 303	0.572 ± 0.054	817.1 < T < 819.7	1.4

Table 4.3 Values of the critical exponent α and the fitting parameter *JA* according to Eq. (3.11) in both ferroelectric ($T<T_C$) and paraelectric ($T>T_C$) phases of $La_{1-x}Nd_xBGeO_5$ with x= 0.05 (T_C= 823.3 K) for the temperature intervals indicated.

Phase		**JA**	**α**	**Temp. interval (K)**	**ΔT (K)**
T_{C3} = 823.3 K (x= 0.05)	**Ferroelectric ($T<T_C$)**	7109 ± 2005	0.146 ± 0.018	819.6 < T < 822.9	3.3
		7431 ± 2145	0.137 ± 0.018	820.0 < T < 822.9	2.9
		8144 ± 2432	0.119 ± 0.019	820.4 < T < 822.9	2.5
		9228 ± 2579	0.094 ± 0.017	820.9 < T < 822.9	1.9
		10421 ±2759	0.072 ± 0.016	821.4 < T < 822.9	1.5
		11103 ± 3103	0.060 ± 0.017	821.6 < T < 822.9	1.2
		12086 ± 3027	0.045 ± 0.015	821.9 < T < 822.9	1.0
	Paraelectric ($T>T_C$)	344 ± 442	0.806 ± 0.047	823.7 < T < 805.8	3.1
		345 ± 646	0.803 ± 0.063	823.7 < T < 804.9	1.9
		432 ± 872	0.700 ± 0.078	823.7 < T < 804.3	1.2
		851 ± 1398	0.526 ± 0.075	823.7 < T < 804.0	0.8
		1678 ± 1369	0.386 ± 0.042	823.7 < T < 803.7	0.6
		2222 ± 1656	0.332 ± 0.039	823.7 < T < 803.4	0.4
		2709 ± 3088	0.295 ± 0.058	823.7 < T < 803.3	0.3

The variation of the critical exponent with respect to the temperature difference ΔT is demonstrated in Figure (4.2). As seen in the figure, in the ferroelectric phase, the critical exponent values decrease slightly while the temperature intervals are getting tight. Nevertheless, in the paraelectric phase, the variation of the α values can be seen clearly for pure and x= 0.05 doped LGB crystal. The x= 0.03 doped sample has a different view compared to the other cases, that has a slight increase while temperature interval decreases.

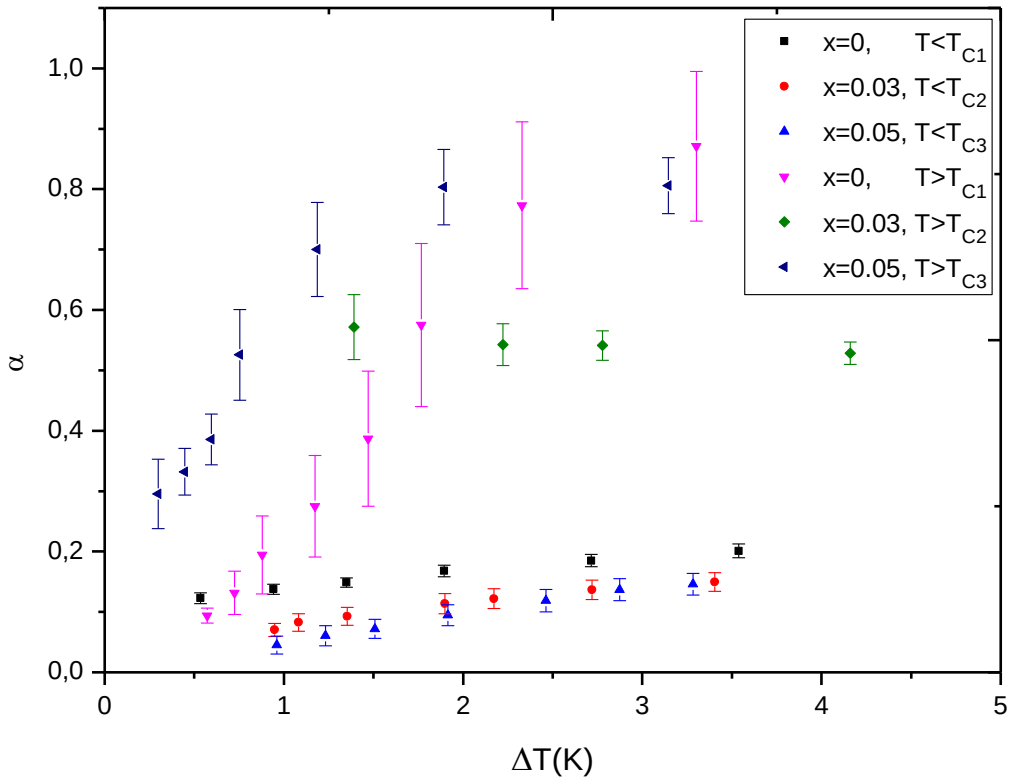

Figure 4.2. Values of the critical exponent α as a function of temperature ΔT (Tables 1-3), calculated from the specific heat data [26] in both ferroelectric ($T<T_C$) and paraelectric ($T>T_C$) phases of $La_{1-x}Nd_xBGeO_5$ with x=0; 0.03 and 0.05 according to Eq. (3.11).

Similarly, the extracted JA values vary with respect to temperature as the variation is demonstrated in Figure (4.3). In the ferroelectric phase, all three combinations have similar tendency, while temperature intervals get larger the JA values decrease. It can be also claimed that the paraelectric phase has the same behavior as the

ferroelectric phase, whereas they approach a smaller value of JA close to zero. The decreasing tendency is seen clearly in Figure (4.3) for the pure (x= 0) LGB crystal (magenta triangle). On the other hand, x = 0.03 sample has approximately the same values for the different temperature intervals. There are limited experimental data to examine at small temperature intervals, so the decreasing tendency cannot be observed. In general, it is seen in the figure that the extracted values are in accordance with each other for each phase.

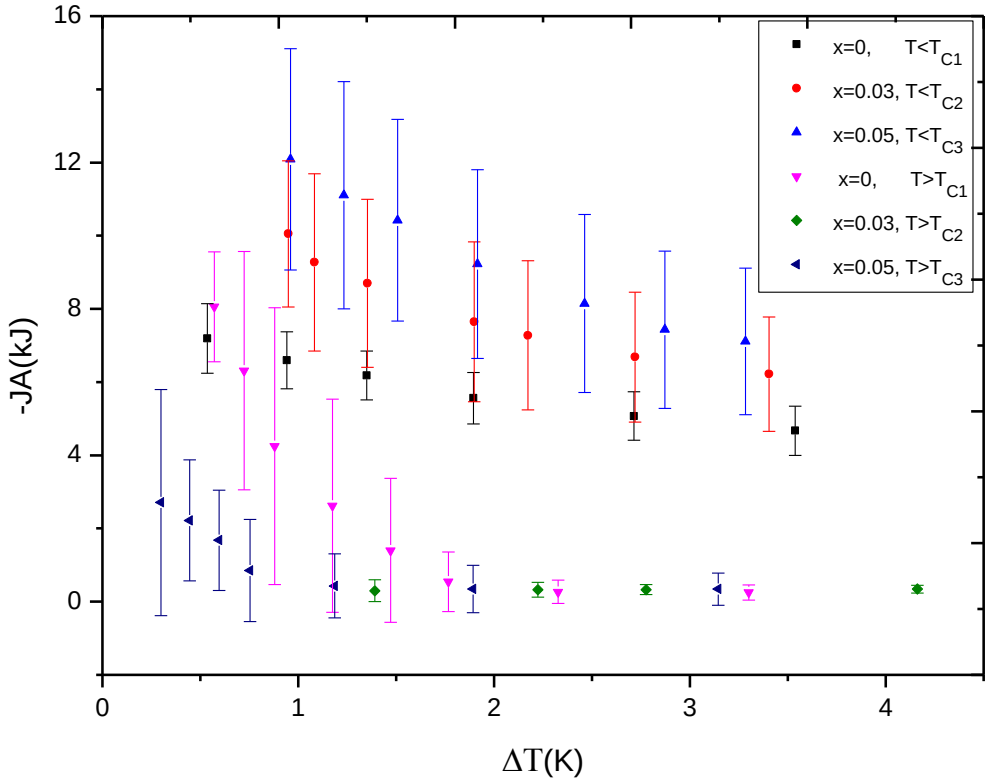

Figure 4.3. Values of the fitting parameter *JA* as a function of temperature ΔT (Tables 1-3) which was calculated from the specific heat data [28] in both ferroelectric ($T<T_C$) and paraelectric ($T>T_C$) phases of $La_{1-x}Nd_xBGeO_5$ with x=0; 0.03 and 0.05 according to Eq. (3.11).

4.2 Calculation of the Enthalpy, Entropy and the Free Energy for $LaBGeO_5$

The change in the enthalpy, $\Delta H = H - H_0$, of the three compositions of $La_{1-x}Nd_xBGeO_5$ crystals was calculated according to Eq (3.13) in both ferroelectric and paraelectric phases. The results are given in Figure (4.4) where H_0 is the enthalpy value at $T = T_C$. For this calculation of ΔH, the extracted values of α and JA (Tables 4.1-4.3) were used.

In Figure (4.4), the three samples on the left demonstrate the ferroelectric phase, and the samples on the right are for the paraelectric phase. The analysis of the graph illustrates that for the ferroelectric phase the enthalpy changes ΔH increase gradually due to the increase in the temperature. The ΔH values corresponding to each critical exponent α, become consistent with each other while the temperature is getting closer to critical temperature T_C. These values approach zero around the critical temperature, and it is expected from the second order phase transition type where there is no latent heat. On the other hand, in the paraelectric phase, the ΔH values are close to each other when the temperature gets close to T_C and spread out slightly while the temperature increases.

Likewise, the entropy change $\Delta S = S - S_0$ was calculated according to Eq (3.15) by using the extracted values of α and JA (Tables 4.1-4.3) in both phases of the three compositions of LBG crystals, as it performed for the calculation of the enthalpy change ΔH. The results of ΔS were demonstrated in Figure (4.5), where S_0 is the entropy value at $T = T_C$. The variation of the entropy ΔS can be observed from the graphs that increases slightly with increasing the temperature both in ferroelectric and paraelectric phase. It is seen that the difference between the results extracted for different α values around the critical temperature, disappears and these values approach each other.

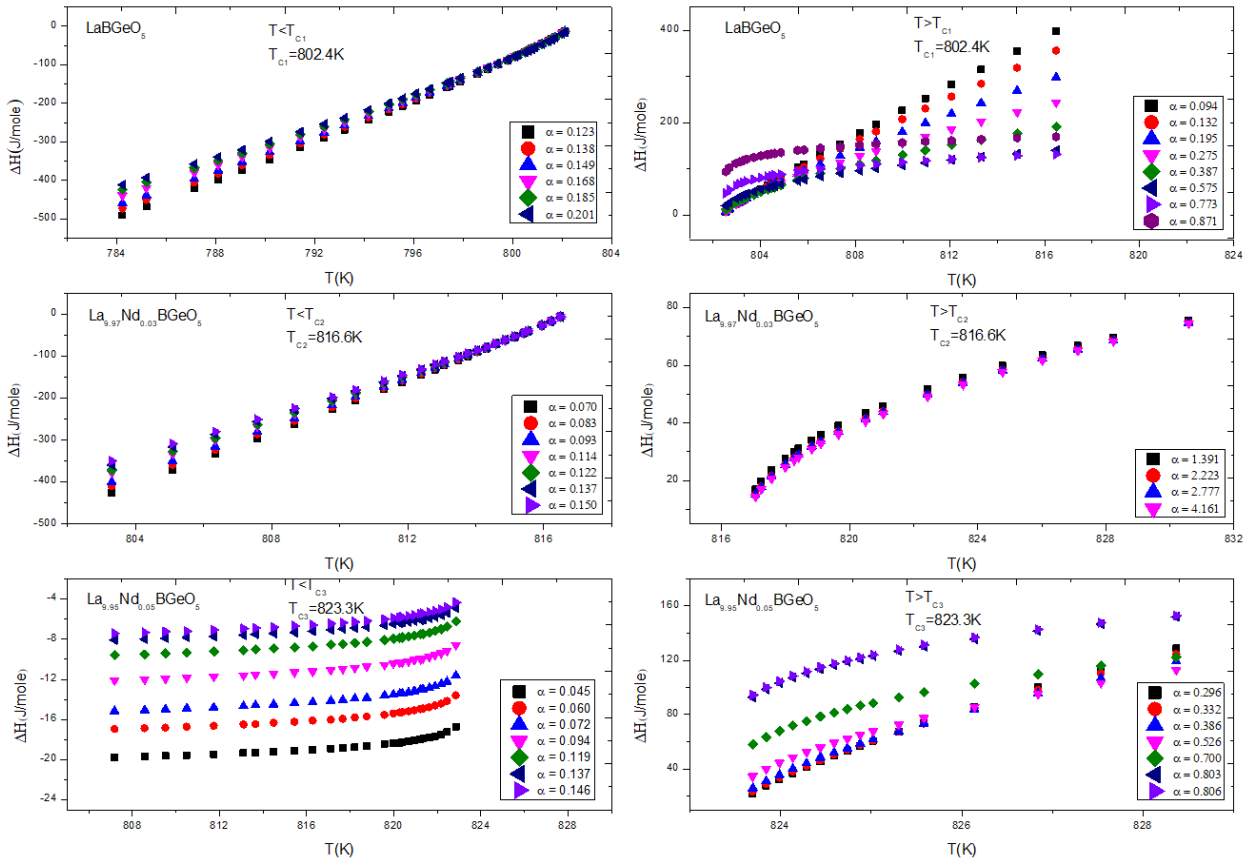

Figure 4.4. The enthalpy difference ΔH as a function of temperature according to Eq (4.2) in both ferroelectric ($T<T_C$) and paraelectric ($T>T_C$) phases of $La_{1-x}Nd_xBGeO_5$ with x=0; 0.03 and 0.05.

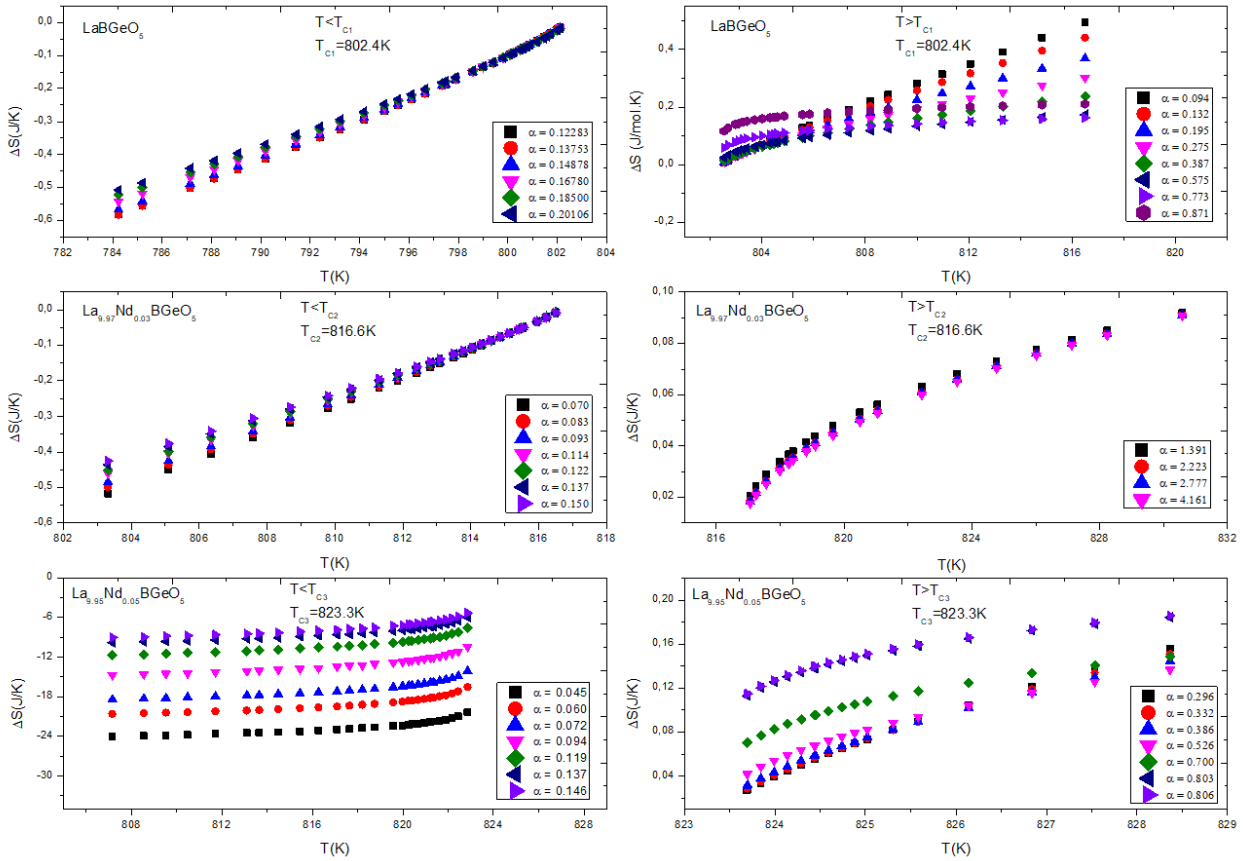

Figure 4.5. The entropy difference ΔS as a function of temperature according to Eq (4.4) in both ferroelectric ($T<T_C$) and paraelectric ($T>T_C$) phases of $La_{1-x}Nd_xBGeO_5$ with x=0; 0.03 and 0.05.

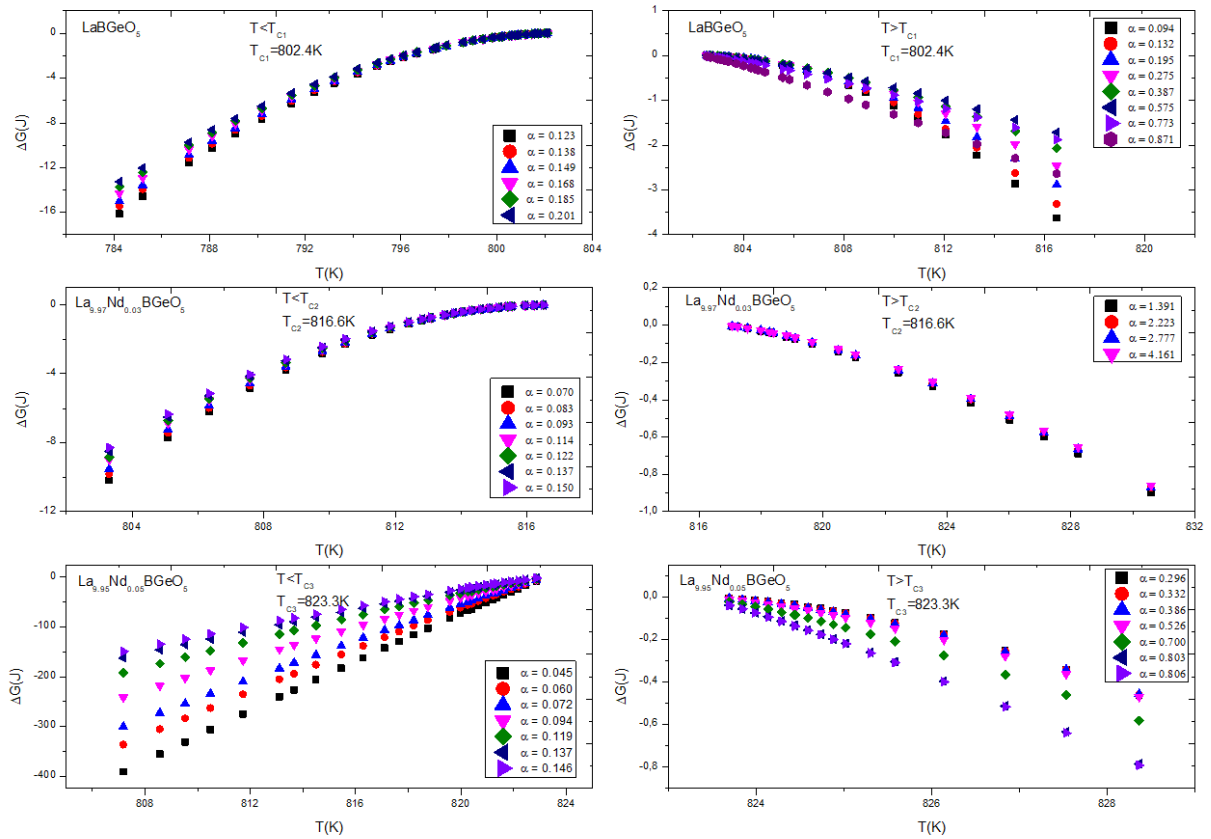

Figure 4.6. The Gibbs free energy ΔG as a function of temperature according to Eq (4.5) in both ferroelectric ($T<T_C$) and paraelectric ($T>T_C$) phases of $La_{1-x}Nd_xBGeO_5$ with x=0; 0.03 and 0.05.

The obtained values of ΔH (Figure 4.4) and ΔS (Figure 4.5) of those three compositions of LBG crystals were inserted into the Eq. (3.16) to calculate the Gibbs free energy ΔG given as Eq (3.16). The temperature dependence of the ΔG was given in Fig (4.6). It can be clearly observed in the graphs that Gibbs free energy tends to increase in ferroelectric phases and decrease in paraelectric phase with increasing temperature. The differences between the results for various α values around the critical temperature vanish, and the values converge, as also observed in enthalpy and entropy changes.

4.3 Analysis of the Birefringence and the Dielectric Constant

The birefringence Δn is proportional to the square of the order parameter η^2 through the Kerr effect. The Kerr effect, which occurs due to the externally applied electric field, expresses the change in the refractive index of the material. It is known that the Kerr effect is directly proportional to the square of the electric field. That is why we can relate the birefringence with the square of the order parameter. Within the framework of the Landau theory (Eq 3.11), the observed [26] birefringence data of the three samples of LBG were analyzed according to

$$\frac{\Delta n}{\Delta n_{max}} = -\frac{a}{a_4}\,(T - T_C) + c_0 \qquad (4.1)$$

where Δn_{max} represents the maximum value of the birefringence, as given in Table (4.4). The normalized $(\Delta n/\Delta n_{max})$ values of the birefringence were taken into consideration because the order parameter could have any value between 0 and 1. The Landau coefficient a_4 and the constant c_0, were extracted from the $(\Delta n/\Delta n_{max})$ versus $(T - T_C)$ graph (Figure 4.7), as given in Table (4.4). Since there are lack of data at about 816.6 K temperature, the relation between birefringence and temperature interval relation cannot be obtained for x= 0.03 composition of the LBG crystals.

Table 4.4 Values of the Landau coefficients a , a_4 (Eq. 4.6) and also the coefficients c_0 , c_1 (Eq. 4.7) for the ferroelectric (T<T_C) phase of $La_{1-x}Nd_xBGeO_5$ with x= 0; 0.03 and 0.05.

Sample (% $\boldsymbol{of\ Nd^{3+}}$)	$\boldsymbol{a\ x\ 10^{-4}}$	$\boldsymbol{a_4}$	$\boldsymbol{c_0}$	$\boldsymbol{c_1\ x10^{-4}}$	$\boldsymbol{T_C(K)}$
0	3.08	0.52	0.98	34.10	804.6
0.03	3.62	-	-	-3.96	810.4
0.05	5.15	1.28	0.98	-12.4	818.4

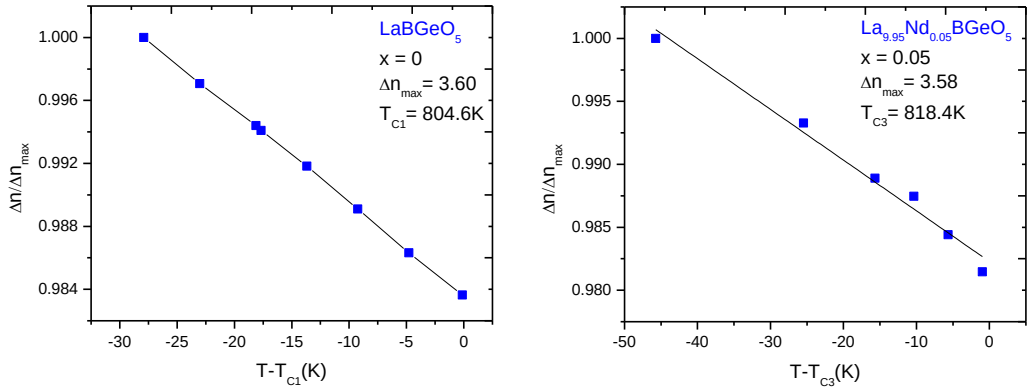

Figure 4.7. The normalized birefringence $\Delta n/\Delta n_{max}$ as a function of T-T_C according to Eq (4.1) in the ferroelectric phase (T>T_C) of $La_{1-x}Nd_xBGeO_5$ with x=0 and 0.05.

The temperature dependence of the inverse dielectric susceptibility χ^{-1} of the three samples of $La_{1-x}Nd_xBGeO_5$ with x= 0, 0.03 and 0.05, was calculated from the observed [26] dielectric constant data according to equation $\chi^{-1}= |\varepsilon - 1|^{-1}$. Within the framework of the Landau phenomenological theory (Eq 3.13), χ^{-1} values were fitted to the following relation

$$\chi^{-1} = -4a\ (T - T_C) + c_1 \qquad (4.2)$$

The Landau coefficient a and the constant c_1 were tabulated in Table 4.4. The χ^{-1} versus $(T - T_C)$ graphs were demonstrated in Figure (4.8). Note that, for the analysis

of $\Delta n/\Delta n_{max}$ and χ^{-1} according to Eqs (4.1) and (4.2), respectively, the observed [26] transition temperatures (T_C) of 804.6 K, 810.4 K and 818.4 K from the dielectric constant measurement, were used for the three samples of the LBG crystals (x= 0, 0.03 and 0.05).

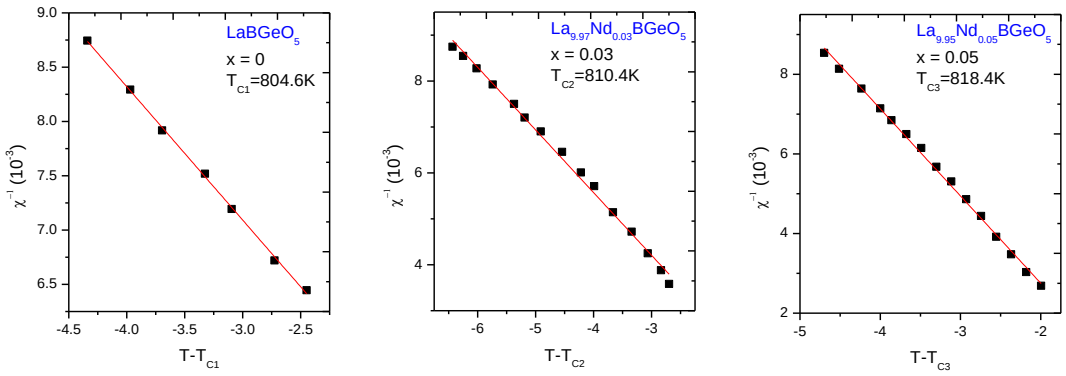

Figure 4.8. The inverse dielectric susceptibility χ^{-1} calculated from the observed [26] dielectric constant data using $\chi^{-1}= |\varepsilon - 1|^{-1}$ as a function of $La_{1-x}Nd_xBGeO_5$ with x=0; 0.03 and 0.05.

4.4 Results and Discussion of $LaBGeO_5$

The phonon dispersion calculations based on the density function theory (DFT), revealed a zone-centered unstable mode, called a rigid unit mode, above the transition temperature of LBG crystal [15]. Also, the valence force field model calculations [75] indicated a strong softening of this rigid unit mode when the ferroelectric phase changed towards the paraelectric phase. Both calculations [15, 73] point out that the rigid rotation of the BO_4 tetrahedra is the main feature of the phase transition mechanism in LBG crystals. By considering the BO_4 tetrahedra as the Ising spin variable, the anomalous behavior of the observed [26] specific heat for Nd^{3+} doped LBG crystals ($La_{1-x}Nd_xBGeO_5$ with x= 0, 0.03 and 0.05) was analyzed in terms of the compressible Ising model (Eq 3.8) approximately 4 K below and above the phase transition temperatures of 802.4 K, 816.6 K and 823.3 K for x= 0, 0.03 and 0.05, respectively. The slope of the $\ln(Cp/T)$ against $\ln|\varepsilon|$ graph

(Figure 4.1) determines the critical exponent α while the intercept allows us to deduce the interaction parameter JA. Calculation of the α and JA were employed for the three samples of LBG crystals in the different temperature intervals as given in Tables (4.1)-(4.3) for x= 0, 0.03 and 0.05, respectively. The evolution of the critical exponent α and the interaction parameter JA were shown in Figs. (4.2) and (4.3), respectively as a function of the change in the temperature (ΔT) according to the temperature intervals indicated in Tables (4.1)-(4.3).

In the ferroelectric phase ($T < T_C$) of those three compositions of LBG crystals, the values of the critical exponents tend to decrease slightly as ΔT decreases. In particular, the α value of 0.12 extracted within the temperature interval of 801.5 < T(K) < 802.0 for the pure LBG crystal (x=0, T_C=802.4 K), is exactly the same as obtained by Lushigton and Garland [76] for a second-order transition in ferroelectric-like NH_4Cl which can be classified as an Ising- like system. Furthermore, the extracted values of 0.07 and 0.04 for the critical exponent α within the temperature intervals of 815.5 < T(K) < 816.5 and 821.9 < T(K) < 822.9 for the $La_{1-x}Nd_xBGeO_5$ with x= 0.03 (T_C= 816.6 K) and x= 0.05 (T_C= 823.3 K), respectively were very close to the expected value of 0.066 (=1/16) for $T<T_C$ according to a 3D-Ising model.

Similarly, in the paraelectric phase ($T>T_C$) of the two samples with x= 0 and x= 0.05, the α values decrease as ΔT gets smaller (Figure 4.2) while the α value for the sample with x= 0.03 is almost constant as ΔT decreases. In some detail, the α value of 1.0 for pure LBG crystals (x= 0; T_C= 802.4K) which was extracted within the temperature interval of 802.5 < T(K) < 808.8 (ΔT=6.3K) is exactly the same value as reported by Strukov et al. [28] for $1 < |T_C-T| <10$K. But, as ΔT decreased to the value of 0.6 K (802.5 < T(K) < 803.1K) we deduce α as 0.09 which can be compared with 0.125 (=1/8) predicted from the 3D-Ising model for $T>T_C$. Furthermore, the extracted value α = 0.5 which is almost independent of ΔT for the samples with x= 0.03 and 0.05 within the temperature interval of 823.6 < T(K) < 824.5K (ΔT = 0.8K) is consistent with that reported by Strukov et. al. [26] above the transition

temperatures of 816.6 K and 823.3 K, respectively. But, as ΔT decreased to a value of 0.3 K (823.6 < T(K) < 823.9K) for the sample with x= 0.05, the α was found to be 0.3 which can be compared with that predicted from the 2-d Pots model. The non-singular (background) part of the specific heat (lattice contribution) which is less dominant when compared with the spin interaction contribution in the vicinity of the phase transition temperature, was not considered in this study.

In addition, the thermodynamic quantities of ΔH (enthalpy), ΔS (entropy) and ΔG (Gibbs free energy) were predicted as a function of temperature according to Eqs (3.13), (3.15) and (3.16), respectively in terms of the obtained values of critical exponent α and the interaction parameter JA (Tables 4.1- 4.3) for both below ($T < T_C$) and above ($T > T_C$) the phase transition temperatures of these three samples of LBG crystals, as given in Fig(4.4)-(4.6).

The observed [26] birefringence data Δn of these three samples of LBG crystal decrease almost linearly below the phase transition temperatures. On the other hand, below T_C the molecular field theory [77] predicts that the order parameter η decreases according to $(\frac{T_C - T}{T_C})^{\beta}$ with the critical exponent $\beta = 0.5$, as the temperature increases toward the T_C. In the light of these information, we associated the normalized birefringence $(\frac{\Delta n}{\Delta n_{max}})$ with the square of the order parameter η^2 in the ferroelectric phase ($T < T_C$). Then, the observed [26] Δn data of LBG crystals with x= 0 and x= 0.05 were analyzed according to Eq (4.6) within the framework of the Landau theory (Figure 4.7). We were unable to do the same analysis for LBG crystal with x= 0.03 due to the lack of the sufficient data of Δn below T_C. In addition, the inverse dielectric susceptibility χ^{-1} calculated from the observed [26] dielectric constant of these three samples of LBG crystals was also analyzed according to Eq (4.2) within the framework of the Landau theory in the ferroelectric phase (Figure 4.8). The slope of Figs (4.7) and (4.8) allows us to extract the coefficients a and a_4 as we tabulated them in Table (4.4). Both a and a_4 were found to be positive as expected from the Landau phenomenological theory for a second-order type of phase transition. The intercepts c_0 and c_1 are also given in Table (4.4).

4.5 Conclusion of $La_{1-x}Nd_xBGeO_5$

The compressible Ising model was used to study the anomalous behavior of the specific heat for Lanthanum Borogermanate ($La_{1-x}Nd_xBGeO_5$) at x = 0, 0.03, and 0.05, which is around 4 K below and above the phase transition temperatures of 802.4 K, 816.6 K, and 823.3 K, respectively. For these three compositions, the critical exponents (α) were calculated in the ferroelectric phase ($T < T_C$), and the extracted values are ranging between 0.04 - 0.12 that are consistent with that predicted from the 3-D Ising model (0.07 for $T < T_C$). Similarly, critical exponent in the paraelectric phase ($T > T_C$) of the sample with x= 0 is also appropriate in 3-D Ising model. However, the deduced value of the sample with x= 0.05 in the paraelectric phase is 0.3, which is same with the predicted one from the 2-D Pots model. It can be concluded that the Compressible Ising Model is adequate to describe the ferroelectric-paraelectric phase transition in pure and Nd^{3+} doped $LaBGeO_5$ crystals.

In addition, the observed birefringence data which were associated with the order parameter (squared) and the observed dielectric constant of the three compositions (x = 0, 0.03, and 0.05) for Lanthanum Borogermanate ($La_{1-x}Nd_xBGeO_5$) were analyzed within the framework of the Landau phenomenological theory to determine the Landau coefficients a and a_4. The Landau coefficients were found to be positive, as expected, which indicates that the phase transition of the samples studied here is of a second order type.

CHAPTER 5

CALCULATION OF THE SPIN- LATTICE RELAXATION TIME AND THE ACTIVATION ENERGY NEAR THE IV-III PHASE TRANSITION IN PYRIDINIUM FLUOROSULFONATE (C_5NH_6)FSO_3

In the scope of the present chapter, the pseudospin-phonon (PS) coupled and energy fluctuation (EF) models are used to compute the spin-lattice relaxation time T_1^H for protons, which is close to the IV-III solid-solid phase transition of $T_C = 235\ K$ in Pyridinium Fluorosulfonate ((C_5NH_6)FSO_3). The observed second moment of the ^1H was used in this calculation as both the order parameter below T_C and the disorder parameter above T_C. This calculation was performed by associating the observed second moment of the ^1H as the order parameter below T_C and the disorder parameter above T_C. The activation energies for the cation reorientation in (C_5NH_6)FSO_3 crystal are calculated by using both PS and EF models. In addition, the Landau theory is used to examine the measured dielectric permittivity of the crystal, and the spontaneous polarization (SP) is calculated as a function of temperature.

5.1 Analysis of the Damping Constant

Temperature dependence of the damping constant Γ_{SP} which is inversely proportional to the spin-lattice relaxation time T_1 can be calculated by using the pseudospin-phonon (PS) coupled model [49] and the energy fluctuation (EF) model [50] for P_yFSO_3. In terms of the order parameter (η), damping constant by considering the pseudospin-phonon interactions (Eq 3.39) in P_yFSO_3 can be expressed as [49]

$$\Gamma_{SP}\ \alpha\ \frac{1}{T_1} = \Gamma_0 + A(1-\eta^2)\ln\left[\frac{T_C}{T - T_C(1-\eta^2)}\right] \tag{5.1}$$

where T_C is the transition temperature, Γ_0 and A are the background damping constant and the amplitude, respectively. Also, the temperature dependence of the damping constant (Eq. 3.41) in terms of the order parameter can be evaluated by using the energy fluctuation (EF) model [50],

$$\Gamma_{SP}\ \alpha\ \frac{1}{T_1} = \Gamma_0' + A'\left[\frac{T(1-\eta^2)}{T - T_C(1-\eta^2)}\right]^{1/2} \tag{5.2}$$

where Γ_0' and A' are the background damping constant and the amplitude. The molecular field theory provides the temperature dependence of the order parameter (η) appearing in Eqs. (5.1) and (5.2) for the different temperature regions below and above T_C given as [77]

$$\eta \approx \begin{cases} 1 - \exp\left(-\dfrac{2T_C}{T}\right) & T \ll T_C \\ \left\{3\left(1 - \dfrac{T}{T_C}\right)\right\}^{\frac{1}{2}} & 0 < (T_C - T) < T_C \\ 0 & T_C < T \end{cases} \tag{5.3}$$

Based on the Ising pseudospin-phonon coupled model of Yamada et al. [78] and Matsushita [77], Eqs. (5.1) and (5.2) have been obtained previously for the KDP type materials [49, 73]. Although it is hard to define its physical meaning without knowledge of the low-temperature crystal structure of P_yFSO_3, the proton second moment M_2 in phase IV behaves like an order parameter as it was pointed out previously [48]. To check this consideration, we associated the observed [48] second moment M_2 of P_yFSO_3 with the order parameter η below the IV-III phase transition temperature $T_C = 235\ K$ according to

$$\frac{M_2}{M_{2,max}} = a\eta + b \tag{5.4}$$

where $M_{2,max}$ is the maximum value of the second moment, a and b are the unitless coefficients (Table 5.1).

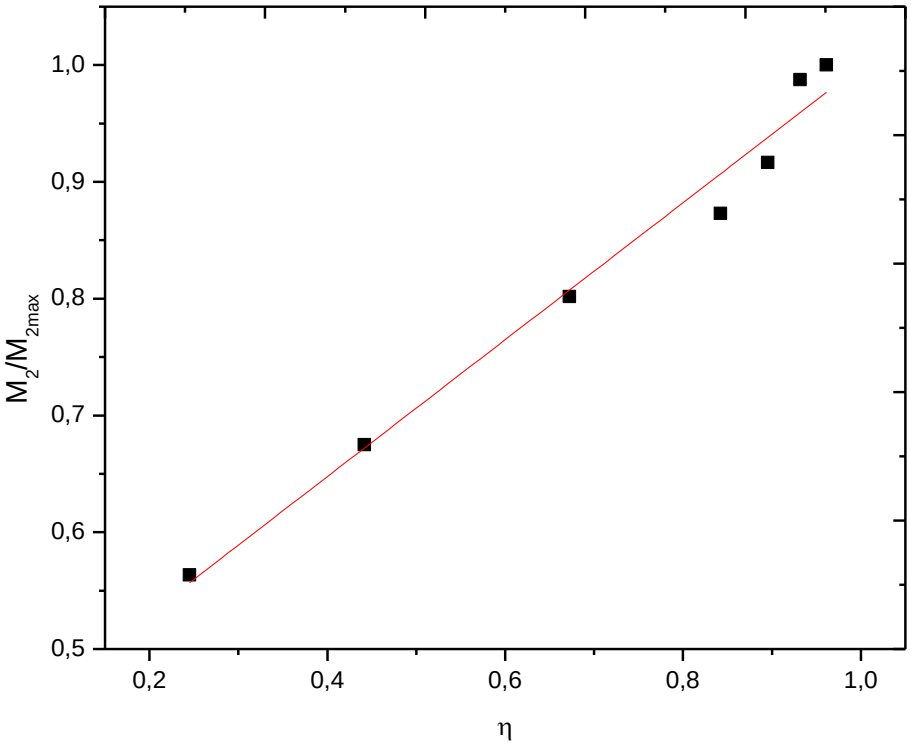

Figure 5.1. $M_2/M_{2,max}$ versus η graph (Eq. 5.4) below the IV-III solid-solid phase transition temperature of $T_C = 235\ K$ in P_yFSO_3.

The values are plotted in Figure (5.1) as $M_2/M_{2,max}$ versus η below the IV-III phase transition temperature. Those $M_2/M_{2,max}$ values were then used as order parameters $[\eta^2 = (M_2/M_{2,max})^2]$ below the IV-III solid-solid transition temperature $T_C = 235\ K$ while it is used as a disorder parameter $[1 - \eta^2 = (M_2/M_{2,max})^2]$ above T_C in Equations (5.1) and (5.2) to calculate the spin-lattice relaxation time of proton T_1. These calculated values of T_1 were fitted to the observed [48] spin-lattice relaxation time (Fig 5.2) and the background damping constant Γ_0 (Γ_0') with the amplitudes A (A') were extracted both below and above T_C, as tabulated in Table (5.2).

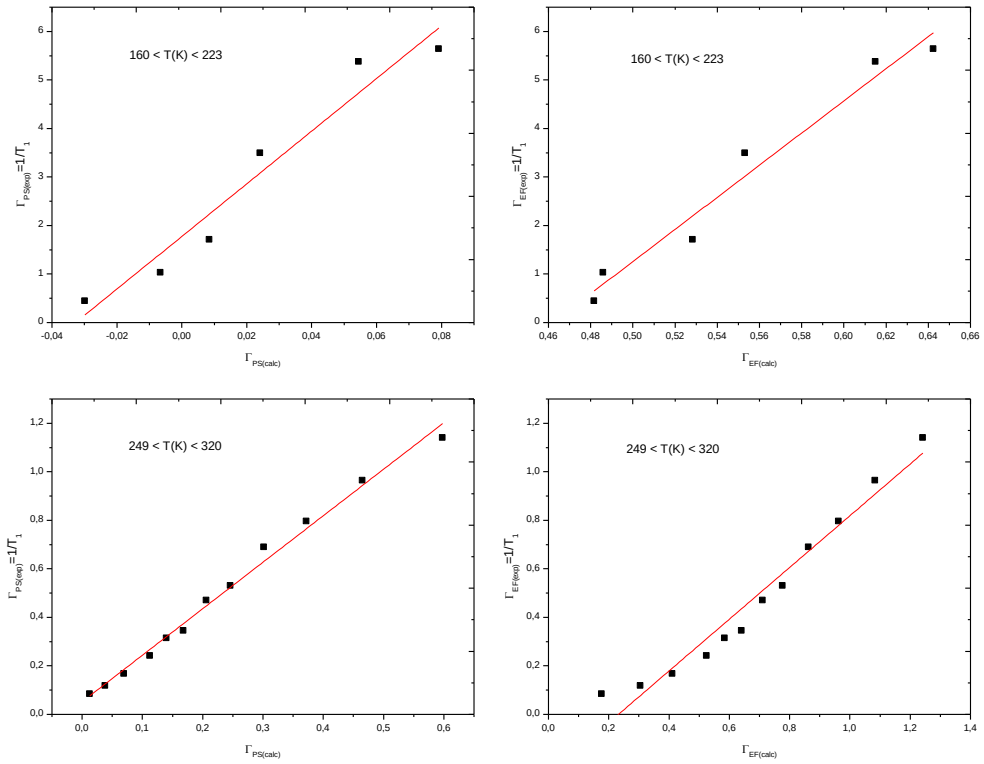

Figure 5.2. The experimental damping constant $(1/T_1)$ against our calculated Γ_{SP} from both PS and EF models below and above the IV-III solid-solid phase transition temperature of $T_C = 235\ K$ in P_yFSO_3.

Table 5.1 Values of the $M_{2,max}$, the parameters a and b according to Eq. (5.4) and values of the α and a_4 according to the Eq. (5.6) below the solid-solid phase transition (IV-III) temperature of $T_C = 235\ K$.

Crystal	$M_{2,max}$	a	b	**α x 10^{-5} (J/K)**	**-a_4**	**Temperature Interval (K)**
P_yFSO_3	7.2 G	4.16	2.93	24.7	0.14	-80 < T-T_C < -40
				33.3	0.12	-38 < T-T_C < 0

Calculated values of the spin-lattice relaxation time T_1 from Eqs. (5.1) and (5.2) were plotted in Figure (5.3) as a function of temperature. The observed data [48] were also given in Figure (5.3) for comparison.

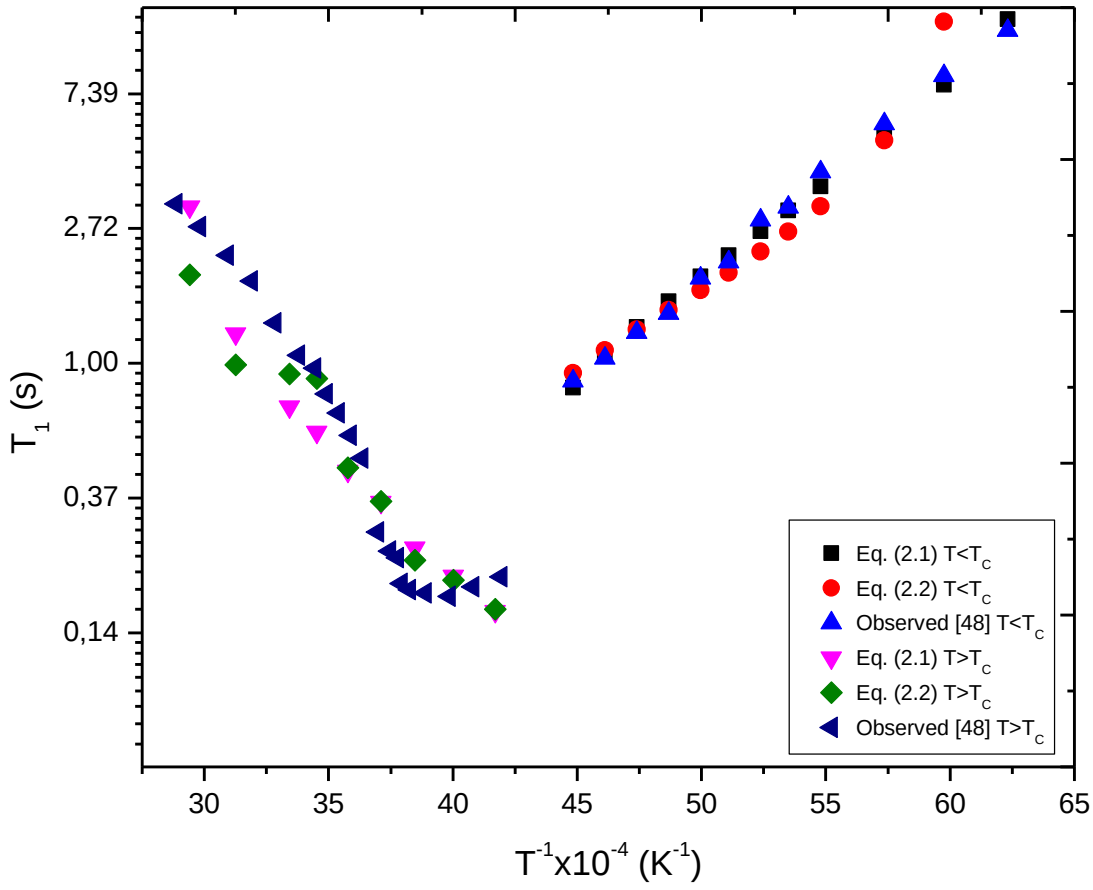

Figure 5.3. The temperature dependence of the spin-lattice relaxation time T_1 calculated from the PS (Eq. 5.1) and EF (Eq. 5.2) models both below and above the IV-III solid-solid phase transition temperature of $T_C = 235\ K$ in P_yFSO_3. The experimental [48] data were also given for comparison.

Table 5.2 Values of the background damping constant Γ_0 (Γ_0') and the amplitude A (A') due to the PS (Eq. 5.1) and EF (Eq. 5.2) models both below and above $T_C = 235\ K$ using the experimental [48] spin-lattice relaxation time of the proton in P_yFSO_3.

Crystal	**Model**	$\boldsymbol{\Gamma_0}$ ($\boldsymbol{\Gamma_0'}$)**(Hz)**	$\boldsymbol{A}$ ($\boldsymbol{A'}$)**(Hz)**	**Temperature Interval**
P_yFSO_3	PS (Eq. 5.1)	0.05	1.92	160 < T (K) < 223
	PS (Eq. 5.1)	1.78	54.25	249 < T (K) < 320
	EF (Eq. 5.2)	-0.25	1.07	160 < T (K) < 223
	EF (Eq. 5.2)	-15.29	33.11	249 < T (K) < 320

The activation energy U for the cation reorientation of crystal can be calculated from the linewidth (damping constant) as given previously [80,81]

$$\ln \Gamma = \ln C - \frac{U}{k_B T} \tag{5.5}$$

where k_B is the Boltzman constant and C is a constant.

The values of the activation energy U were deduced from the Arrhenius plot (Figure 5.4) and they were tabulated in Table (5.3). For this extraction of U, calculated values of the damping constant from the PS and EF models (Eqs. 5.1 and 5.2) were used.

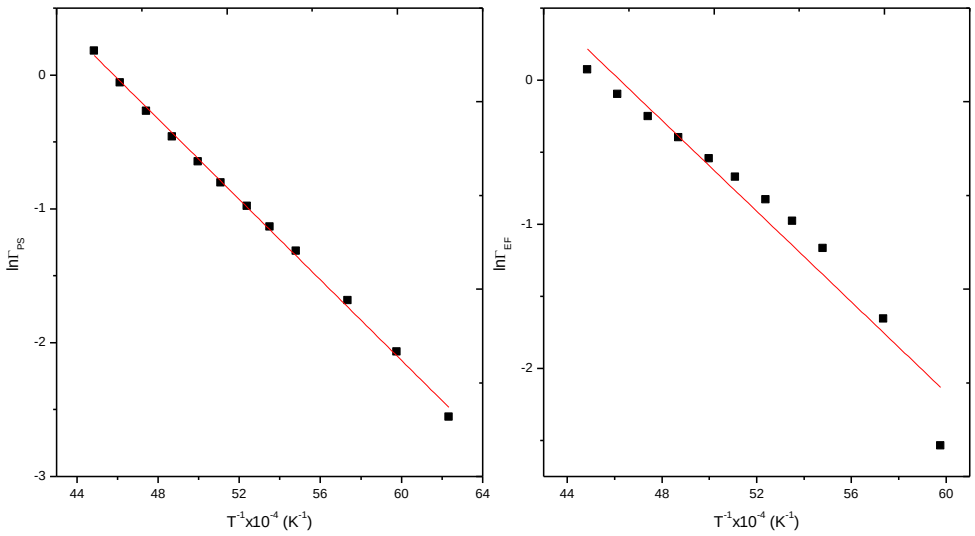

Figure 5.4. The damping constant Γ_{SP} calculated from Eqs. (5.1) and (5.2) as a function of the reciprocal temperature to extract the activation energy for the cation reorientation in P_yFSO_3.

Table 5.3 Values of the activation energy U for the cation reorientation and the constant $ln\ C$ according to Eq. (5.5) for the temperature interval indicated in P_yFSO_3.

Crystal	**Model**	$\boldsymbol{U(kJ/mol)}$	**ln $\boldsymbol{C}$**	**Temperature Interval**
P_yFSO_3	PS (Eq. 5.1)	12.5	6.89	160 < T (K) < 223
	EF (Eq. 5.2)	13.1	7.27	160 < T (K) < 223

The dielectric susceptibility χ of P_yFSO_3, which was calculated from the observed [49] dielectric permittivity ε ($\varepsilon = \chi + 1$), was analyzed within the framework of the Landau theory according to [81]

$$\chi^{-1} = (\varepsilon - 1)^{-1} = -12\alpha(T - T_C) + \frac{16}{3}\frac{a_4^2}{a_6} \qquad (5.6)$$

where α, a_4, and a_6 are the coefficients of the free energy F expanded in terms of the spontaneous polarization P as

$$F = a_0 + \alpha(T - T_C)P^2 + a_4P^4 + a_6P^6 \tag{5.7}$$

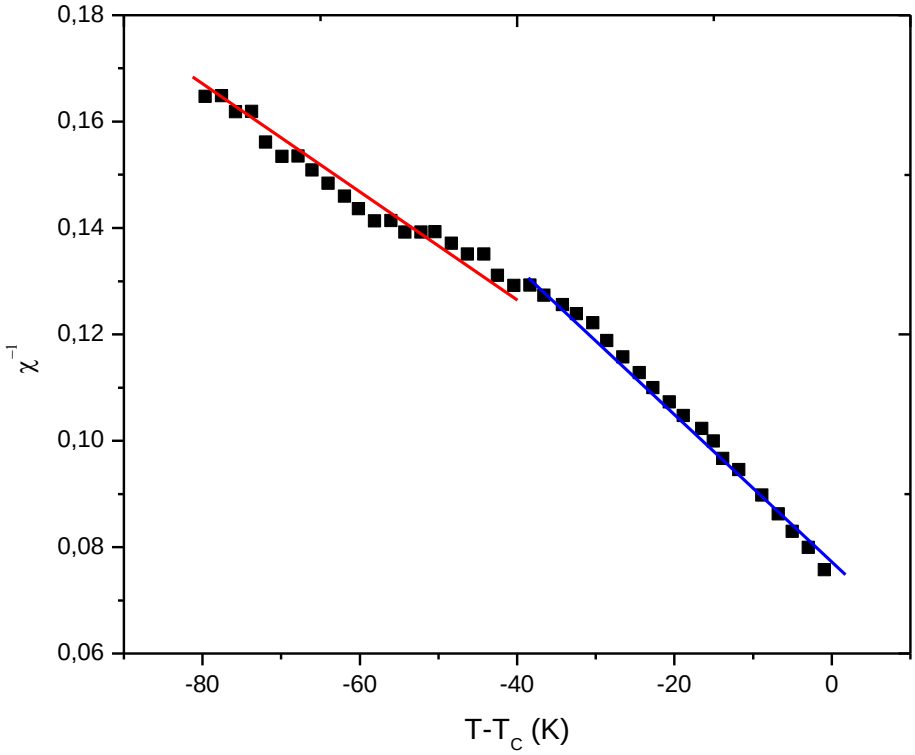

Figure 5.5. Temperature dependence of the inverse dielectric susceptibility χ^{-1} below the IV-III solid-solid phase transition temperature $T_C = 235\ K$ in P_yFSO_3.

Figure 5.5 shows χ^{-1} versus $T - T_C$ graph for this crystal below T_C. The coefficient α and a_4 (Table 5.1) extracted from Figure (5.5) according to Eq. (5.6) were then used to predict the spontaneous polarization P which reads as [81]

$$P^2 = \frac{\alpha\ (T - T_C)}{2a_4} - \frac{2a_4}{3a_6} \tag{5.8}$$

For simplicity a_6 was taken as unity. The spontaneous polarization calculated from Eq. (5.8) were then used as order parameter to calculate the damping constant from the PS and EF models (Eqs. 5.1 and 5.2). Finally, the activation energy for the reorientation of the dipole moment was calculated according to Eq. (5.5) for the temperature intervals indicated in Table (5.4).

Table 5.4 Values of the activation energy U and the constant lnC according to Eq. (5.5) for the reorientation of the dipole moment in P_yFSO_3.

Crystal	**Model**	$\boldsymbol{U(kJ/mol)}$	**ln** $\boldsymbol{C}$	**Temperature Interval**
P_yFSO_3	PS (Eq. 5.1)	21.9	12.8	159 < T (K) < 212
	EF (Eq. 5.2)	11.2	7.0	159 < T (K) < 212

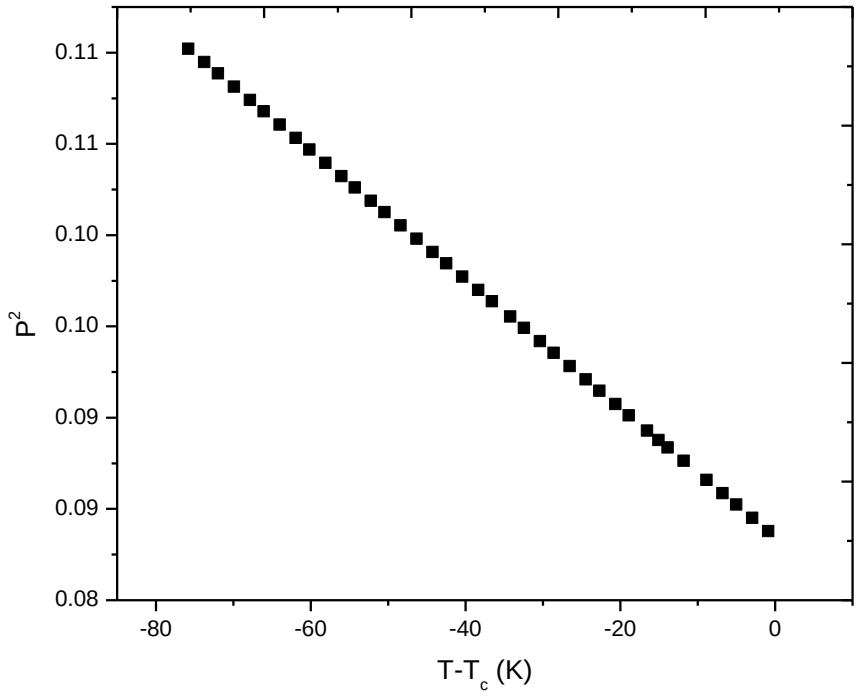

Figure 5.6. The temperature dependence of the spontaneous polarization P below the IV-III solid-solid phase transition temperature of $T_C = 235\ K$ in P_yFSO_3.

5.2 Results and Discussion of Pyridinium Fluorosulfonate (C_5NH_6)FSO_3

The observed [48] proton second moment M_2 for P_yFSO_3 decreases in phase IV as the temperature increases toward the solid-solid phase transition (IV-III) temperature of $T_C = 235\,K$. This behavior is very similar to the order parameter η that was predicted from the mean field theory (Figure 5.1). This then allows us to associate the normalized proton second moment ($M_2/M_{2,max}$) with the order parameter η according to Eq (5.4). The fitting parameters (a and b) of Eq (5.4) were tabulated in Figure (5.1). On the other hand, above $T_C = 235\,K$ the observed [48] proton second moment M_2 decrease further as the temperature increases due to the infrequent reorientation of the cation between probably non-equivalent potential wells. That is why above T_C the observed M_2 [48] was associated with the disorder parameter ($1-\eta^2$) according to $1-\eta^2 = (M_2/M_{2,max})^2$.

The spin lattice relaxation time (SLRT) of proton T_1 for P_yFSO_3 was calculated in terms of the pseudo-spin phonon (PS) coupled (Eq. 5.1) and the energy fluctuation (EF) models (Eq. 5.2) with the help of the observed [48] second moment M_2 of this crystal both below and above the solid phase transition (IV-III) temperature of $T_C = 235\,K$. The background damping constant Γ_0 (Γ_0') and the amplitudes A (A') of Eqs. 5.1 and 5.2 were extracted through a fitting procedure (Figure 5.2) and they were tabulated in Table (5.2) for the temperature intervals indicated. Those calculated values of SLRT from PS and EF models and the observed data were given in Figure 5.3 as a function of inverse temperature T^{-1}. The SLRT predicted from both PS and EF models are adequate to explain the observed [48] data. We extracted the values of 12.6 kJ/mol and 13.1 kJ/mol for the cation reorientation activation energy through Eq (5.5) by using the damping constant, which were calculated from the PS model (Eq. 5.1) and EF model (Eq. 5.2) respectively. Both values are almost the same with the calculated value (12.7 kJ/mol) [48].

Regarding the calculation of the activation energy (Eq. 5.5) for the reorientation of the dipole moment in phase IV of P_yFSO_3 within the framework of the Landau

theory, we first calculated the dielectric susceptibility χ of P_yFSO_3 below the solid-solid phase transition (phase IV-III) temperature $T_C = 235\,K$ from the observed dielectric permittivity ε ($\varepsilon = \chi + 1$). A fitting procedure for χ^{-1} versus $T - T_C$ (Figure 5.5) was performed according to Eq (5.6), which is a simplified form of χ [81], and the fitting parameters α and a_4 were extracted (Table 5.1). The coefficient a_6 was taken unity due to the fact that our solution of χ^{-1} was based on the approximation ($a_2 a_6 / a_4^2 << 1$) in order to simplify the solution by regarding very small values of α and almost ~0.1 value of a_4 [81]. We then predicted values of the spontaneous polarization P by using these coefficients α, a_4 (Table 5.1) according to Eq (5.8).

These predicted values of P (Eq. 5.8) were then used as an order parameter in Eqs. (5.1) and (5.2) to calculate the damping constant Γ from both PS and EF models, respectively. Finally, by using Γ values through Eq (5.5) we expected the activation energy for the reorientation of the dipole moment within the temperature intervals of $159 < T(K) < 212$ as given in Table (5.4). Our expected value of 22 kJ/mol from the PS model (Eq. 5.1) for the temperature interval of $159 < T(K) < 212$ can be compared with the experimental value of 26 kJ/mol which was extracted from the dielectric correlation time within the same temperature interval [48] while our expected value of 11 kJ/mol from the EF model (Eq. 5.2) was very small when compared with the experimental value of 26 kJ/mol. This is an indication of that PS model works better than the EF model to explain the reorientation of the effective dipole moment of the P_yFSO_3 arising from the cation-anion interaction.

As a result, the energy fluctuation (EF) and the pseudospin-phonon coupled (PS) models were used to determine the spin-lattice relaxation time for protons nuclei in Pyridinium Fluorosulfonate ($PyFSO_3$). The activation energy for the cation reorientation in the P_yFSO_3 crystal can be calculated using both models as accurate as that which can be deduced from the experimental spin-lattice relaxation time data. Additionally, the activation energy for the reorientation of the dipole moment estimated from the PS model within the context of the Landau theory is nearly

identical to that obtained from the experimental dielectric correlation time, while the EF model was unable to achieve the same result. The phase transition mechanisms of other pyridinium salts could be investigated using PS and EF models.

CHAPTER 6

ANALYSIS OF THE SPECIFIC HEAT AND CALCULATION OF THE RELAXATION TIME, ACTIVATION ENERGY, ENTROPY, AND ENTHALPY CLOSE TO THE LOWER PHASE TRANSITION IN IMIDAZOLIUM PERCHLORATE

In the present chapter, the phase transition mechanism of the Imidazolium Perchlorate (Im-ClO_4) crystal has been investigated in terms of thermodynamic properties; specific heat, activation energy, entropy, and enthalpy. Im-ClO_4 crystal demonstrates anamolous behaviour around various temperatures; 245K [61, 63], 247K [63], and 373K [83] according to the literature, which were accepted as transition temperatures and they were investigated by different methods. Both relaxation time and specific heat calculations are performed at around 245 K, and entropy and entalpy changes are deduced. At around 247 K, only the specific heat calculations were done, and similar to 245K, some thermodynamic behaviors were investigated. Lastly at 373 K, the analysis of critical exponents was carried out and it was checked whether they are compatible with Rushbrooke's inequality or not.

6.1 Calculation of the Relaxation Time and Activation Energy

6.1.1 Calculations and Results

The temperature dependence of the spin lattice relaxation time (τ) for the Imidazolium Perchlorate (Im-ClO_4) crystal has been calculated from the pseudospin-phonon (PS) coupled (Eq. 5.1) and energy fluctuation (EF) models (Eq 5.2) in the vicinity of the phase transition temperature of $T_C = 247\,K$. The observed [61] normalized proton second moment M_2/M_{2max} was associated with the order parameter η according to

$$M_2/M_{2max} = a_0 + a_1\eta \tag{6.1}$$

Thus, by fitting the order parameter from the mean field theory (Eq. 5.3) to the experimental [61] M_2/M_{2max} data for Im-ClO_4, the coefficients a_0 and a_1 were determined as given in Table 6.1. In Figure 6.1 (Eq. 6.1) normalized proton second moment M_2/M_{2max} and order parameter η (Eq. 5.3) are given as a function of temperature for Im-ClO_4.

Table 6.1 Values of the coefficients a_0 and a_1 according to Eq. (6.1) below the transition temperature (T_C= 247 K) of Im-ClO_4**.**

Crystal	$M_{2,max}$	a_0	a_1
ImClO_4	7.50 G	0.76	0.27

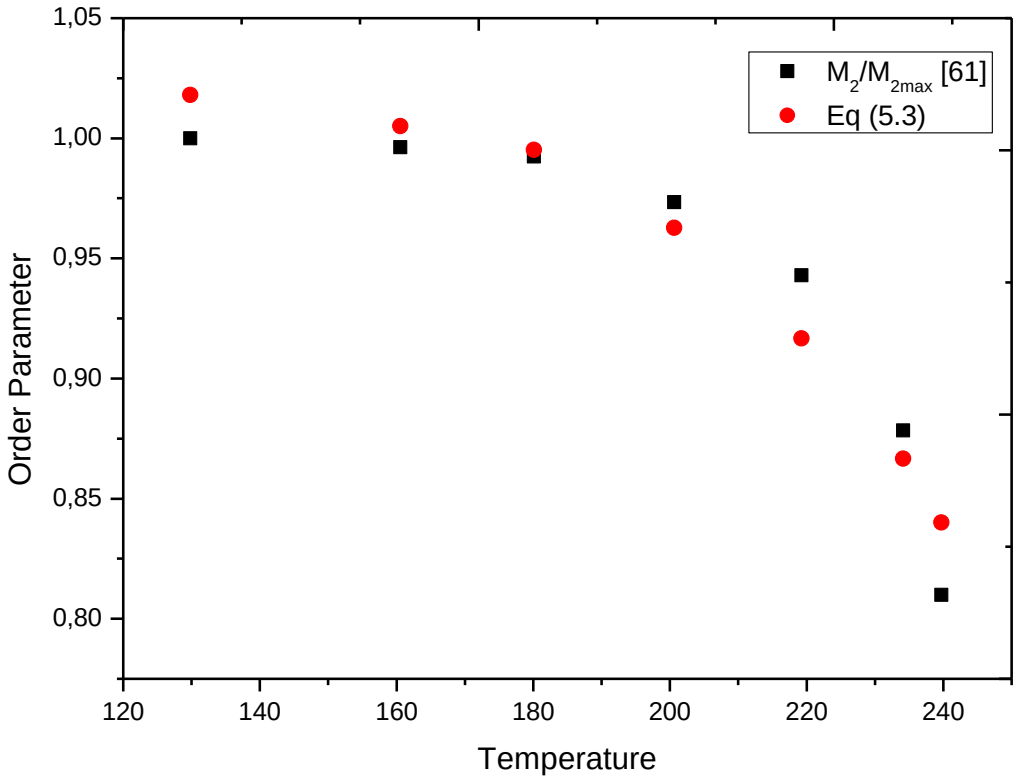

Figure 6.1. The order parameters (observed ($M_2/M_{2,max}$) [61] and calculated η (Eq. 5.3)) versus temperature graph below the phase transition temperature of T_C = 247 K in ImClO_4.

As indicated in Figure (6.1), observed and calculated values are in a good agreement. Therefore, the normalization of the square of the observed [61] proton second moment ($M_2^2/M_{2,max}^2$) has been associated with the square of the order parameter (η^2) for the calculations. On the other hand, above T_C, the observed M_2 [61] decreases very rapidly as the temperature increases due to the infrequent reorientation of the cation between the non-equivalent potential wells. This caused us to associate the values above T_C with the disorder parameter ($1-\eta^2$) instead of the order parameter.

Then, the spin lattice relaxation time (demonstrated by τ_{cal}) from both PS and EF models were calculated according to damping constant equations; Eq 5.1 and 5.2 by the order and disorder parameters below and above T_C, respectively. The calculated relaxation time τ_{cal} was fitted to the observed relaxation time τ_{obs} [61] according to

$$1/\tau_{obs} = b_0 + b_1(1/\tau)_{cal} + b_2(1/\tau)_{cal}^2 \qquad (6.2)$$

where b_0, b_1, and b_2 are the fitting parameters that are constant and they are listed in Table 6.2 for both models in the ferroelectric and paraelectric phases.

Table 6.2 Values of the coefficients b_0, b_1 and b_2 according to Eq. (6.1) below and above the transition temperature (T_C= 247 K) of Im-ClO_4

Crystal	**Model**	b_0 **x** 10^{-2} **(**s^{-1}**)**	b_1 **x** 10^{-2} **(**s^{-1}**)**	b_2 **x** 10^{-2} **(**s^{-1}**)**	**Temperature Interval**
$ImClO_4$	PS (Eq. 5.1)	1.505	38.6	-213.3	142.9 < T (K) < 236.0
	PS (Eq. 5.1)	16.2	644.7	15776.0	251.0 < T (K) < 357.4
	EF (Eq. 5.2)	1.3	5.1	-3.1	142.9 < T (K) < 236.0
	EF (Eq. 5.2)	39.0	-261.6	587.3	251.0 < T (K) < 357.4

Calculated (Eqs. 5.1 and 5.2) values of τ_{cal} were fitted to the measured data [61] as given in Figure 6.2. Both models displayed similar curves for the ferroelectric and paraelectric phase. In the paraelectric phase of EF model, there is an irregularity but the relation can be examined by general tendency.

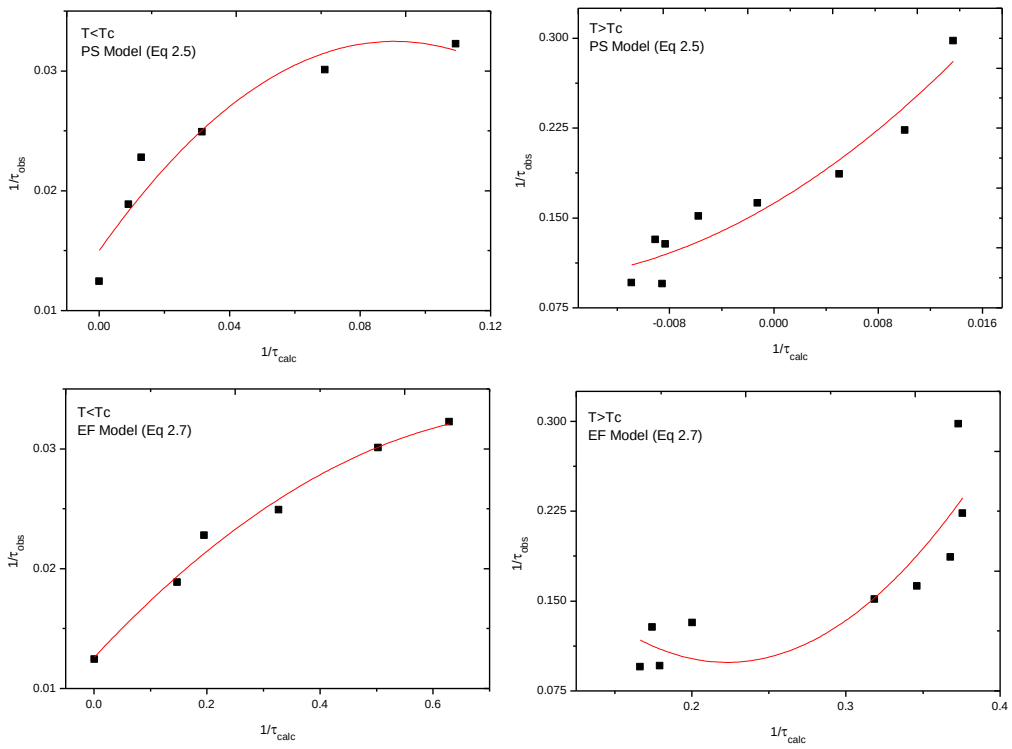

Figure 6.2. The experimental [61] versus calculated (Eqs. 5.1 and 5.2) spin lattice relaxation time at various temperatures. The solid curves represent the best fit to the experimental data.

In Figure 6.3 both calculated (Eqs. 5.1 and 5.2) values and measured data [61] of the inverse spin lattice relaxation time are demonstrated as a function of temperature. The discontinuity in the vicinity of the transition temperature T_C is clearly seen in the figure. Additionally, it can be claimed that the tendency of the observed and calculated values of the spin lattice relaxation time are compatible with each other in both phases as seen in Figure (6.3).

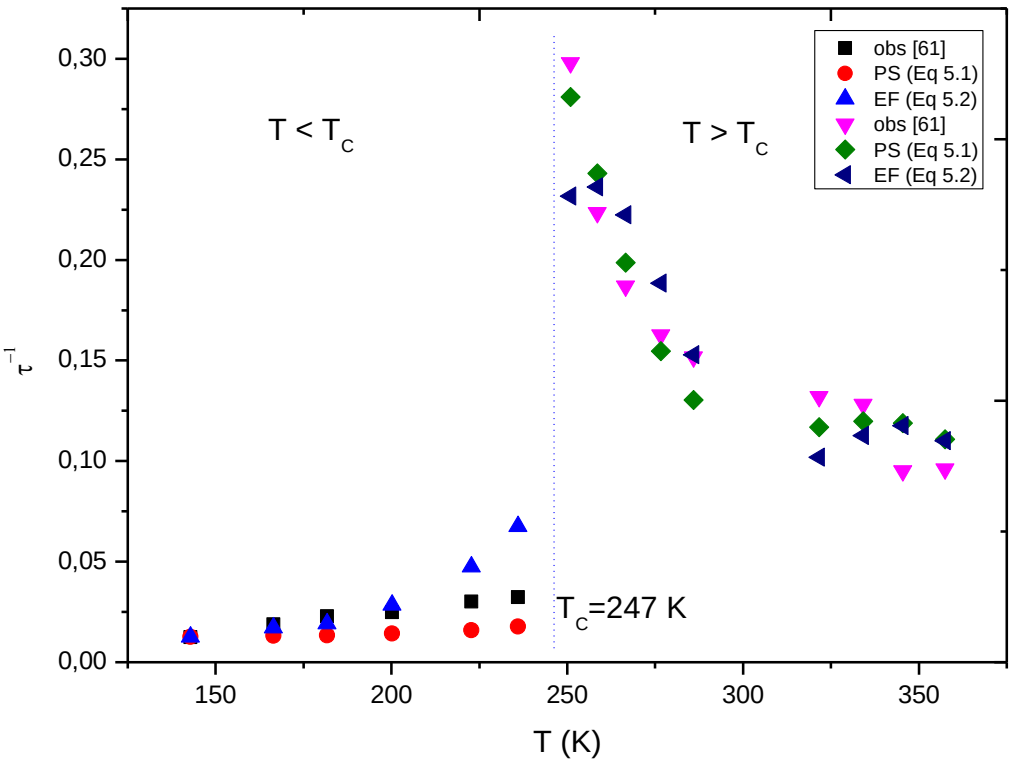

Figure 6.3. The temperature dependence of the inverse spin lattice relaxation time τ that was calculated from the PS and EF models both below and above the solid-solid phase transition temperature of T_C = 247 K in $ImClO_4$.

The activation energy U can be calculated from the spin lattice relaxation time by the following relation [80]

$$\ln(1/\tau) = \ln C - U/k_B T \tag{6.3}$$

Calculated $\ln(\tau^{-1})$ from both PS (Eq 5.1) and EF (Eq 5.2) models were plotted as a function of T^{-1} according to Eq. (6.3) as given in Figure 6.4. The slope of the graphs allows to find the activation energy U and intersection points allow to calculate the constant C in Eq (6.3). The values of activation energy U and the constant C were then extracted below and above T_C for Im-ClO_4 as given in Table 6.3.

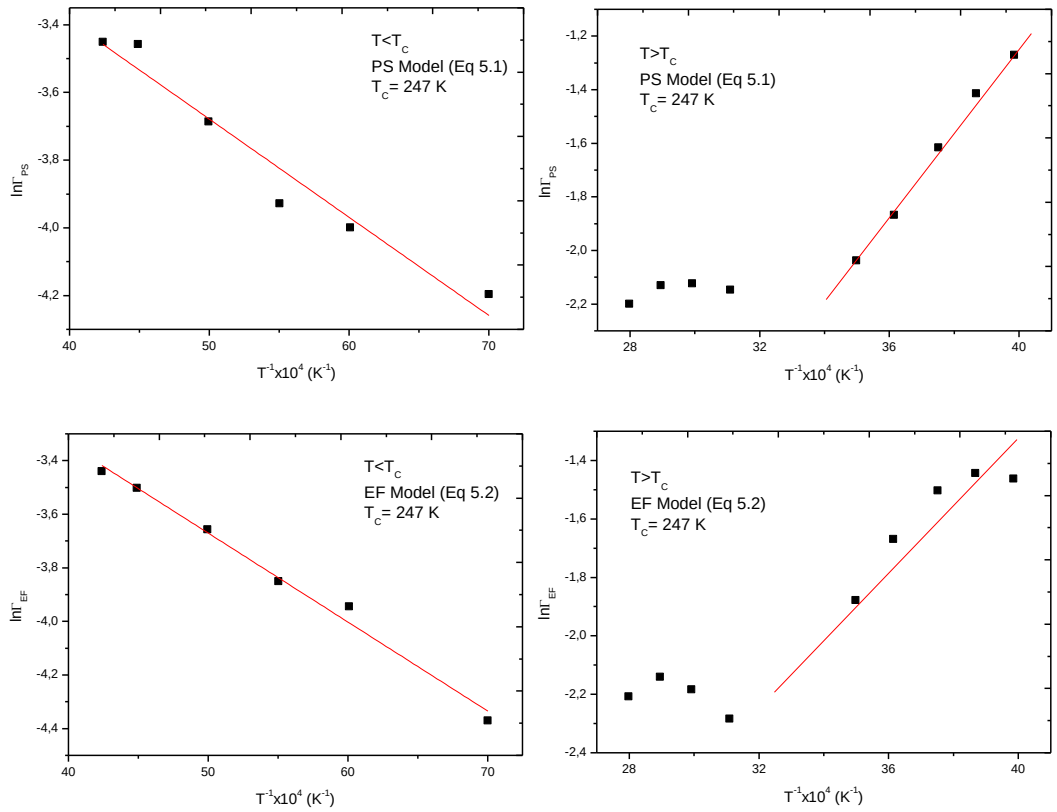

Figure 6.4. The damping constant Γ_{SP} calculated from Eqs. 5.1 (PS) and Eqs. 5.2 (EF) as a function of the reciprocal temperature to extract the activation energy for the cation reorientation in $ImClO_4$.

Table 6.3 Values of the activation energy U and the constant C according to Eq. (6.3) for the cation reorientation in Im-ClO_4.

Crystal	Model	$U(kJ/mol)$	C x 10^{-3}	Temperature Interval
$ImClO_4$	PS (Eq. 5.1)	2.4	107.7	142.9 < T (K) < 236.0
	PS (Eq. 5.1)	13.5	0.4	251.0 < T (K) < 285.9
	EF (Eq. 5.2)	4.9	650.9	142.9 < T (K) < 236.0
	EF (Eq. 5.2)	9.8	2.5	251.0 < T (K) < 285.9

6.1.2 Discussion

Although it is difficult to explain the physical mechanism without knowledge of the low temperature crystal structure of Im-ClO_4, the proton second moment M_2 below T_C = 247 K can be considered as an order parameter η, as pointed out previously for pyridinium periodate [38] and pyridinium flurosulfonate [48]. The molecular field theory provides the temperature dependence of the order parameter η below the phase transition as given in Chapter 5, which was calculated according to Eq (5.3) for Im-ClO_4. Then, the observed [61] proton second moment M_2/M_{2max} was associated with the order parameter η from the mean field theory (Eq. 5.3) for Im-ClO_4. The parameters of Eq. (6.1) were determined by the fitting procedure below the transition temperature T_C. Above T_C, on the other hand, the observed M_2 [61] decreases very rapidly as the temperature increases due to the infrequent reorientation of the cation between the non-equivalent potential wells. So that, the square of the observed [61] M_2/M_{2max} was associated with the disorder parameter [1- η^2] above T_C for Im-ClO_4.

Then, the temperature dependence of the spin lattice relaxation time was calculated from PS (Eq 5.1) and EF (Eq 5.2) models below and above T_C for Im-ClO_4 as given in Figure 6.3. Our results indicate that the inverse spin lattice relaxation time increases very slightly as the temperature increases below the transition temperature of T_C= 247 K. At the transition temperature T_C, it increases anomalously and reaches its maximum value. Above T_C, it decreases very rapidly up to the 300 K and it is almost constant above 300 K. Although both models (PS and EF) were in good agreement with the observed data [61], the PS model seems to describe it better than EF model (Fig 6.3) with the fitting parameters of Eq. (6.2) as given in Table 6.2. These calculated values of the spin lattice relaxation time from both models were then used to deduce the activation energy U according to Eq. (6.3) as given in Figure 6.4. A significant deviation of $ln\Gamma$ from linearity above the transition temperature of 247 K (Figure 6.3), which starts at about 320 K (10^4/T= 31.25 K^{-1}) is occurred. A similar deviation is observed at about 320 K in the unit cell volume of Im-ClO_4, so

this illustrates reasonably well the pretransition effects which were pronounced in the DSC experiments, as pointed out previously [61]. Our extracted values of U from the PS model 2.4 and 13.5kJ/mol (Table 6.3) below and above T_C, respectively, are close to that reported [61] values of 3.0 and 16.0 kJ/mol.

6.2 Analysis of the Specific Heat

6.2.1 Calculation of the Entropy, Enthalpy, and Free Energy

The anomalous behavior of the measured [63] specific heat data was analyzed according to the Ising model (Eq (3.11)) close to the phase transition temperature of Im-ClO_4. Interestingly, two peaks at T=245.8 K and 247.1 K have been reported by Przesławski and Czapla [63] for the specific heat of Im-ClO_4, which are given in Figure (6.5). So, both of 245.8 K and 247.1 K have been considered as transition temperatures and the analysis has been carried out below and above those two temperatures.

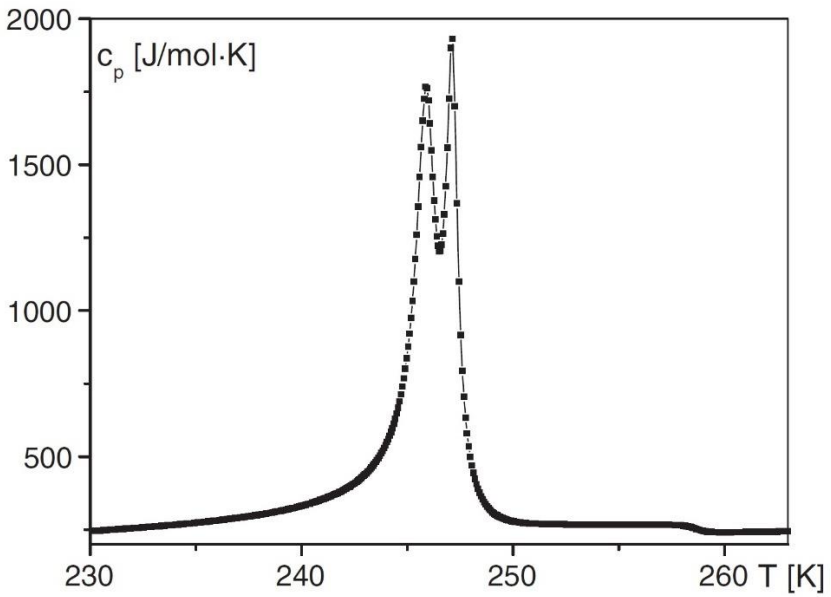

Figure 6.5. Temperature dependence of the specific heat observed during the heating at the lower-temperature phase transition [63]

The analysis has been performed according to Eq. (3.11) by taking the logarithmic (ln) function of both sides. $ln\,(Cp/T)$ versus $ln\,(\varepsilon)$ graphs were plotted for all regions of both transitions. As seen in Figure (6.6), linear correlation has been captures in all regions. The critical exponent α and the interaction parameter JA were deduced from tangent and intersection of the graphs, respectively, in the vicinity of these transition temperatures (245.8 K and 247.1 K). The extracted values of α and JA were tabulated in Table (6.4). While all critical exponent values appear to be in harmony with each other, it is seen that the value in the paraelectric region at of T_{C2} = 247.1 K is clearly greater than the others.

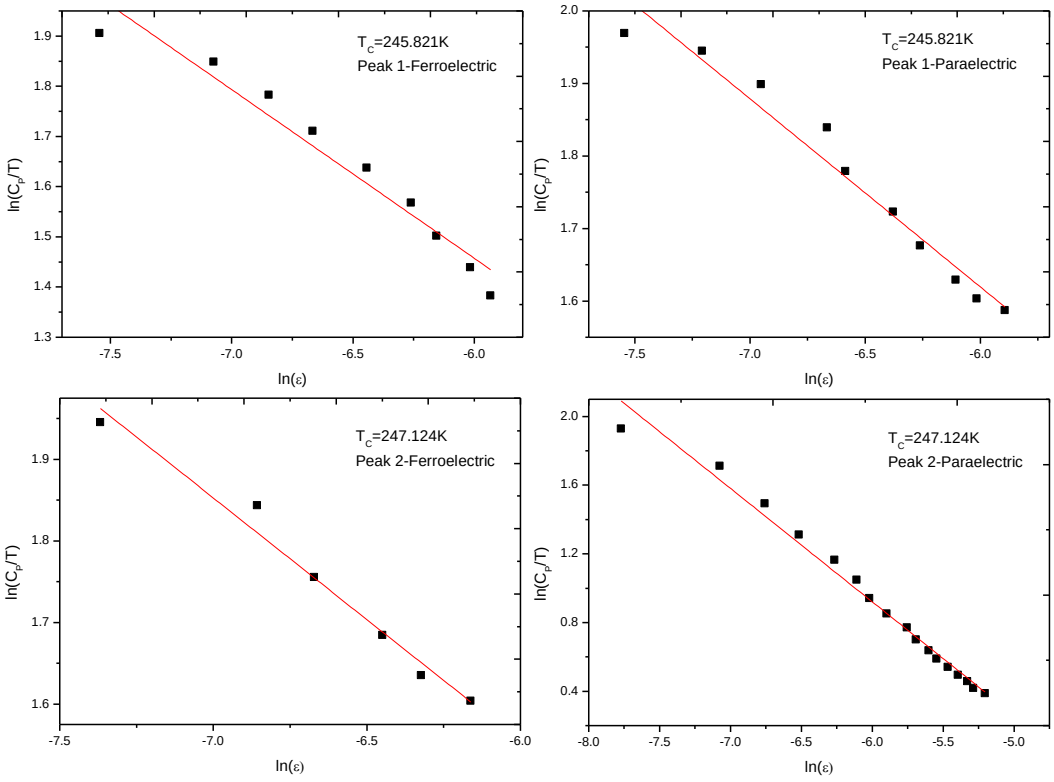

Figure 6.6. Specific heat (C_P) [63] as a function of the reduced temperature ε in an ln-ln scale according to Eq. (3.11) in the vicinity of these transition temperatures 245.8 K and 247.1 K in Im-ClO_4.

Table 6.4 Values of the critical exponent α and the fitting parameter JA according to Eq. (3.11) in the vicinity of these transition temperatures 245.8 K and 247.1 K in Im-ClO_4.

	Phase	**-JA**	**α**	**Temp. interval (K)**
T_{C1} = 245.8 K	Ferroelectric	31317	0.33	245.2-245.7
	Paraelectric	49926	0.26	245.9-246.5
T_{C2} = 247.1 K	Ferroelectric	40403	0.30	246.6-246.9
	Paraelectric	6411	0.66	247.3-247.9

Another discussion that has been carried out in this analysis, is about the thermodynamic properties of Im-ClO_4, such as enthalpy, entropy, and free energy. The thermodynamic definition of the enthalpy $H = \int C_P \, dT$ can be used to predict the temperature dependence of H close to the phase transition temperatures T_C. By substituting the expression of C_P (Eq. (3.11)) in this definition, the enthalpy (H) expression in terms of the critical exponent and reduced temperature can be obtained as

$$\Delta H = H - H_0 = -JA[(1-\alpha)|\varepsilon|^{2-\alpha} + (2-\alpha)|\varepsilon|^{1-\alpha}] \qquad (6.4)$$

where H_0 is the enthalpy value at $T = T_C$, α is the critical exponent, and $\varepsilon = |T-T_C|/T_C$ is the reduced temperature. The extracted values of α and JA (Table 6.4) were used to predict the temperature dependence of the enthalpy (H) of Im-ClO_4. The predicted values of enthalpy change ΔH have been demonstrated in Figure (6.7) for both critical temperatures.

Similarly, from the definition of entropy $S = (C_P/T)\ dT + S_0$, one can calculate the entropy as a function of temperature by replacing the specific heat (Eq. (3.11)) in this basic definition which gives

$$\Delta S = S - S_0 = -JA\frac{(2-\alpha)}{T_C}\,|\varepsilon|^{1-\alpha} \tag{6.5}$$

where S_0 is the entropy at the transition temperature. The computed values of ΔS for Im-ClO_4 were given in Figure 6.8 as a function of temperature for both critical temperatures. Similar to the enthalpy calculations, the extracted values of JA and α (Table 6.4) from the specific heat data were used for the computation of ΔS.

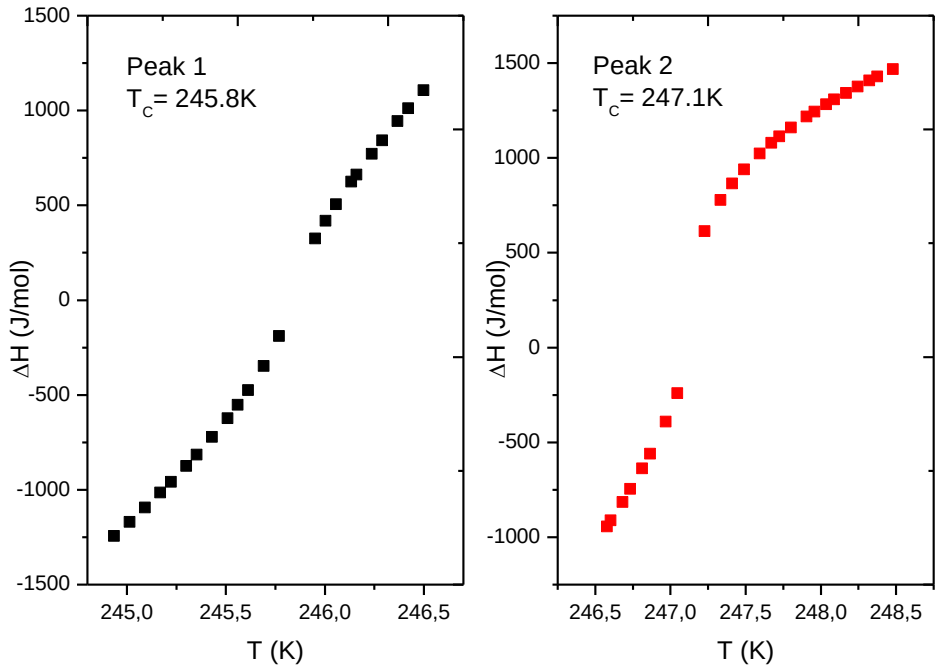

Figure 6.7. The enthalpy difference ΔH as a function of temperature according to Eq. (6.4) around both transition temperatures 245.8 K and 247.1 K in Im-ClO_4.

The obtained values of ΔH (Figure 6.7) and ΔS (Figure 6.8) of Im-ClO_4 crystals were inserted into the expression of the Gibbs free energy ΔG;

$$\Delta G = \Delta H - T\Delta S \tag{6.6}$$

The temperature dependence of the ΔG was demonstrated in Fig (6.9). It can be clearly observed in the graphs that Gibbs free energy tends to increase in ferroelectric phases and it decreases in the paraelectric phase with increasing temperature, as expected.

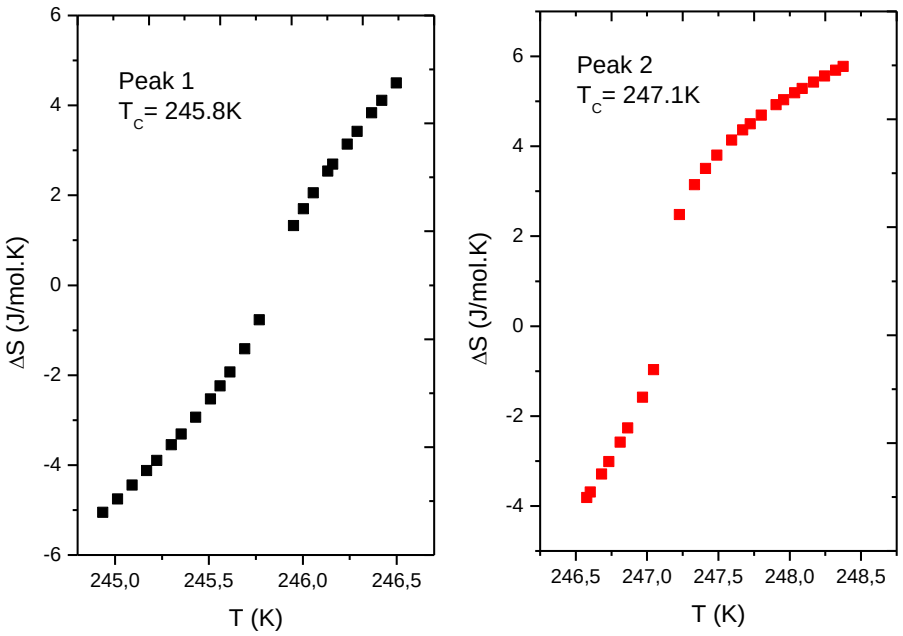

Figure 6.8. The entropy difference ΔS as a function of temperature according to Eq. (6.5) around both transition temperatures 245.8 K and 247.1 K in Im-ClO_4.

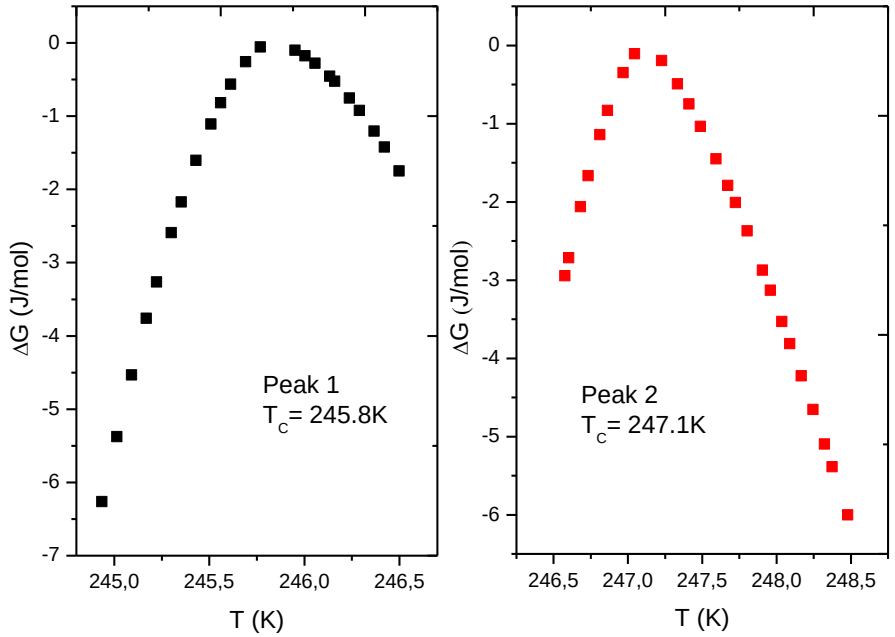

Figure 6.9. The Gibbs free energy difference ΔG as a function of temperature according to Eq. (6.6) around both transition temperatures 245.8 K and 247.1 K in Im-ClO_4.

6.2.2 Calculation of the Critical Exponents

Another discussion about the analysis of Im-ClO_4 has been continued on the critical exponents of an Ising model. The variation of certain thermodynamic properties of a system around its phase transition temperature can be expressed by critical exponents. The order parameter, specific heat, susceptibility, and other system characteristics can exhibit some sharp changes or jumps close to the transition point. The power laws can be used to describe critical behavior of the system which was caused by these discontinuities or singularities. The power laws can be expressed generally as

$$A(-\varepsilon)^{\emptyset} \tag{6.7}$$

where $\emptyset$ denotes the critical exponent, A is any constant and ε is the reduced temperature ($\varepsilon = |T-T_C|/T_C$).

For this analysis, another temperature value, 373 K has been chosen as the transition temperature that has been widely studied in the literature and the transition is already defined as a second order phase transition [63, 82, 83]. By using the definition of the power law, the reduced temperature has been correlated to the specific heat C_P according to the Eq. (3.11), polarization, and susceptibility in the vicinity of second-order transition temperature T_C = 373 K and then the critical exponents were extracted for each relation.

The power-law rise of specific heat ($C \sim |\varepsilon|^{-\alpha}$) and susceptibility ($\chi \sim |\varepsilon|^{-\gamma}$) near Tc, as well as their divergences at Tc, characterize the second-order phase transition [82]. Firstly, the reduced temperature ε was correlated to the specific heat Cp to extract the critical value of α according to the scaling law. The relation has been revealed by the ln-ln scale graph for the reduced temperature and specific heat. The linear relation can be seen in Figure (6.10), so by the tangent of the graph, the critical exponent α can be extracted. In addition, to observe the changes in the critical exponent (α) values with respect to the temperature, we examined it at different temperature ranges, which diverge to the critical phase transition temperature as T_C

demonstrated in Figure (6.11). As can be seen from the figure, while the temperature ranges get narrow, α values gradually decrease and approach zero.

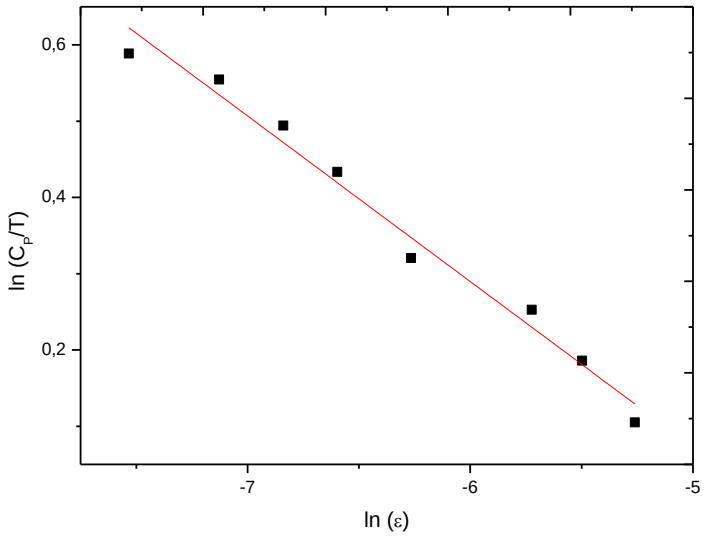

Figure 6.10. Specific heat (C_P) [63] as a function of reduced temperature ε in an ln-ln scale according to Eq. (3.11) in the vicinity of second-order phase transition temperatures 373 K in Im-ClO_4.

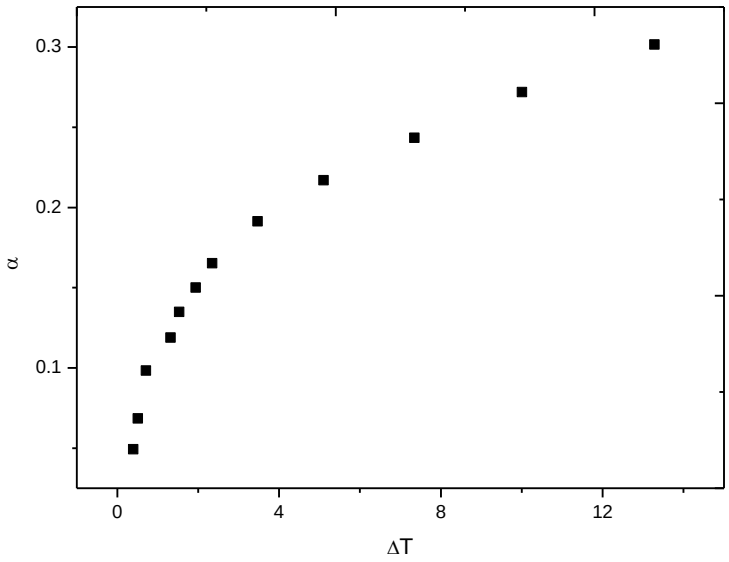

Figure 6.11. Critical exponent α as a function of temperature interval ΔT that approaches the second-order phase transition temperatures (373 K) in Im-ClO_4.

Then, the correlation between the reduced temperature and polarization has been investigated. According to scaling laws, the value of the critical exponent β can be calculated by using the value of the average dipole [83] at the critical temperature T_C. The average polarization data [83] have been used to extract the critical exponent β, by the power-law $P \sim |\varepsilon|^{\beta}$. The expected linear relation has been obtained and it was demonstrated in Figure (6.12). The slope of the graph was used to calculate the β values. Also, temperature interval analysis has been made for polarization, the ranges have been chosen as approaching the critical temperatures.

Lastly, the susceptibility data obtained from the permittivity relation ($\chi = \varepsilon - 1$) and it was given in an ln-ln scale graph as a function of the reduced temperature as discussed for the specific heat and polarization. The linear relation can be seen in the Figure (6.13) and it was used to extract γ values in different temperature intervals.

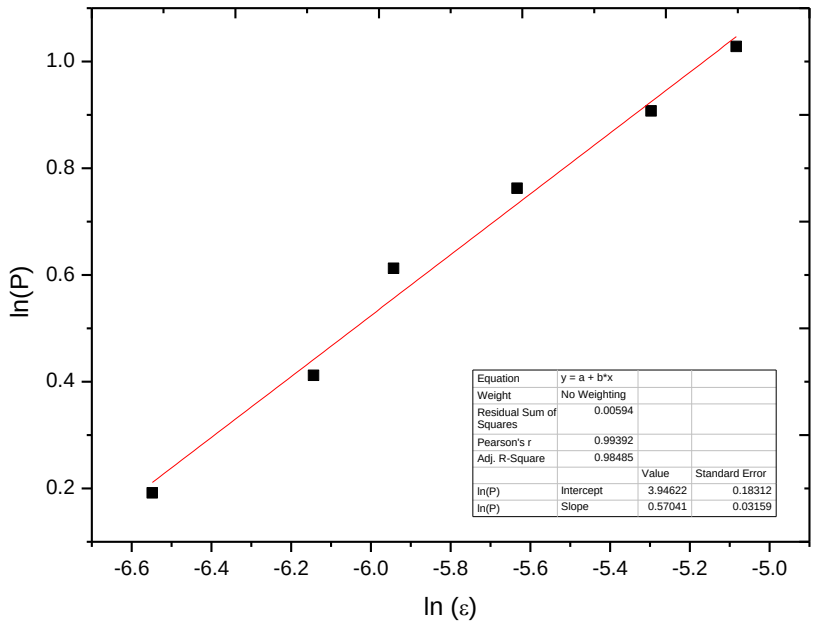

Figure 6.12. Polarization P as a function of reduced temperature ε in an ln-ln scale in the vicinity of the second-order phase transition temperatures 373 K in Im-ClO_4.

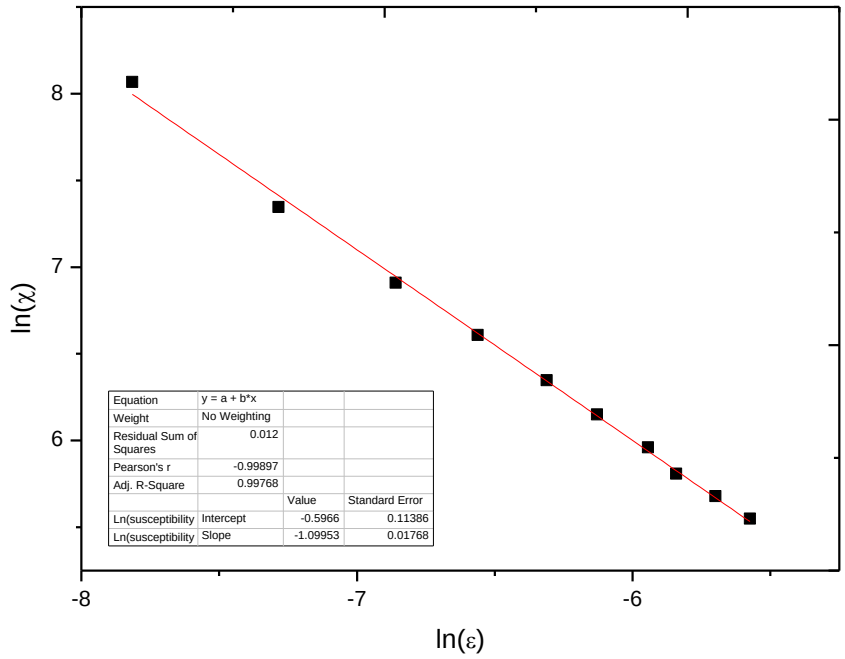

Figure 6.13. The susceptibility χ as a function of reduced temperature ε in an ln-ln scale in the vicinity of the second-order phase transition temperatures (373 K) in Im-ClO_4.

The temperature interval analysis was made for all three critical exponents. As mentioned earlier, α approaches zero when intervals get narrow, whereas β and γ values did not change drastically. The critical exponent values for the specific temperature interval ΔT at about 2 K are demonstrated in Table (6.5) with their errors.

Table 6.5 The critical exponents deduced from the specific heat, polarization, and susceptibility in the vicinity of the second-order phase transition temperature T_C = 373 K.

Critical Exponents	**α ± Δα**	**β ± Δβ**	**γ ± Δγ**
Calculated Values	0.19 ± 0.01	0.58 ± 0.01	1.10 ± 0.20

The fact that various systems might exhibit the same critical exponents close to the transition point, is known as the universal critical behavior. Such a classification (scaling) allows us to determine the characteristics of the transitions. The Rushbrooke inequality (RI), which reduces to equality under the static scaling hypothesis [82], is one of the most remarkable scaling relations.

$$\alpha + 2\beta + \gamma \geq 2 \tag{6.8}$$

As an extension to critical exponent calculations, the values of the extracted critical exponents were checked to see if they were consistent with any of the universality classes listed in the literature.

6.2.3 Results and Discussions about Calculations of Im-ClO_4

The critical behavior of the observed specific heat data for Im-ClO_4 [63] was analyzed according to Eq. (3.11) close to the transition temperatures of T_{C1} = 245.8 K and T_{C2} = 247.1 K (Figure 6.6). Table (6.4) gives our extracted values of the critical exponent α and the interaction parameters JA for the temperature intervals indicated. While the values of 0.33 ($T < T_{C1}$), 0.26 ($T > T_{C1}$) and 0.30 ($T < T_{C2}$), can be compared with that predicted from the 2d Potts model (α = 0.30), the value of 0.66 ($T > T_{C2}$) is much greater than the predicted value. So, it is reasonable to argue that the Im-ClO_4 undergoes a second-order phase transition at T_{C1} = 245.8 K, while it exhibits a first-order phase transition at T_{C2} = 247.1 K.

Regarding the prediction of the enthalpy ΔH (Eq. 6.4), the entropy ΔS (Eq. 6.5) and free energy ΔG for $ImClO_4$, the extracted values of the critical exponent α and the interaction parameters from the observed [63] specific heat data of this crystal (Table 6.4) were used. The results have been given in Figs. (6.7), (6.8), and (6.9) as a function of temperature for the enthalpy, entropy, and free energy, respectively. The predictions for ΔH (Figure 6.7) and ΔS (Figure 6.8) can be compared with the measured values when they are available in the literature.

When we evaluated the critical exponent α, we obtained it in the 2 K neighborhood of second-order phase transition temperature T_C, which was approximately 0.15 (Table 6.5). It is compatible with the 3D Ising model which predicts 0.11. However, as we approach the critical temperature closer than 2 K, the α value approaches zero, as predicted by the mean field theory. As the discussion continues for the critical exponent β, by the correlation between reduced temperature and polarization, the value of 0.57 (Table 6.5) has been attained, while T_C has been approached around 2.3 K temperature difference. However, when we approach more than 2 K to T_C, this value has increased slightly. It can be claimed that it is still close to 0.5, as suggested by the mean field theory.

The last critical exponent which is of interest is γ that was related to the susceptibility. Its value has been obtained from Figure (6.13), at around 1.10 (Table 6.5) and the value did not change noticeably as it approaches the critical temperature T_C. This critical exponent value is less than 1.23 as suggested by the 3d Ising model and it is greater than 1.0 as suggested by mean field theory. However, it has been extracted between the values of both models, which seems to be in agreement with both.

Finally, the extracted values of critical exponents α, β, and γ (Table 6.5) have been used to control the applicability of the Rushbrooke inequality [82] given in Eq. (6.8). The extracted values are 0.19, 0.58, and 1.10 for α, β, and γ, respectively. As easily can be calculated from Eq. (3.11), the result of the scaling law gives 2.43 at the temperature close as 2 K to the second-order phase transition temperature T_C. As a result of this discussion, we can conclude that the extracted values of the critical exponents have been compatible with Rushbrooke's inequality.

6.2.4 Conclusion of Im-ClO_4

The phase transition mechanism in Im-ClO_4 crystal was investigated by calculating the relaxation time and the activation energy of the crystal close to the phase

transition temperature T_C. The calculated values of the relaxation time from the pseudospin-phonon (PS) and the energy fluctuation (EF) models fit the observed data well. The phase transition mechanism in Im-ClO_4 was investigated by analyzing the specific heat of this crystal around the phase transition temperatures; T_{C1} = 245.8 K and T_{C2} = 247.1 K. The results from the analysis of the specific heat indicate a second order phase transition at T_{C1} = 245.8 K and a first order transition at T_{C2} = 247.1 K. According to the specific heat analysis of the Im-ClO_4, it can be concluded that in the vicinity of both transition temperatures, the anomalous behavior of the specific heat of Im-ClO_4 was investigated in terms of a power-low formula, comprising the critical exponent α and the interaction parameter JA, as obtained from the Ising model. Furthermore, using the values of α and JA which were derived from the measured specific heat data of Im-ClO_4, various thermodynamic functions such as entropy and enthalpy were projected as a function of temperature.

Additionally, the critical exponents of Imidazolium Perchlorate ($ImClO_4$) that have been associated using the reduced temperature to specific heat C_P, polarization P, and susceptibility χ at around the second-order transition temperature T_C = 373 K, were studied, and the critical exponents for each relation were extracted. After that, the values of the extracted critical exponents were checked whether they were consistent with any of the universality classes listed in the literature. Finally, the well-known scaling relation, Rushbrooke inequality (RI), was studied and it was concluded that corresponds to the critical exponent values as obtained.

CHAPTER 7

RAMAN WAVENUMBERS CALCULATED AS A FUNCTION OF PRESSURE FROM THE GRÜNEİSEN PARAMETER OF ZIRCONIA

7.1 Calculations and Results

Changes in temperature and pressure can affect the size and dynamics of a crystal lattice, which in turn can cause slight changes in the vibrational frequencies of atoms in a molecular crystal. The Grüneisen parameter (denoted by γ) is a dimensionless parameter that expresses the change in volume of the crystal lattice as a function of temperature and pressure. The parameter can be hardly determined experimentally so a detailed knowledge of the phonon distribution spectrum is necessary to investigate by macroscopic parameters. For this purpose, investigation of microscopic parameters requires experimental measurements of thermodynamic properties at high pressure and temperature.

The isothermal Grüneisen parameter of the Raman modes in ZrO_2 was calculated according to the Eq. (3.44). To get the calculation, the observed Raman shift [68] and volume data [69] were analyzed as a function of pressure according to

$$w(P) = a_0 + a_1 P + a_2 P^2 \tag{7.1}$$

and

$$V(P) = b_0 + b_1 P + b_2 P^2 \tag{7.2}$$

The fitting parameters a_0, a_1, a_2 of Eq. (7.1) and b_0, b_1, b_2 and of Eq. (7.2) were given in Tables (7.1) and (7.2), respectively, in the pressure intervals indicated.

Table 7.1 The values of the fitting parameter of Eq. (7.1) for the Raman modes in ZrO_2.

Frequencies T = 298 K	a_0 **(cm^{-1})**	a_1 **(cm^{-1}/GPa)**	a_2 **(cm^{-1}/GPa^2)**	**Pressure Interval (GPa)**
150 cm^{-1}	142.54879	4.06387	-0.1454	$0 \leq P \leq 40$
260 cm^{-1}	273.08047	- 4.92692	0.07759	
320 cm^{-1}	318.35292	3.46741	-0.02443	
480 cm^{-1}	462.18435	5.01944	0.01056	
602 cm^{-1}	602.48966	2.41407	-0.0228	
650 cm^{-1}	645.81203	3.66497	-0.06053	

Table 7.2 The values of the fitting parameter of Eq. (7.2) for the cell volume in ZrO_2.

Cell Volume ($Å^3$)	b_0 **(cm^{-1})**	b_1 **(cm^{-1}/GPa)**	b_2 **(cm^{-1}/GPa^2)**	**Pressure Interval (GPa)**
ZrO_2	67.21242	-0.32874	0.00322	0 < P <50

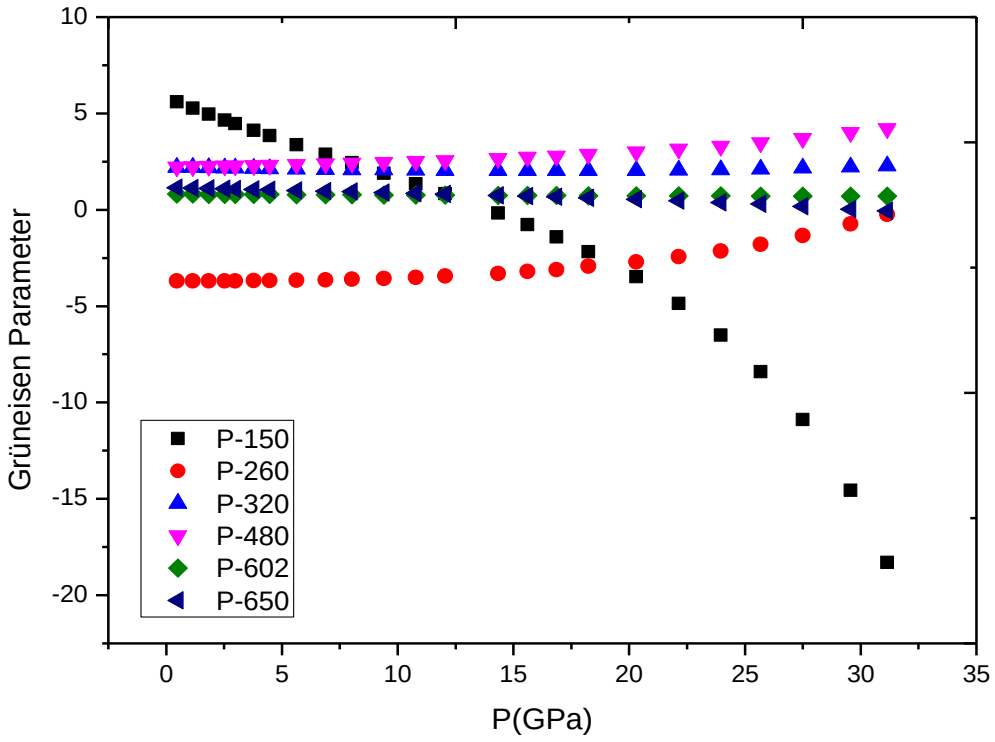

Figure 7.1. Isothermal Grüneisen parameter $\gamma_T(P)$ calculated (Eq 3.44) as a function of pressure for the Raman frequencies of ZrO_2.

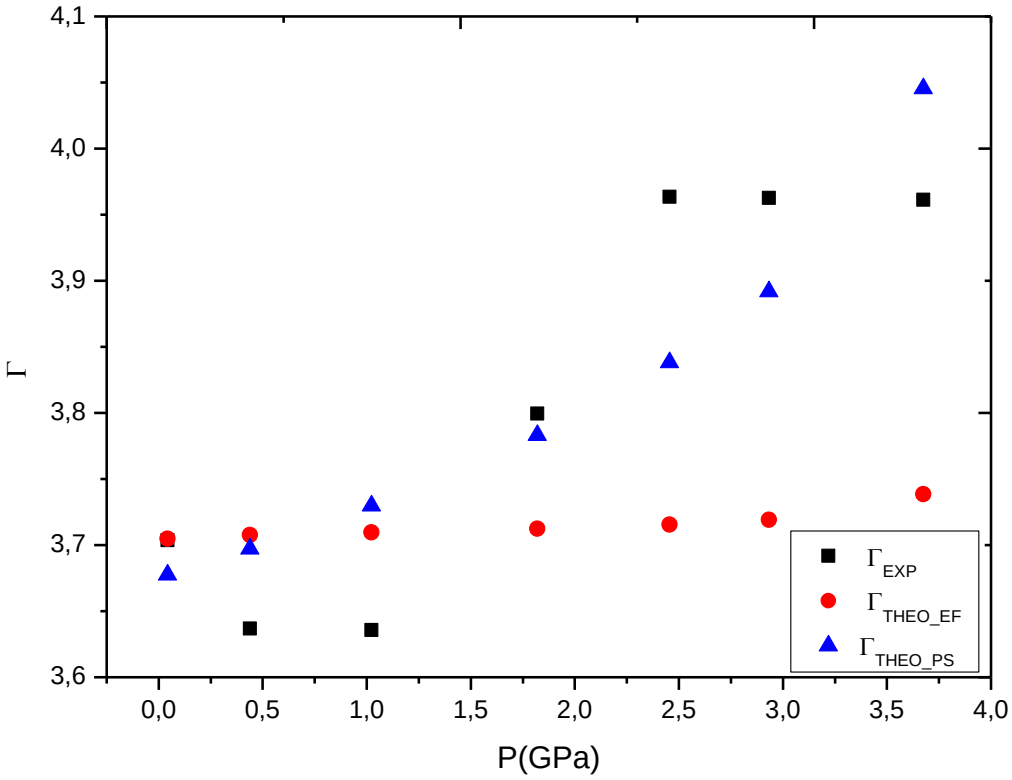

Figure 7.2. The damping constant Γ_{SP} calculated from Eqs (5.1) and (5.2) as a function of pressure for the Raman frequency band at 150 cm^{-1} in ZrO_2.

We used the psuedospin-phonon coupled (Eq 5.1) and energy fluctuation (Eq. 5.2) models to investigate the pressure dependence of the HWHM of the lowest two Raman modes (150 and 260 cm^{-1}). The calculated HWHM values were fitted to the observed data [68]. The fitting parameters of Eqs. (5.1) and (5.2) were then deduced as given in Table 7.3 for the pressure intervals indicated. The results are given in Figs (7.2) and (7.3) for 150 and 260 cm^{-1} Raman frequency, respectively.

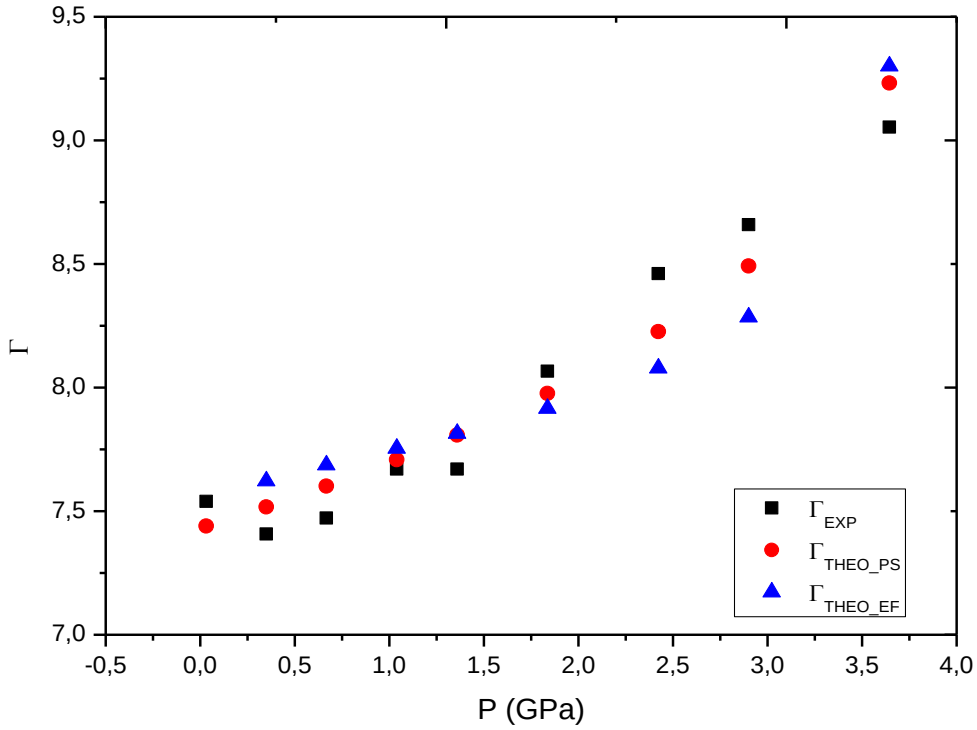

Figure 7.3. The damping constant Γ_{SP} calculated from Eqs. (5.1) and (5.2) as a function of pressure for the Raman frequency band at 260 cm^{-1} in ZrO_2.

Table 7.3 Values of the damping constant Γ_0 (Γ_0') and the amplitude A (A') due to the PS (Eq. 5.1) and EF (Eq. 5.2) models both Raman frequency bands at 150 and 260 cm^{-1} in ZrO_2.

Crystal	**Raman Frequency Band (w)**	**Model**	$\boldsymbol{\Gamma_0}$ **(**$\boldsymbol{\Gamma_0'}$**) (Hz)**	$\boldsymbol{A}$ **(**$\boldsymbol{A'}$**) (Hz)**	**Pressure Interval**
$\boldsymbol{ZrO_2}$	150 cm^{-1}	PS (Eq. 5.1)	3.677	0.755	0 < P (GPa) < 4
		EF (Eq. 5.2)	3.705	0.245	
	260 cm^{-1}	PS (Eq. 5.1)	7.439	3.796	
		EF (Eq. 5.2)	7.493	1.381	

7.2 Discussion

The observed [68] Raman frequency data for the bands at 150, 260, 320, 480, 602, 650 cm^{-1}, were analyzed according to Eq. (7.1) in the pressure intervals and the fitting paramerters were determined, as given in Table 7.1. In addition, the observed [69] cell volume dependence with the pressure of ZrO_2 were also analyzed according to Eq. (7.2) with the fitting parameters as given in Table 7.2. Once we get the fitting parameters of Eqs of (7.1) and (7.2), we were able to calculate the isothermal Grüneisen parameters through Eq 3.44, as given in Fig 7.1. It is seen from Fig 7.1 that the Grüneisen parameter from the Raman frequency of ZrO_2 for the band at 150 cm^{-1} decreases drastically as the pressure increases, whereas the 260 cm^{-1} band and the others (320, 480, 603 and 650 cm^{-1}) which were calculated increase slightly.

Regarding the calculation of the HWHM (damping constant) of the lowest modes (150 and 260 cm^{-1}), the frequency softening of those two modes that have been represented by a power-law according to $w = a(P^0 - P)^b$ where a = 16.25, P^0 = 38.03 GPa and b = 0.472, were associated with the order parameter η according to

$$\left(\frac{w}{w_{max}}\right)^2 \alpha\, \eta^2 \tag{7.3}$$

Since the order parameter η can take any value between 0 and 1, the normalization was performed for the values of the frequency (Eq 7.3).

It is possible to investigate the evaluation of the HWHM of the Raman modes indicated by considering the psuedospin-phonon interactions in ZrO_2. For this reason, the psuedospin-phonon coupled (Eq 5.1) and energy fluctuation (Eq. 5.2) models have been taken into account. Although the PS (Eq 5.1) and EF (Eq 5.2) models have been derived at various temperatures, the pressure dependence of the HWHM (damping constant) can also be predicted by considering the pressure-temperature (P-T) phase diagram of ZrO_2, as considered in the present study. A lineer

relation between T and P were obtained from the analysis of the observed [69] P-T graph that reads

$$T_C = 3787.66 - 173.62\,P \tag{7.4}$$

By replacing Eqs. (7.3) and (7.4) into both Eqs. (5.1) and (5.2), we were able to predict the pressure dependence of the HWHM of the lowest two Raman modes (150 and 260 cm^{-1}) in ZrO_2, as given in Figures (7.2) and (7.3), respectively.

Although the EF model (Eq. 5.2) explains well the observed HWHM data of the 260 cm^{-1}, it fails to explain the observed HWHM data of the 150 cm^{-1}. On the contrary, the PS model fits well the observed data of both 150 and 260 cm^{-1} bands, as given in Figures (7.2) and (7.3).

CHAPTER 8

SUMMARY

In the scope of the present thesis, the phase transition mechanisms of some ferroelectric crystals were investigated by the phenomenological methods. Particularly, we made use of the compressible Ising model and Landau phenomenological theory to explain the anomalous behavior of ferroelectrics exhibiting second-order phase transitions in the vicinity of the transition temperatures. Besides, the temperature dependence of some thermodynamic functions such as internal energy, enthalpy, entropy, and free energy of some ferroelectric materials was predicted. The thermodynamic quantities of ferroelectrics were obtained by calculating the order parameters using the experimental data from the literature. Investigation on different ferroelectric materials in the present thesis can be summarized in the following order:

Firstly, the compressible Ising model was used to study the anomalous behavior of the specific heat for $La_{1-x}Nd_xBGeO_5$ with x= 0, 0.03, and 0.05, at about 4 K below and above the phase transition temperatures of 802.4 K, 816.6 K, and 823.3 K, respectively. According to the results obtained, the extracted values of the critical exponent vary between 0.04 - 0.12 in the ferroelectric phase ($T < T_C$) of these three compositions and also in the paraelectric phase ($T > T_C$) of the sample with x= 0 they are consistent with those predicted from the 3-D Ising model (0.07 for $T < T_C$ and 0.13 for $T > T_C$). On the other hand, the deduced value of 0.3 in the paraelectric phase of the sample with x= 0.05, is the same as that predicted from the 2-D Pots model. So, it can be argued that the compressible Ising model is adequate to describe the ferroelectric-paraelectric phase transition in pure and Nd^{3+} doped $LaBGeO_5$ crystals. Additionally, birefringence data which were associated with the order parameter (squared) and the observed dielectric constant of the three compositions of $La_{1-x}Nd_xBGeO_5$ were analyzed. The Landau phenomenological theory was used

to extract the coefficients a and a_4. As expected, all these coefficients were found to be positive, which also indicates that the phase transition of the $La_{1-x}Nd_xBGeO_5$ with x= 0, 0.03, and 0.05 is of a second order type.

Secondly, two phenomenological models, namely the pseudospin -phonon coupled and the energy fluctuation (EF) models, were used to calculate the spin-lattice relaxation time for protons nuclei in Pyridinium Fluorosulfonate ($(C_5NH_6)FSO_3$). The results indicated that both models explain well the observed anomalous behavior of the sample during the phase transition. In addition, the activation energy was calculated for the reorientation of the cation in this crystal. Also, both models are adequate to calculate the activation energy as close as those extracted from the experimental spin-lattice relaxation time data. Then, the activation energy for the reorientation of the dipole moment as calculated from the PS model within the framework of the Landau theory is almost the same as that extracted from the experimental dielectric correlation time, while the EF model fails to find the same result. As a consequence of this, those two models (PS and EF) work well to explain the phase transition mechanism and they can be used to examine the mechanism of other pyridinium salts.

Thirdly, the phase transition mechanism in Imidazolium Perchlorate (Im-ClO_4) crystal was investigated by calculating the relaxation time and the activation energy by using the pseudospin-phonon (PS) and the energy fluctuation (EF) models close to the phase transition temperature T_C = 247 K. The calculated values of the relaxation time from both models fit to the observed data well. Then, the phase transition mechanism in Im-ClO_4 was investigated by analyzing the specific heat of this crystal in the vicinity of the two phases transition temperatures T_{C1} = 245.8 K and T_{C2} = 247.1 K. The results from the analysis of the specific heat indicate a second order phase transition at T_{C1} = 245.8 K and a first order transition at T_{C2} = 247.1 K. According to the specific heat analysis of the Im-ClO_4, it can be concluded that in the vicinity of the lower phase transition temperature of T_C = 247 K, the anomalous behavior of the specific heat of Im-ClO_4 was investigated in terms of a power-law formula, comprising the critical exponent α and the interaction parameter JA, as

obtained from the Ising model. Furthermore, using the values of α and JA which were derived from the measured specific heat data of Im-ClO_4, various thermodynamic functions such as entropy and enthalpy were projected as a function of temperature.

Additionally, the critical exponents of Imidazolium Perchlorate that have been associated using the reduced temperature to the specific heat C_P, polarization P and susceptibility χ at around the second-order transition temperature T_C = 373 K, were studied and they for each relation. After that, the values of the extracted critical exponents were checked to see if they were consistent with any of the universality classes listed in the literature. As a result of the critical exponent study the well-known scaling relation, the Rushbrooke inequality (RI), was studied and I was concluded that the critical exponent values which were obtained, are in accordance with the Rushbrooke inequality.

Finally, the Grüneisen parameter γ_T of various Raman modes in Zirconia (ZrO_2) was calculated as a function of pressure at room temperature. For this calculation of γ_T, the pressure dependence of both Raman frequencies of the 150, 260, 320, 480, 602, and 650 cm^{-1} bands, and the volume of the ZrO_2 cell were used as given in the literature. The results demonstrate that the two lowest modes (150 and 260 cm^{-1}) exhibit unusual overdamped behavior of the soft mode with increasing pressure. From both Figures (7.2) and (7.3), it can be easily seen that the calculated damping constant values of pseudospin-phonon coupled model is in good agreement with the observed experimental data.

REFERENCES

[1] C. Kittel, *Introduction to Solid State Physics*. Wiley, 2004.

[2] N. W. Ashcroft & N. D. Mermin, *Solid-state physics*. New York: Holt, Rinehart, and Winston, 1976.

[3] R. Whatmore, *Ferroelectric Materials.* In: Kasap S., Capper P. (eds) Springer Handbook of Electronic and Photonic Materials. Springer Handbooks. Springer, Cham., 2017.

[4] J. Valasek, "Piezo-electric and allied phenomena in Rochelle salt," *Physical Review*, vol. 17, no. 4, pp.75-481, 1921.

[5] N. Nuraje and K. Su, "Perovskite ferroelectric nanomaterials," *Nanoscale*, vol. 5(19), pp. 8752-8780, 2013.

[6] W. Gao, L. Chang, H. Ma, L. You, J. Yin, J. Liu, Z. Liu, J. Wang, G. Yuan, "Flexible organic ferroelectric films with a large piezoelectric response," *NPG Asia Materials*, vol. 7(6), e189, 2015.

[7] Y. Hu, Z. Guo, A. Ragonese, T. Zhu, S. Khuje, C. Li, J. C. Grossman, C. Zhou, M. Nouh, S. Ren, "A 3D-printed molecular ferroelectric metamaterial," *PNAS*, vol. 117(44), pp. 27204-27210, 2020.

[8] D. W. Fu, H. L. Cai, Y. Liu, Q. Ye, W. Zhang, Y. Zhang, X. Y. Chen, G. Giovannetti, M. Capone, J. Li, R. G. Xiong, "Diisopropylammonium bromide is a high-temperature molecular ferroelectric crystal," *Science*, vol. 25, no. 339, pp. 425-428, 2013.

[9] C. K. Yang, W. N. Chen, Y. T. Ding, J. Wang, Y. Rao, W. Q. Liao, Y. Xie, W. Zou, R. G. Xiong, "Directional Intermolecular Interactions for Precise Molecular Design of a High- Tc Multiaxial Molecular Ferroelectric," *Journal of the American Chemical Society*, 141, 4, pp. 1781–1787, 2019.

[10] S. Horiuchi and Y. Tokura, “Organic ferroelectrics,” *Nature Materials*, 7: pp. 357–366, 2008.

[11] J. Li, Y. Liu, Y. Zhang, H. L. Cai, R. G. Xiong, “Molecular ferroelectrics: where electronics meet biology,” *Physical Chemistry Chemical Phys*ics, vol. 15(48), pp. 20786-20796, 2013.

[12] A. A. Kaminskii, A. V. Butashin, J. A. Maslyanizin, B. V. Mill, V. S. Mironov, S. P. Rozov, S. E. Sarkisov, V. D. Shigorin, “Pure and Nd^{3+}-, Pr^{3+}- Ion doped trigonal acentric $LaBGeO_5$ single crystals nonlinear optical properties, Raman scattering, spectroscopy, Crystal-Field analysis, and simulated emission of their activators,” *Physics Status Solidi A*, vol. 125, pp. 671-696, 1991.

[13] A. Rulmont and P. Tarte, “Lanthanide borogermanates $LnBGeO_5$: Synthesis and structural study by X-ray diffractometry and vibrational spectroscopy,” *Journal of Solid State Chemistry*, vol. 75, pp. 244-250, 1988.

[14] N. V. Sigaev, P. D. Sarkinson, E. V. Lopatina, S. J. Stefanovich, V.I. Molev, “Ferroelectric-pyroelectric texture based on glass-ceramic materials containing the $LaBGeO_5$ stillwellite-like phase,” *Glass Phys. and Chemistry*, vol. 22, p. 117, 1996.

[15] B. J. Demaske, A. Chernatynskiy, S. R. Phillpot, “First-principles investigation of ferroelectricity in $LaBGeO_5$,” *Journal of Physics: Condensed Matter*, 28, 165901 (9pp). , 2016.

[16] A. Onodera, B. A. Strukov, A. A. Belov, S. A. Taraskin, H. Haga1, H. Yamashita, Y. Uesu, “Thermal and dielectric properties of a new ferroelectric $LaBGeO_5$,” *Journal of the Physical Society of Japan*, vol. 62, pp. 4311- 4315, 1993.

[17] S. J. Stefanovich, B. V. Mill, A. V. Butashin, “Ferroelectric and phase transition in stillwellite $LaBGeO_5$,” *Kristallografiya*, vol. 37, pp. 965-970, 1992.

[18] E. L. Belokoneva, W. I. F. David, J. B. Forsyth, K. S. Knight, "Structural aspects of the 530^0C phase transition in $LaBGeO_5$," *Journal of Physics: Condensed Matter*, vol. 9, pp. 3503-3519, 1997.

[19] M. Tokunaga, "Two Different Mechanisms of the Curie-Weiss Dielectric Susceptibility in Ferroelectrics," *Journal of the Physical Society of Japan*, vol. 57, pp. 4275-4283, 1988.

[20] I. Hrubá, S. Kamba, J. Petzelt, I. Gregora, Z. Zikmund, D. Ivannikov, G. Komandin, A. Volkov, B. Strukov, "Optical Phonons and Ferroelectric Phase Transition in the $LaBGeO_5$ Crystal," *Physica Status Solidi B*, vol. 214, pp. 423-439, 1999.

[21] R.V. Pisarev and M. Serhane, "Raman scattering study of the ferroelectric $LaBGeO_5$," *Physics of the Solid State*, vol. 37, p. 2022, 1995.

[22] V. Califano, B. Champagnon, E. Fanelli, P. Pernice, V. Sigaev, D. Zakharkin, V. Sakharov, P. Baskov, "Anisotropy in extruded lanthanum borogermanate glasses? Structural study by Raman spectroscopy," *Philosophical Magazine*, vol. 84, pp. 1639-1644, 2004.

[23] E. V. Milov and B. A. Strukov, "Piezoelectric effect in the $LaBGeO_5$ ferroelectric crystal," *Moscow University Physics Bulletin*, vol. 62, pp. 48-50, 2007.

[24] R. Shaltaf, H. K. Juwhari, B. Hamad, J. Khalifeh, G. M. Rignanese, X. Gonze, "Structural, electronic, vibrational, and dielectric properties of $LaBGeO_5$ from first principles," *Journal of Applied Physics*, vol. 115, 074103, 2014.

[25] Y. Takahashi, A. Iwasaki, Y. Benino, T. Fujiwara, T. Komatsu, "Ferroelectric Properties and Second Harmonic Intensities of Stillwellite-Type (La,Ln)$BGeO_5$ Crystallized Glasses," *Japanese Journal of Applied Physics*, vol. 41, pp. 3771-3777, 2002.

[26] B. A. Strukov, Y. Uesu, A. Onodera, S. N. Gorshkov and I. V. Shnaidshtein, "Effect of Nd^{3+} doping upon ferroelectric properties of $LaBGeO_5$ crystals," *Ferroelectrics*, vol. 218, pp. 249-255, 1998.

[27] O. K. Rice, "Thermodynamics of phase transitions in compressible solid lattices," *The Journal of Chemical Physics*, vol. 22, pp. 1535-1543, 1954.

[28] A. I. Larkin and S. A. Pikin, "Phase transitions of the first order but nearly of the second," *Soviet Physics JETP*, vol. 29, pp. 891-896, 1969.

[29] G. A. Baker and J. W. Essam, "Effects of lattice compressibility on critical behaviour," *Physical Review Letters*, vol. 24, pp. 447-449, 1970.

[30] H. Yurtseven, "Phase transitions of weakly first order or nearly second order," *Phase Transition*, vol. 47, pp. 59-68, 1994.

[31] H. Yurtseven and A. Yanik, "Specific heat of NH_4Cl and $NH_4Br_xCl_{1-x}$ crystals close to the ferro-ordered phase," *Journal of The Chemical Society of Pakistan*, vol. 31, pp. 207-213, 2009.

[32] H. Yurtseven, D. Kayisoglu and W. H. Sherman, "Calculation of the specific heat for the first order, tricritical and second order phase transitions in NH_4Cl," *Phase Transitions*, vol. 67, pp. 399-412, 1999.

[33] H. Yurtseven, D. V. Tirpanci and H. Karacali H, "Analysis of the specific heat of Ru doped $LiKSO_4$ close to phase transitions," *High Temperature*, vol. 56, pp. 462-465, 2018.

[34] A. Kiraci, "Analysis of the specific heat and the free energy of $[N(CH_3)_4]_2ZnBr_4$ close to the ferro-paraelastic phase transition," *Phase Transitions*, vol. 92, pp. 249-258, 2019.

[35] A. Kiraci, "A phenomenological study on ferroelectric pyridinium tetrafluoroborate $(C_5NH_6)BF_4$," *Thermochimica Acta*, vol. 680, 178371, 2019.

[36] A. Costa, J. Noro, A. Brito, F. Proença, "Tandem cyclization of a bispyridinium chloride: facile synthesis of substituted indolizines," *Synlett*, vol. 24, pp. 2255–2258, 2013.

[37] M. Franconetti, L. C. Bernal, F. C. Escribano, “From Pyrylium to Pyridinium Salts: Understanding Physicochemical Features,” *ECSOC*-17, 2013.

[38] Z. Pajak, P. Czarnecki, J. Wasicki, and W. Nawrocik, “Ferroelectric properties of pyridinium periodate,” *The Journal of Chemical Physics*, vol. 109, 6420, 1998.

[39] Y. Ito, T. Asaji, R. Ikeda, D. Nakamura, “^{1}H NMR and ^{35}Cl NQR Studies on the Motion of Pyridinium Ions in Crystalline Pyridinium Tetrachloro and Tetrabromoaurate (III): (pyH)AuX_4 (X = Cl, Br),” *Ber. Bunsenges. Phys. Chem*, vol. 92, pp. 885–891, 1988.

[40] A. Kozak, M. Grottel, J. Wasicki, Z. Pajak, “Temperature variation of asymmetry in potential barriers in pyridinium nitrate,” *Physica Status Solidi A Applied Research*, vol. 143, pp. 65–70, 1994

[41] J. Ripmeester, “Molecular motion, phase transitions, and disorder in the pyridinium halides,” *Canadian Journal of Chemistry*, vol. 54, pp. 3453–3457, 1976.

[42] J. W. Wasicki, A. Kozak, Z. Pajak, P. Czarnecki, A. V. Belushkin, M. A. Adams, “Neutron, nuclear magnetic resonance, and dielectric study of ion motion in pyridinium hexafluorophosphate,” *The Journal of Chemical Physics*, vol. 105, pp. 9470–9477, 1996.

[43] A. Kozak, J. Wasicki, Z. Pajak, “Molecular reorientation and phase transition in pyridinium hexafluoroantimonate,” *Phase Transition*, vol. 57, pp. 153–159, 1996.

[44] I. Szafraniak, P. Czarnecki, P. U. Mayr, “Thermodynamics of the phase transitions in ferroelectric pyridinium tetrafluoroborate $[C_5NH_6]^{+}BF_4^{-}$,” *Journal of Physics: Condensed Matter*, vol. 12, pp. 643–652, 2000.

[45] P. Czarnecki, W. Nawrocik, Z. Pajak, J. Wasicki, “Ferroelectric properties of pyridinium perchlorate,” *Journal of Physics: Condensed Matter*, vol. 6, pp. 4955–4960, 1994.

[46] J. Wąsicki, P. Czarnecki, Z. Pająk, W. Nawrocik, W. Szczepanski, "Ferroelectric properties of pyridinium perrhenate," *The Journal of Chemical Physics*, vol 107, pp. 576–579, 1997.

[47] J. Ripmeester, "^{1}H and ^{2}H NMR study of pyridinium iodide. Disorder and molecular motion between inequivalent sites," *The Journal of Chemical Physics*, vol. 85, pp. 747-750, 1986.

[48] Z. Pajak, P. Czarnecki, H. Małuszynska, B. Szafranska, "Ferroelectric properties of pyridinium fluorosulfonate," *The Journal of Chemical Physics*, vol. 113, pp. 848-853, 2000.

[49] I. Laulicht, "The drastic temperature broadening of hard mode Raman lines of ferroelectric KDP type crystals near Tc," *Journal of Physics and Chemistry of Solids*, vol. 39 (8), pp. 901-906, 1978.

[50] G. Schaack and V. Winterfeldt, "Temperature behaviour of optical phonons near Tc in triglycine sulphate and triglycine selenate, II. Evidence of non-linear pseudospin-phonon interaction," *Ferroelectrics*, vol. 15 (1), pp. 35-41, 1977. DOI: 10.1080/00150197708236718.

[51] E. B. Anderson and T. E. Long, "Imidazole- and imidazolium-containing polymers for biology and material science applications," *Polymer*, vol. 51(12), pp. 2447–2454, 2010.

[52] S. N. Riduan and Y. Zhang, "Imidazolium salts and their polymeric materials for biological applications," *Chemical Society Review*, vol. 42(23), pp. 9055-9070, 2013.

[53] L. Zhao, C. Zhang, L. Zhuo, Y. Zhang, J. Y. Ying, "Imidazolium Salts: A Mild Reducing and Antioxidative Reagent," *Journal of the American Chemical Society*, vol. 130(38), pp. 12586–12587, 2008.

[54] C. G. Hanke, S. L. Price, R. M. Lynden-Bell, "Intermolecular potentials for simulations of liquid imidazolium salts," *Molecular Physics*, vol. 99(10), pp. 801–809, 2001.

[55] Y. Zhang and J. Y. G. Chan, “Sustainable chemistry: imidazolium salts in biomass conversion and CO_2 fixation,” *Energy Environmental Science*, vol. 3(4), pp. 408–417, 2010.

[56] S. Lee, “Functionalized imidazolium salts for task-specific ionic liquids and their applications,” *Chemical Communications*, vol. 37(31), pp. 1049-1063, 2006.

[57] O. A. El Seoud, A. Koschella, L. C. Fidale, S. Dorn, T. Heinze, “Applications of ionic liquids in carbohydrate chemistry: A window of opportunities,” *Biomacromolecules*, vol. 8(9), pp. 2629–2647, 2007.

[58] B. Yu, F. Zhou, H. Hu, C. Wang, W. Liu, “Synthesis and properties of polymer brushes bearing ionic liquid moieties,” *Electrochimica Acta*, vol. 53(2), pp. 487-494, 2007.

[59] H. Ma, W. Gao, J. Wang, T. Wu, G. Yuan, J. Liu, Z. Liu, “Ferroelectric polarization switching dynamics and domain growth of Triglycine Sulfate and Imidazolium Perchlorate,” *Advance Electronic Materials*, vol. 2, 1600038, 2016.

[60] Y. Zhang, Y. Liu, H. Y. Ye, D. W. Fu, W. Gao, H. Ma, Z. Liu, Y. Liu, W. Zhang, J. Li, G. L. Yuan, R. G. Xiong, “A molecular ferroelectric thin film of imidazolium perchlorate that shows superior electromechanical coupling,” *Angewandte Chemie International Edition*, vol. 126, pp. 5164-5168, 2014.

[61] Z. Pająk, P. Czarnecki, B. Szafrańska, H. Małuszyńska, Z. Fojud, “Ferroelectric ordering in imidazolium perchlorate,” *The Journal of Chemical Physics*, vol. 124(14), 144502, 2006.

[62] Z. Czapla, S. Dacko, B. Kosturek, A. Waskowska, “Dielectric and optical properties related to phase transitions in an imidazolium perchlorate [$C_3N_2H_5ClO_4$] crystal,” *Physica Status Solidi B*, vol. 242, pp. 122-124, 2005.

[63] J. Przesławski and Z. Czapla, “Calorimetric studies of phase transitions in imidazolium perchlorate crystal,” *Journal of Physics: Condensed Matter*, vol. 18(23), pp. 5517–5524, 2006.

[64] Y. Hu, Z. Liu, C. C. Wu, J. L. Gottfried, R. Pesce-Rodriguez, S. D. Walck, P. W. Chung, S. Ren, “Chemically driven energetic molecular ferroelectrics,” *Nature Communications*, vol. 12, no. 5696, pp. 1-7, 2021.

[65] N. Kara, A. Kiraci, H. Yurtseven, “Calculation of the Relaxation Time and the Activation Energy Close to the Lower Phase Transition in Imidazolium Perchlorate,” *Journal of Basic Applied Science*, vol. 17, pp. 53-63, 2021.

[66] R. Terki, G. Bertrand, H. Aourag, C. Coddet, “Structural and electronic properties of zirconia phases: A FP-LAPW investigations,” *Materials Science in Semiconductor Processing*, vol. 9, pp. 1006-1013, 2006.

[67] P. Bouvier and G. Lucazeau, “Raman spectra and vibrational analysis of nanometric tetragonal zirconia under high pressure,” *Journal of Physics and Chemistry of Solids*, vol. 61, pp. 569-578, 2000.

[68] P. Bouvier, E. Djurado, G. Lucazeau, T. Le Bihan, “High-pressure structural evolution of undoped tetragonal nanocrystalline zirconia,” *Physical Review B*, vol. 62, pp. 8731-8737, 2000.

[69] M. Gitterman, *Phase Transitions: Modern Applications*. World Scientific, 2014.

[70] P. Papon, J. Lebland, P. H. E. Meijer, *The Physics of Phase Transitions*. Springer, 2002.

[71] H. Yurtseven and W. H. Sherman, “Weakly first order or nearly second order phase transitions in ammonium halides,” *Phase Transition*, vol. 47, pp. 69–75, 1994.

[72] I. Laulicht and N. Luknar, “Internal-mode line-broadening by proton jumps in KH_2PO_4,” *Chemical Physics Letters*, vol. 47(2), pp. 237–240, 1977.

[73] G. Lahajnar, R. Blinc, S. Zumer, “Proton spin-lattice relaxation by critical polarization fluctuations in KH_2PO_4,” *Physics of Condensed Matter*, vol. 18(4), pp. 301–316, 1974.

[74] M. B. Smirnov, A. V. Menschikova, I. Kratochvilova-Hruba, Z. Zikmund, “Lattice dynamics and phase transition in $LaBGeO_5$,” *Physica Status Solidi B*, vol. 241, pp. 1017-1025, 2004.

[75] K. J. Lushington and C. W. Garland, “Critical heat capacity of NH_4Br and $NH_4Br_xCl_{1-x}$ single crystals,” *The Journal of Chemical Physics*, vol. 72, pp. 5752-5759, 1980.

[76] M. Matsushita, “Anomalous temperature dependence of the frequency and damping constant of phonons near T_C in ammonium halides,” *The Journal of Chemical Physics*, vol. 65, pp. 23-28, 1976.

[77] Y. Yamada, M. Mori, Y. Noda, “A microscopic theory on the phase transitions in NH_4Br- An ising spin phonon coupled system,” *Journal of the Physical Society of Japan*, vol. 32 (6), pp. 1565–1576, 1972.

[78] V. Rakov, “The influence of intermolecular interaction on linewidth in the Raman spectra of liquids,” *Optical Spectroscopy*, vol. 7, pp. 128-133, 1959.

[79] F. F. Bartoli and T. A. Litovitz, “Raman scattering: orientational motions in liquids,” *Journal of Chemical Physics*, vol. 56 (1), pp. 413-425, 1972.

[80] H. Yurtseven and A. Kiraci, “Temperature dependence of the damping constant and the relaxation time close to the tetragonal-cubic phase transition in $SrZrO_3$,” *Journal of Molecular Structure*, vol.1128, pp. 51-56, 2017.

[81] M. K. Hassan, D. Alam, Z. I. Jitu, M. M. Rahman, “On entropy, specific heat, susceptibility, and Rushbrooke inequality in percolation,” *Physical Review E*, vol. 96(5), pp. 50101-50106, 2017.

[82] E. Almahmoud, I. Kornev, L. Bellaiche, “Critical Behavior in Ferroelectrics from First Principles,” *Physical Review Letters*, vol. 102(10), 105701, 2009.

[83] V. P. Gorelov, “High-Temperature Phase Transitions in ZrO_2,” *Physics of Solid State*, vol. 61, pp. 1288–1293, 2019.

[84] J. H. Park, I. H. Bang, S. J. Lee, “Phase Transition and Thermal Expansion Behavior of Zirconia Setter Fabricated from Fused CaO Stabilized Zirconia,” *Journal of the Korean Ceramic Society*, vol. 56(2), pp. 184-190, 2019.

[85] S. Block, J. A. Jornada, G. J. Piermarini, “Pressure-Temperature Phase Diagram of Zirconia,” *Journal of the American Ceramic Society*, vol. 68(9), pp. 497-499, 1985.

[86] A. Kiraci and H. Yurtseven, “Temperature dependence of the Raman frequency, damping constant and the activation energy of a soft-optic mode in ferroelectric barium titanate,” *Ferroelectrics*, vol. 432, pp. 14-21, 2012.

[87] H. Yurtseven and A. Kiraci, “Calculation of the damping constant and the relaxation time for the soft-optic and acoustic mode in hexagonal barium titanate,” *Ferroelectrics*, vol. 437, pp. 137-148, 2012.

[88] H. Karacali, A. Kiraci, H. Yurtseven, “Calculation of the Raman frequency and the damping constant of a coupled mode in the ferroelectric and paraelectric phases in KH_2PO_4,” *Physica Status Solidi B*, vol. 247, pp. 927-936, 2010.

[89] A. Kiraci and H. Yurtseven, “Damping constant and the relaxation time calculated for the lowest-frequency soft mode in the ferroelectric phase of $Cd_2Nb_2O_7$,” *Optik*, vol. 127, pp. 11497- 11504, 2016.

[90] A. Kiraci and H. Yurtseven, “Calculation of the Raman frequency, damping constant (Linewidth) and the relaxation time near the tetragonal-cubic transition in $PbTiO_3$,” *Optik*, vol. 142, pp. 311- 319, 2017.

[91] H. Yurtseven and A. Kiraci, “Damping Constant (Linewidth) and the Relaxation Time of the Brillouin LA Mode for the Ferroelectric-Paraelectric Transition in $PbZr_{1-x}$ Ti_xO_3,” *IEEE Trans Ultrason Ferroelectric Frequency Control*, vol. 63, pp. 1647-1655, 2016.

[92] A. Kiraci and H. Yurtseven, “Analysis of the integrated intensity of the central peaks calculated as a function of temperature in the ferroelectric phase of lithium tantalite,” *Thermal Science*, vol. 22(1), pp. 221-227, 2018.

CURRICULUM VITAE

Surname, Name: Kara, Nazan

EDUCATION

Degree	Institution	Year of Graduation
MS	METU Physics	2013
BS & MS (Non-Thesis)	METU Sec. School Physics Education	2006
High School	Hamdi Bozbağ Anadolu High School, Giresun	1999

FOREIGN LANGUAGES

Advanced English

PUBLICATIONS

1. Kara N., Kiraci A. and Yurtseven H. "Calculation of the Relaxation Time and the Activation Energy Close to the Lower Phase Transition in Imidazolium Perchlorate", J Basic Appl Sci, 17, 53-63 (2021).

2. Kara N., Kiraci A. and Yurtseven H. "Phenomenological approaches on the Nd^{3+} doped ferroelectric $LaBGeO_5$", Ferroelectrics, 572(1), 13-26 (2021).

3. Kara N., Kiraci A. and Yurtseven H. "Calculation of the spin-lattice relaxation time and the activation energy near the IV–III phase transition in pyridinium fluorosulfonate $(C_5NH_6)FSO_3$", Ferroelectrics, 589(1), 45-54 (2022).

4. Kara N., Kiraci A. and Yurtseven H. "Analysis of the Specific Heat and Calculation of the Entropy, Enthalpy, and Free Energy Close to the Lower Phase Transition in Imidazolium Perchlorate", CUSJE, 19(2), 95-101 (2022).

INSTERESTS

Cycling, Camping, Outdoor Sports, Sea Kayaking, Photography and Videography